AD-A087 367 WYOMING UNIV LARAMIE DEPT OF MECHANICAL ENGINEERING F/G 11/4
NONLINEAR VISCOELASTIC BEHAVIOR OF A COMPOSITE MATERIAL USING A--ETC(U)
JUN 80 B G SCHAFFER, D F ADAMS DAAG29-79-C-0189
UNCLASSIFIED UWME-DR-001-101-1 ARO-16370.1-MS NL

1 OF 2

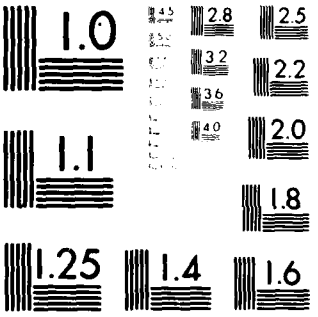

MICROSCOPY RESOLUTION TEST CHART
NATIONAL BUREAU OF STANDARDS 1963 A

ARO 16370.1-MS

5

DEPARTMENTAL REPORT UWME-DR-001-101-1

ADA087367

NONLINEAR VISCOELASTIC BEHAVIOR of a COMPOSITE MATERIAL USING a FINITE ELEMENT MICROMECHANICAL ANALYSIS

LEVEL II

(12)

Brent G. Schaffer

Donald F. Adams

June 1980

DTIC ELECTE AUG 1 1980 S D A

INTERIM REPORT

U.S. Army Research Office

Grant No. DAAG 29-79-C-0189

DDC FILE COPY

Approved for Public Release; Distribution Unlimited

COMPOSITE MATERIALS RESEARCH GROUP

DEPARTMENT of MECHANICAL ENGINEERING

University of Wyoming Laramie, Wyoming 82071

THE VIEWS, OPINIONS, AND/OR FINDINGS CONTAINED IN THIS REPORT ARE THOSE OF THE AUTHORS AND SHOULD NOT BE CONSTRUED AS AN OFEICIAL DEPARTMENT OF THE ARMY POSITION, POLICY, OR DECISION, UNLESS SO DESIGNATED BY OTHER DOCUMENTATION.

DEPARTMENT REPORT
UWME-DR-001-101-1

NONLINEAR VISCOELASTIC BEHAVIOR OF A COMPOSITE MATERIAL USING A FINITE ELEMENT MICROMECHANICAL ANALYSIS

INTERIM REPORT

BRENT G. SCHAFFER
DONALD F. ADAMS

JUNE 1980

U.S. ARMY RESEARCH OFFICE
GRANT NO. DAAG 29-79-C-0189

COMPOSITE MATERIALS RESEARCH GROUP
MECHANICAL ENGINEERING DEPARTMENT
UNIVERSITY OF WYOMING
LARAMIE, WYOMING 82071

APPROVED FOR PUBLIC RELEASE;
DISTRIBUTION UNLIMITED

Unclassified (18) ARO (19) 16370.1-MS

SECURITY CLASSIFICATION OF THIS PAGE (When Data Entered)

REPORT DOCUMENTATION PAGE

READ INSTRUCTIONS BEFORE COMPLETING FORM

1. REPORT NUMBER

2. GOVT ACCESSION NO. AD-A087367

3. RECIPIENT'S CATALOG NUMBER (9)

4. TITLE (and Subtitle) (6)

NONLINEAR VISCOELASTIC BEHAVIOR OF A COMPOSITE MATERIAL USING A FINITE ELEMENT MICROMECHANICAL ANALYSIS.

5. TYPE OF REPORT & PERIOD COVERED

Interim Report.

6. PERFORMING ORG. REPORT NUMBER (14)

UWME-DR-001-101-1

7. AUTHOR(s) (10)

Brent G. Schaffer
Donald F. Adams

8. CONTRACT OR GRANT NUMBER(s) (15)

DAAG 29-79-C-0189

9. PERFORMING ORGANIZATION NAME AND ADDRESS

Composite Materials Research Group
Mechanical Engineering Department, University of Wyoming, Laramie, Wyoming 82071

10. PROGRAM ELEMENT, PROJECT, TASK AREA & WORK UNIT NUMBERS

11. CONTROLLING OFFICE NAME AND ADDRESS (11)

U.S. Army Research Office
P.O. Box 12211
Research Triangle Park, NC 27709

12. REPORT DATE

Jun[redacted]80

13. NUMBER OF PAGES

141

14. MONITORING AGENCY NAME & ADDRESS (if different from Controlling Office) (12) 156

15. SECURITY CLASS. (of this report)

Unclassified

15a. DECLASSIFICATION/DOWNGRADING SCHEDULE

NA

16. DISTRIBUTION STATEMENT (of this Report)

Approved for public release; distribution unlimited

17. DISTRIBUTION STATEMENT (of the abstract entered in Block 20, if different from Report)

NA

18. SUPPLEMENTARY NOTES

The view, opinions, and/or findings contained in this report are those of the author(s) and should not be construed as an official Department of the Army position, policy, or decision, unless so designated by other documentation.

19. KEY WORDS (Continue on reverse side if necessary and identify by block number)

Composite Materials	Micromechanics Analysis
Viscoelasticity	Finite Element Analyses
Nonlinear Viscoelasticity	Mechanical Properties
Creep	Thermal Effects

20. ABSTRACT (Continue on reverse side if necessary and identify by block number)

The analysis uses an elastoplastic finite element micromechanics computer program to model a unidirectional composite subjected to any combination of longitudinal, transverse, and hygrothermal loadings. Time-dependent effects are included by means of nonlinear viscoelastic constitutive equations. The method of solution is based upon the conditions for generalized plane strain which permits a pseudo-three-dimensional analysis. It also contains two failure criteria, viz., an octahedral shear stress criterion and a hydrostatic criterion.

(continued)

DD FORM 1 JAN 73 1473 EDITION OF 1 NOV 65 IS OBSOLETE

Unclassified

SECURITY CLASSIFICATION OF THIS PAGE (When Data Entered)

408984

Application of load or changes in temperature or moisture are input through time-independent increments. A plotting package is also included which allows the user to obtain a total of eight different plots; octahedral shear stress and strain, maximum and minimum principal stress, in-plane shear stress, out-of-plane longitudinal stress, and normal and tangential shear stress on the fiber-matrix interface. The study demonstrates that the associated program is able to model essentially any type of stress input or hygrothermal history.

Accession For
NTIS GRA&I
DDC TAB
Unannounced
Justification
By
Distribution/
Availability Codes
Dist. | Avail and/or special
A

FORWARD

This Interim Report presents the preliminary results of one phase of a comprehensive study, "Laminate Analyses, Micromechanical Creep Response, and Fatigue Behavior of Polymer Matrix Composites," being performed under Grant DAAG 29-79-C-0189 for the U.S. Army Research Office, Durham, North Carolina. This study was initiated in September 1979. The ARO Program Monitor is Dr. John C. Hurt, Associate Director, Metallurgy and Materials Science Division.

Program Manager and Principal Investigator at the University of Wyoming is Dr. Donald F. Adams, Professor of Mechanical Engineering. Co-Principal Investigator is Mr. David E. Walrath, Staff Scientist in Mechanical Engineering.

The task being reported here was performed by Mr. Brent G. Schaffer, Graduate Student in Mechanical Engineering, as a Masters Thesis under the direction of Dr. D. F. Adams.

Special appreciation is due to Dr. Richard A. Schapery, Professor of Civil and Aerospace Engineering, Texas A & M University, for his many valuable discussions and suggestions.

The assistance of graduate students Mohamed M. Monib and Daniel P. Murphy, and Staff Scientist David E. Walrath, is gratefully acknowledged. Additional acknowledgments are extended to Stephen R. Ownbey, Programmer Analyst, for his assistance in identifying programming errors, and to undergraduate students Kevin M. Kiger, John S. Huenefeld, and David W. Peterson, for their efforts during the experimental program.

TABLE OF CONTENTS

Chapter		Page
I.	INTRODUCTION	1
II.	LITERATURE SURVEY	5
	Empirical Approaches	5
	Mechanical Models	7
	Differential Operator Form	7
	Integral Representation	9
III.	ANALYSIS METHOD	13
	A Statement of Linearity	13
	Constitutive Equations	15
	Method of Solution	17
	Multiple Step Loading	26
IV.	EXPERIMENTAL CHARACTERIZATION	29
	Test Method	29
	Experimental Results	31
V.	NUMERICAL EXAMPLES	39
	Creep of Epoxy Resin	40
	Creep of a Composite	45
	Effect of Fiber Volume	58
	Relaxation After Cure	59
	Cyclic Loading	62
	Multiaxial Loading	68

TABLE OF CONTENTS (Continued)

Chapter		Page
VI.	SUMMARY AND CONCLUSIONS	75
	REFERENCES	80
	APPENDICES	83
	A. Evaluation of the Constitutive Equations	83
	B. Computer Program	90
	C. Experimental Results	98
	D. Numerical Results	115

LIST OF FIGURES

Figure		Page
1.	Illustrative examples of creep-recovery, relaxation, and the three stages of creep	6
2.	Plots of stress versus time for three different specimens	14
3.	Fiber packing arrangement of a unidirectional composite	18
4.	Unit cell for the finite element analysis	19
5.	The finite element grid used in the present analysis	21
6.	Plot of stress versus time for a two-step input	26
7.	Plot of stress versus time for a creep-recovery test	31
8.	Plot of a_σ versus stress for Hercules 3501-6 epoxy resin	33
9.	Plot of g_1 versus stress for Hercules 3501-6 epoxy resin	34
10.	Plot of g_0D_0 versus stress for Hercules 3501-6 epoxy resin	36
11.	Plot of g_2 versus stress for Hercules 3501-6 epoxy resin	37
12.	Plots of strain versus time for Shell 58-68R epoxy resin subject to a 2.1 hour creep and a 2.1 hour recovery test	41
13.	Expanded scale plots of strain versus time for Shell 58-68R epoxy resin subject to a 2.1 hour creep and a 2.1 hour recovery test	42
14.	Plot of strain versus time for an S2 glass composite (using Shell 58-68R epoxy resin) subject to a 2.1 hour creep and a 2.1 hour recovery test.	47
15.	Plot of strain versus time for an S2 glass composite (using Hercules 3501-6 epoxy resin) subject to a 50 hour creep test	50
16.	Plot of strain versus time for an S2 glass composite (using Hercules 3501-6 epoxy resin) subject to a 14 hour creep test	51

LIST OF FIGURES (continued)

Figure		Page
17.	Plot of strain versus time for an S2 glass composite (using Hercules 3501-6 epoxy resin) subject to a 14 hour creep test	52
18.	Plot of strain versus time for an AS graphite composite (using Hercules 3501-6 epoxy resin) subject to a 14 hour creep test	53
19.	Plot of strain versus time for two different fiber volume glass/epoxy composites subject to the same -20 ksi stress for 140 hours	60
20.	Plot of strain versus time for a glass/epoxy composite subject to a ±5000 psi stress for 2.1 hour intervals . . .	63
21.	Plot of strain versus time for a glass/epoxy composite subject to a ±20,000 psi stress for 2.1 hour intervals . .	65
22.	Plot of strain versus time (x-direction) for a glass/ epoxy composite subjected to a 5000 psi stress in the x-direction and a 5000 psi stress in the y-direction . . .	69
23.	Plot of strain versus time (x-direction) for a glass/ epoxy composite subjected to a 15,000 psi stress in the x-direction and a 5000 psi stress in the y-direction . . .	70
24.	Plot of strain versus time (y-direction) for a glass/ epoxy composited subjected to a 15,000 psi stress in the x-direction and a 5000 psi stress in the y-direction . . .	71
A-1.	Plot of stress versus time for a single-step input	84
A-2.	Plot of stress versus time for a two-step input	85
A-3.	Plot of stress versus time for a creep-recovery input . . .	88
B-1.	Analysis procedure flowchart	92
C-1.	Experimental creep-recovery data for Hercules 3501-6 epoxy resin subject to a 2000 psi uniaxial compressive stress . .	100

LIST OF FIGURES (continued)

Figure		Page
C-2.	Experimental creep-recovery data for Hercules 3501-6 epoxy resin subject to a 2000 psi uniaxial compressive stress . .	101
C-3.	Experimental creep-recovery data for Hercules 3501-6 epoxy resin subject to a 6000 psi uniaxial compressive stress . .	102
C-4.	Experimental creep-recovery data for Hercules 3501-6 epoxy resin subject to a 6000 psi uniaxial compressive stress . .	103
C-5.	Experimental creep-recovery data for Hercules 3501-6 epoxy resin subject to a 8000 psi uniaxial compressive stress . .	104
C-6.	Experimental creep-recovery data for Hercules 3501-6 epoxy resin subject to a 8000 psi uniaxial compressive stress . .	105
C-7.	Experimental creep-recovery data for Hercules 3501-6 epoxy resin subject to a 16,000 psi uniaxial compressive stress .	106
C-8.	Experimental creep-recovery data for Hercules 3501-6 epoxy resin subject to a 16,000 psi uniaxial compressive stress .	107
C-9.	Experimental creep-recovery data for Hercules 3501-6 epoxy resin subject to a 19,000 psi uniaxial compressive stress .	108
C-10.	Experimental creep-recovery data for Hercules 3501-6 epoxy resin subject to a 19,000 psi uniaxial compressive stress .	109
C-11.	Plot of strain versus time for Hercules 3501-6 epoxy resin subjected to a one-hour creep test	110
C-12.	Plot of strain versus time for Hercules 3501-6 epoxy resin subjected to a one-hour creep test	111
C-13.	Plot of strain versus time for Hercules 3501-6 epoxy resin subjected to a one-hour creep test	112
C-14.	Plot of strain versus time for Hercules 3501-6 epoxy resin subjected to a one-hour creep test	113
C-15.	Plot of strain versus time for Hercules 3501-6 epoxy resin subjected to a one-hour creep test	114

LIST OF FIGURES (continued)

Figure		Page
D-1.	Plot of strain versus time for Hercules 3501-6 epoxy resin subjected to a 2.1 hour creep and a 2.1 hour recovery test	116
D-2.	Expanded scale plot of strain versus time for Hercules 3501-6 epoxy resin subjected to a 2.1 hour creep and a 2.1 hour recovery test	117
D-3.	Plot of strain versus time for Hercules 3501-6 epoxy resin subjected to a 2.1 hour creep and a 2.1 hour recovery test	118
D-4.	Expanded scale plot of strain versus time for Hercules 3501-6 epoxy resin subjected to a 2.1 hour creep and a 2.1 hour recovery test	119
D-5.	Plot of strain versus time for Hercules 3501-6 epoxy resin subjected to a 2.1 hour creep and a 2.1 hour recovery test	120
D-6.	Expanded scale plot of strain versus time for Hercules 3501-6 epoxy resin subjected to a 2.1 hour creep and a 2.1 hour recovery test	121
D-7.	Octahedral shear stress (normalized) and octahedral shear strain plots for glass/epoxy subjected to a cooldown from the 177°C cure temperature to 21°C, followed by a 140 hour relaxation period, and then a -20 ksi stress for another 140 hours	122
D-8.	Interface stresses for glass/epoxy subjected to a cool-down from the 177°C cure temperature to 21°C, followed by a 140 hour relaxation period, and then a -20 ksi stress for another 140 hours	125
D-9.	Octahedral shear stress (normalized) and octahedral shear strain plots for glass/epoxy subjected to a -20 ksi stress for 140 hours	127
D-10.	Octahedral shear stress (normalized) and octahedral shear strain plots for a 50 percent fiber volume glass/epoxy composite subjected to a -20 ksi stress for 140 hours	128

LIST OF FIGURES (continued)

Figure		Page
D-11.	Interface stresses for a 50 percent fiber volume glass/epoxy composite subjected to a -20 ksi stress for 140 hours	129
D-12.	Octahedral shear stress (normalized) and octahedral shear strain plots for glass/epoxy subjected to a cooldown from the 177°C cure temperature to 99°C, a 2.1 hour relaxation period, further cool from 99°C to 21°C, and another 2.1 hour relaxation period	130
D-13.	Octahedral shear stress (normalized) and octahedral shear strain plots for glass/epoxy subjected to a +20 ksi stress for 2.1 hours, a -20 ksi stress for 2.1 hours, and a +20 ksi stress for another 2.1 hours	132
D-14.	Interface stresses for glass/epoxy subjected to a +20 ksi stress for 2.1 hours, a -20 ksi stress for 2.1 hours, and a +20 ksi stress for another 2.1 hours	135
D-15.	Octahedral shear stress (normalized) and octahedral shear strain plots for glass/epoxy subjected to a 5 ksi stress in the x-direction and a 5 ksi stress in the y-direction	138
D-16.	Octahedral shear stress (normalized) and octahedral shear strain plots for glass/epoxy subjected to a 15 ksi stress in the x-direction and a 5 ksi stress in the y-direction	139
D-17.	Interface stresses for glass/epoxy subjected to a 5 ksi stress in the x-direction and a 5 ksi stress in the y-direction	140
D-18.	Interface stresses for glass/epoxy subjected to a 15 ksi stress in the x-direction and a 5 ksi stress in the y-direction	141

LIST OF SYMBOLS

a_σ	Temperature- and moisture-dependent time shift factor
$[B]_i$	Element shape matrix
C	Constant
D_0	Initial or time-independent compliance
ΔD	Transient or time-dependent compliance
$\hat{D}$	Nonlinear uniaxial creep compliance
D^*	Nonlinear uniaxial creep compliance evaluated at the midpoint of a time increment
D_{ijkl}	Creep compliance tensor
$[D]_i$	Element material properties matrix
E	Young's modulus
$\{\dot{F}\}_i$	Incremental element nodal force vector due to externally applied loads
$\{\dot{F}_{\varepsilon_0}\}_i$	Incremental element nodal force vector due to temperature, moisture, or time changes
g_0, g_1, g_2	Constants (kernels) which are functions of temperature, moisture, and stress
$[K]_i$	Element stiffness matrix
M	Moisture content
n	Exponent used in the power law
P,Q	Series of linear differential operators with respect to time
T	Temperature
t	Real time
t_i	Element thickness

LIST OF SYMBOLS (Continued)

Δt	Time increment
γ	Shear strain
$\gamma_{xy}, \gamma_{xz}, \gamma_{yz}$	Shear strain components
Δ_i	Area of an element
$\{\dot{\delta}\}_i$	Incremental element nodal displacement vector
δ_{ij}	Kronecker delta
ε	Strain
$\varepsilon_x, \varepsilon_y, \varepsilon_z$	Normal strain components
$\varepsilon_x(t), \varepsilon_y(t), \varepsilon_z(t)$	Time-dependent normal strain components
λ	Nondimensional time
ν	Poisson's ratio
$\nu(t)$	Time-dependent Poisson's ratio
ν^*	Time-dependent Poisson's ratio evaluated at the mid-point of a time increment
σ	Stress
$\sigma_x, \sigma_y, \sigma_z$	Normal stress components
$\sigma(t)$	Time-dependent stress
τ	Shear stress
$\tau_{xy}, \tau_{xz}, \tau_{yz}$	Shear stress components
τ'	Time variable of integration
Ψ, Ψ'	Reduced times

CHAPTER I

INTRODUCTION

As the demand for more precise control of material parameters such as thermal expansion, directional strength and stiffness, and impact and fatigue resistance in structures has increased, designers have begun to move away from metal components and are now attempting to "tailor" composite materials to suit their particular needs. Thus, the use of fiber-reinforced composites such as graphite/epoxy and glass/epoxy has increased rapidly over the past ten years.

While an extensive effort during the past decade has been devoted to studying the above topics, it has only been recently that viscoelastic, i.e., time-dependent, behavior of composites has been investigated. The viscoelastic behavior of a material can be of paramount importance when a composite component is subjected to repeated loading cycles or substantial loads at moderately high temperatures for long periods of time. Environmental cycling or fluctuations of the ambient temperature and/or relative humidity can also have considerable influence on the performance of the composite. Under such conditions, the internal stress distributions and overall strain of the composite could ultimately change enough with time to cause failure of the component. Alternatively, the stress state could also change so as to relieve high stress states in certain areas of the composite, preventing failure of the component.

It is not possible to accurately simulate environmental or loading

cycles with a time-independent analysis. This approach does not realistically model the situation since it neglects any redistribution or changes in the internal stress state with time. And, since the distribution of stresses can change one way or another with time, the ability to predict these changes can be extremely important.

As an example, graphite/epoxy or other composite components on aircraft are often exposed to significant environmental changes. Whether these are detrimental to the performance of the composite or not can be determined by means of a time-dependent analysis. Spacecraft and satellite components must be dimensionally stable throughout their service lifetime, to preserve the functional integrity of the optical or electronic hardware which they carry. During fabrication, storage, and launch, the satellite sees a variety of environmental fluctuations, which cause dimensional changes to the structure and the instruments it carries. To accurately determine these dimensional changes, a time-dependent analysis should be used. Automotive components such as driveshafts and engine motor mounts must be able to withstand sustained loading and/or cyclic loadings for long periods of time. Whether the composite is capable of such performance may also be determined by means of a time-dependent analysis.

In order to experimentally characterize the time-dependent behavior of a composite material, a number of tests must be conducted. There are many factors (e.g., temperature, moisture, loading rate, and stress level) that affect the viscoelastic properties of a composite. Thus, an extensive amount of testing must be undertaken to determine how and to what extent each of these factors will affect the composite. While a particu-

lar composite material system might be adequately characterized by such a testing program, if a designer wishes to use a different fiber-matrix combination, he must re-evaluate all the properties determined in the previous testing program. This can be a problem since there are numerous fiber-matrix combinations available to a designer.

To overcome this difficulty, a micromechanics analysis and associated computer code has been developed in the present study which includes time-dependent effects. By inputing the appropriate constituent viscoelastic properties to the program, the designer can try any combination of fiber and matrix material, to determine if that composite will satisfy his need. Since only the individual constituent properties need to be determined experimentally, this analysis becomes extremely cost effective considering the amount of time and experimental testing saved by not having to evaluate all fiber-matrix combinations. Also, most fibers do not exhibit time-dependence. Therefore, only the candidate matrix materials need be tested.

To model the various fiber-matrix combinations, the analysis uses a finite element model capable of simulating a unidirectional composite subjected to any combination of longitudinal and transverse normal loadings, as well as hygrothermal loading. Time-independent nonlinear (elastoplastic) material behavior is included, as is a creep formulation which uses stresses as the independent state variable. The program also contains two failure criteria, viz., an octahedral shear stress criterion and a hydrostatic criterion.

Since the effects of temperature and moisture are included in the analysis, it is possible to examine the internal stress state of a com-

posite as a function of time after curing a laminate, as well as during external loading. The analysis can also model any arbitrary multiple step loading (stress reversal, cycling, etc.) as well as recovery. Some numerical examples of the capability are presented in Chapter V.

CHAPTER II

LITERATURE SURVEY

Whether considering creep or relaxation there are numerous theories available, each having its strong and weak points. A review of various theories will be presented in this chapter and the relative advantages and disadvantages of each will be discussed. Before this discussion begins, a few of the terms, viz., creep, recovery, and relaxation will be briefly defined.

In a creep test, stress is the independent state variable, while in a relaxation test, strain is the independent state variable. Recovery occurs when all of the stress is removed after a creep test. There are usually three stages of creep: primary, during which a rapid decrease of the creep rate occurs, secondary, where the creep rate is more or less constant, and tertiary, where a rapid increase in creep rate occurs. The tertiary stage of creep is usually brief, leading quickly to failure and is not of much use in design. Illustrative examples of creep-recovery and relaxation are shown in Figures 1a and 1b, respectively. The three stages of creep are shown in Figure 1c.

Empirical Approaches

Observation of the time-dependence or creep of metals was first reported around the mid-nineteenth century [1]. Early investigators used an empirical approach in dealing with the observed time-dependence

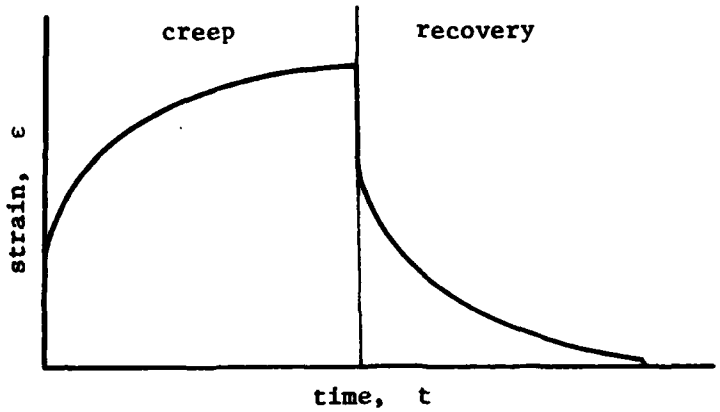

a) Plot of strain versus time for σ = constant (creep) and σ = zero (recovery)

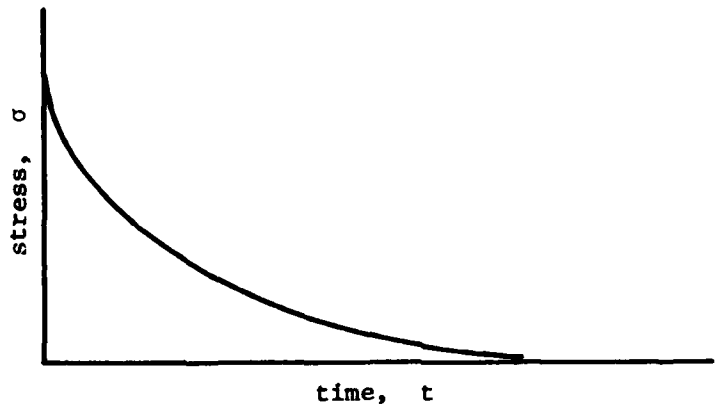

b) Plot of stress versus time for ε = constant (relaxation)

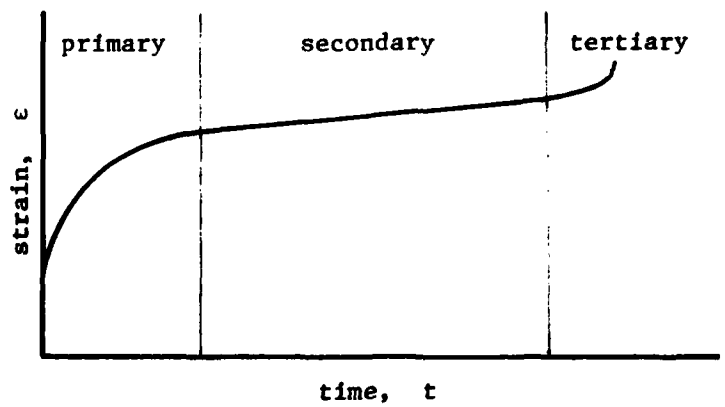

c) Plot of strain versus time showing the three stages of creep

Figure 1. Illustrative examples of creep-recovery, relaxation, and the three stages of creep

of metals [1,2]. Many equations were written which yielded good agreement with experimental data for uniaxial creep at low stresses under a constant externally applied load. These equations were found to be adequate to describe either primary or secondary stages of creep, but rarely both. Difficulties arose when investigators tried to describe combined states of stress using this empirical approach. The multiaxial stress experiments necessary were not easily performed, and the mathematical representation became more involved than those for uniaxial creep. Also, if the situation involved a changing stress history or a loading that was a function of time, the equation for the creep rate had to be a function of strain as well as the applied stress in order to fit the experimental data. This fact, along with the difficulty of multiaxial representation, caused many to realize that a more rigorous approach was necessary.

Mechanical Models

A number of investigators have utilized mechanical models to represent the creep behavior of materials [1,3]. By assembling springs and dashpots in a variety of configurations, they have been able to describe many different types of materials; from stainless steels, which exhibit a great deal of secondary creep, to polymers, which do not. These models become extremely difficult to visualize, much less formulate, when a combined stress state is considered.

Differential Operator Form

Both of the time-dependent stress-strain formulations just discussed were primarily phenomenological, models being constructed and equa-

tions written to describe specific experimental data. In creep, actual values of strain (response) depend upon the entire stress (input) history and not just the current value of stress. That is, the creep behavior of most materials, composites included, are affected by the total loading history. In order to account for this, a more mathematical representation is needed.

One of these mathematical forms is the differential operator method [1,3]. A differential equation is written

$$P\sigma = Q\varepsilon \tag{1}$$

where P and Q are a series of linear differential operators with respect to time. By choosing the proper terms in P and Q and excluding others, any material behavior may be represented. It can be shown that Eq. (1) can be reduced to give a representation of any of the mechanical model combinations. A generalization to multiaxial stress states is given by Findley and Lai [1].

A common solution technique for Eq. (1) utilizes the Correspondence Principle [1]. This method utilizes a known linearly elastic (time-independent) solution, selected in accordance with the particular problem. The Laplace transform of this solution is then taken to obtain equations of state in the imaginary or s-domain. Next, a substitution is made for the modulus and Poisson's ratio, e.g., $E = s\hat{E}(s)$ and $\nu = s\hat{\nu}(s)$, so that these quantities will become time-dependent terms when the inverse Laplace transform is taken. Following this substitution, the desired quantities are solved for. The solution in the real (time) domain is then generated by taking the inverse Laplace transform of the resulting equation. The limitation in using this solution technique is that Eq. (1) is

of metals [1,2]. Many equations were written which yielded good agreement with experimental data for uniaxial creep at low stresses under a constant externally applied load. These equations were found to be adequate to describe either primary or secondary stages of creep, but rarely both. Difficulties arose when investigators tried to describe combined states of stress using this empirical approach. The multiaxial stress experiments necessary were not easily performed, and the mathematical representation became more involved than those for uniaxial creep. Also, if the situation involved a changing stress history or a loading that was a function of time, the equation for the creep rate had to be a function of strain as well as the applied stress in order to fit the experimental data. This fact, along with the difficulty of multiaxial representation, caused many to realize that a more rigorous approach was necessary.

Mechanical Models

A number of investigators have utilized mechanical models to represent the creep behavior of materials [1,3]. By assembling springs and dashpots in a variety of configurations, they have been able to describe many different types of materials; from stainless steels, which exhibit a great deal of secondary creep, to polymers, which do not. These models become extremely difficult to visualize, much less formulate, when a combined stress state is considered.

Differential Operator Form

Both of the time-dependent stress-strain formulations just discussed were primarily phenomenological, models being constructed and equa-

tions written to describe specific experimental data. In creep, actual values of strain (response) depend upon the entire stress (input) history and not just the current value of stress. That is, the creep behavior of most materials, composites included, are affected by the total loading history. In order to account for this, a more mathematical representation is needed.

One of these mathematical forms is the differential operator method [1,3]. A differential equation is written

$$P\sigma = Q\varepsilon \tag{1}$$

where P and Q are a series of linear differential operators with respect to time. By choosing the proper terms in P and Q and excluding others, any material behavior may be represented. It can be shown that Eq. (1) can be reduced to give a representation of any of the mechanical model combinations. A generalization to multiaxial stress states is given by Findley and Lai [1].

A common solution technique for Eq. (1) utilizes the Correspondence Principle [1]. This method utilizes a known linearly elastic (time-independent) solution, selected in accordance with the particular problem. The Laplace transform of this solution is then taken to obtain equations of state in the imaginary or s-domain. Next, a substitution is made for the modulus and Poisson's ratio, e.g., $E = s\hat{E}(s)$ and $\nu = s\hat{\nu}(s)$, so that these quantities will become time-dependent terms when the inverse Laplace transform is taken. Following this substitution, the desired quantities are solved for. The solution in the real (time) domain is then generated by taking the inverse Laplace transform of the resulting equation. The limitation in using this solution technique is that Eq. (1) is

now restricted to the linear viscoelastic range since linearly elastic (time-independent) equations are used. This restriction means that the solution is only applicable to a material which is subjected to stresses (or strains) that are sufficiently low. This restriction will be discussed in more detail in the next chapter. Of course, it is possible to find a solution without using the Correspondence Principle, but the differential equations can become cumbersome and extremely difficult to solve.

Integral Representation

Another and more widely used mathematical model is the integral representation [1,3-8]. The advantages of this method over the differential operator form are the relative ease of incorporating measured experimental data and the inclusion of temperature and moisture effects. For these reasons this method has been very appealing to many investigators, and consequently is becoming increasingly popular.

Probably the simplest of the integral representations is the Boltzmann superposition principle [1]. It states that the sum of the strain (stress) outputs caused by several stress (strain) inputs equals the sum of the strain (stress) outputs caused by each stress (strain) input individually. Thus, this representation is restricted to linear viscoelastic behavior, and as discussed before, can only be used when the applied stresses (or strains) are sufficiently low.

A slightly more general integral form was proposed by Leaderman [9]. This representation, referred to as the modified superposition principle, modified the Botlzmann superposition integral slightly so that

stress-dependence could be accounted for. For instance, the creep compliance is usually divided into two portions, i.e., a time-dependent portion and a time-independent portion. While this method allows for the stress-dependence of the time-dependent portion, it does not for the time-independent portion. This method has been useful; however, it lacks the complete generality necessary to describe nonlinear behavior.

Lai and Findley [10] have recently used the modified superposition principle in conjunction with other theories to represent the nonlinear viscoelastic behavior of aluminum. In this study, multiaxial creep tests were run to verify their hybrid theory with experimental data. Excellent-to-fair agreement was obtained between the measured data and the predictions based on constant-stress tests. This relatively new theory, while having potential applications, has not been applied to many different types of materials. Also, it is somewhat empirical in nature and requires several experimental tests to obtain the parameters used in the constitutive equations.

Multiple integral representations [5,6] are very attractive in that they are completely general in nature and can account for any degree of nonlinearity. Hence, they are not limited to any one type or class of materials. The difficulty with this method arises when the material contains a high degree of nonlinearity, making simplification of many terms impossible. Without such simplification, the experimental requirements of this theory are overwhelming and the kernels, i.e., the stress-, temperature-, moisture-dependent parameters in the equations, extremely difficult to evaluate experimentally.

Schapery has developed much simpler, single-integral nonlinear con-

stitutive equations, derived from thermodynamic theory in terms of strains [7] or stresses [8]. These equations contain kernels which are written in terms of linear viscoelastic properties, and are much easier to evaluate than those in the multiple integral forms. In fact, the equations can be reduced to the Boltzmann superposition principle by equating certain terms to one; and experimental determination of the kernels requires only uniaxial creep tests followed by a recovery period.

For these reasons, the theory developed by Schapery [8] was chosen for use in the present analysis. This decision was based upon the facts that the number of tests required to obtain the necessary experimental parameters is minimal, and the generality present in the constitutive equations is adequate to describe nonlinear viscoelastic behavior.

In summary, while the empirical approaches are useful, they do not readily allow for the incorporation of temperature or moisture effects. On the other hand, mechanical models are very difficult if not impossible to visualize for a combined stress state. Differential operator methods rely upon linear solution techniques, which restrict the applicable range of solutions. Multiple integral representations can be extremely difficult to evaluate experimentally.

As will be shown in Chapter IV, it is quite easy to incorporate the measured material parameters into the equations derived by Schapery [8]. Also, it has been demonstrated by Schapery [11] that for a multiaxially stressed material, the properties can be expressed as a function of the local octahedral shear stress in the material. This allows one to completely characterize a material by a series of uniaxial tests. In order to include the effects of temperature and moisture, one need

simply repeat the above uniaxial tests for a range of constant temperature and moisture levels, to determine the dependence of certain constants in the constitutive equations upon these parameters.

A detailed description of the analysis method, utilizing the constitutive equations developed by Schapery [8] in a finite element micromechanical analysis, is given in the following chapter. Succeeding chapters present some numerical results and conclusions based upon these results.

CHAPTER III

ANALYSIS METHOD

A Statement of Linearity

It is important to first examine the concept of linear viscoelastic material behavior and its range of applicability, in order for nonlinear viscoelastic constitutive equations to be meaningful.

While certain materials may behave in a linear manner up to some relatively high stress level (for a fixed temperature, and for certain composites, moisture content), others may be quite nonlinear in that same stress range. In order to differentiate between linear and nonlinear behavior, a definition of linearity is necessary.

There are two criteria which must be met in order for material response to be considered linear [1,12]. The first of these is the property of homogeneity. This property, sometimes referred to as the proportionality property, states that the material response is linearly proportional to the input history. That is, if the stress (input) is doubled, the strain response (output) is correspondingly doubled. This can be written as

$$\varepsilon\{C\sigma(t)\} = C\varepsilon\{\sigma(t)\} \tag{2}$$

where C is any constant, $\sigma(t)$ is the stress input function, and $\varepsilon\{\}$ is the material response based upon the entire history of $\sigma(t)$.

The second criterion is the superposition principle. This property states that the response due to a multistep input of stress with time is identical to the sum of the responses due to individual, independent

stress inputs at corresponding times. This can be written as

$$\varepsilon\{\sigma_1(t) + \sigma_2(t) + \cdots\} = \varepsilon\{\sigma_1(t)\} + \varepsilon\{\sigma_2(t)\} + \cdots \tag{3}$$

where $\sigma_1(t)$, $\sigma_2(t)$, $\cdots$ represent any type of stress input history.

This second property can be demonstrated by an example. Assume three identical pieces of material, each subjected to a different loading history. Specimen A is subjected to a load input described by Figure 2a. Specimen B by that of Figure 2b, and Specimen C by that of Figure 2c. If the material behavior is linear viscoelastic, the superposition principle states that the sum of the strain responses from the loadings shown in Figures 2b and 2c will be identical to the response from the loading shown in Figure 2a.

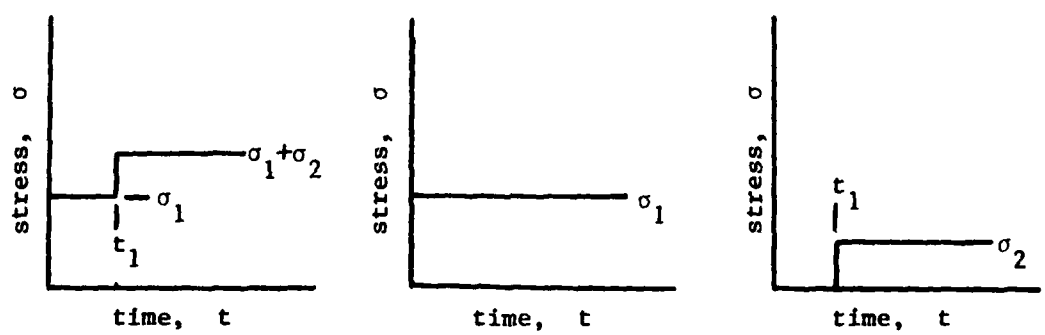

a) Stress input history for Specimen A

b) Stress input history for Specimen B

c) Stress input history for Specimen C

Figure 2. Plots of stress versus time for three different specimens

Many investigators assume linearity if a material satisfies the homogenity principle alone, while in fact the material may be quite nonlinear. It can be shown [1,12] that if the material satisfies the super-

position criterion, it will automatically satisfy homogenity, but the opposite is not true. Thus, if a material is to be examined for linear viscoelastic behavior, the superposition test must be applied.

Constitutive Equations

The single integral nonlinear viscoelastic constitutive equation derived by Schapery [8] for an isotropic material under isothermal conditions and uniaxial loading can be written as

$$\varepsilon(t) = g_0 D_0 \sigma(t) + g_1 \int_{0^-}^{t} \Delta D(\Psi-\Psi') \frac{d[g_2\sigma(t)]}{d\tau'} d\tau' \tag{4}$$

where D_0 is the initial (time-independent) value of the compliance and $\Delta D(\Psi)$ is the transient (time-dependent) value of the compliance. Note that $\Delta D(\Psi)$ is a function of reduced time Ψ. The reduced times are defined as

$$\Psi \equiv \int_0^t \frac{dt'}{a_\sigma} \quad \text{and} \quad \Psi' \equiv \int_0^{\tau'} \frac{dt'}{a_\sigma} . \tag{5}$$

The terms g_0, g_1, g_2, and a_σ are all functions of stress and have certain thermodynamic significance [8]; for example, g_0, g_1, and g_2 reflect stress-dependence on Gibb's free energy while changes in a_σ signify effects of both entropy production and free energy. The term a_σ in Eq. (5) is also a function of temperature, and for certain composites, moisture content. This factor tends to accelerate or decelerate the influence of time, meaning that changes in temperature, moisture, or stress produce the same output of events (with respect to some reference value), but at a faster or slower rate.

Multiaxial relationships as defined by Schapery [8] are somewhat more complicated in that they allow for any degree of coupling between the applied stresses. In the present analysis it is assumed that this coupling (except Poisson effects) is of higher order and is neglected. The constitutive equations used in the present analysis can be written in the simple form

$$\varepsilon_{ij}(t) = D_{ijkl}(t,T,M,\sigma)\sigma_{kl} \tag{6}$$

where $D_{ijkl}(t,T,M,\sigma)$ is the time-dependent nonlinear creep compliance tensor, and is a function of time, temperature, moisture, and applied stress level.

In order to use Eq. (6) in a finite element analysis scheme, it becomes necessary to simplify the convolution integrals (Eq. 4) contained in D_{ijkl}.

In the current analysis an incremental procedure is used, all loading, temperature, and moisture increments being applied in time-independent steps. That is, these increments are assumed to occur instantaneously, and to be held constant during succeeding time steps. Time-dependent response is determined by the application of finite increments of time; no increments of stress, temperature, or moisture are permitted during a time increment. In other words, stress is a constant during any time increment.

By substituting $\sigma(t) = \sigma_a$ (a constant value) and integrating, Eq. (4) yields

$$\varepsilon(t) = [g_0 D_0 + g_1 g_2 \Delta D(t/a_\sigma)]\sigma_a. \tag{7}$$

Details of this integration are presented in Appendix A. Note that ΔD is a function of the ratio of real time to the time shift factor a_σ.

From Eq. (7), the nonlinear creep compliance for a constant applied stress σ_a is defined as

$$\hat{D} = \frac{\varepsilon(t)}{\sigma_a} = g_0 D_0 + g_1 g_2 \, \Delta D(t/a_\sigma) \tag{8}$$

where the term $g_0 D_0$ is the instantaneous (time-independent) portion and the term $g_1 g_2 \, \Delta D(t/a_\sigma)$ is the transient (time-dependent) portion of the creep compliance.

As mentioned previously, no coupling between multiaxial loading is assumed except for Poisson effects. If the material is isotropic (as is typically the case of the matrix material in a composite), the creep compliance tensor in Eq. (6) is simplified to three time-dependent terms, two of which are independent.

The isotropic elastic constitutive equations for multiaxial loading, written in tensorial form, are [13]

$$\varepsilon_{ij} = \frac{(1+\nu)}{E} \sigma_{ij} - \frac{\nu}{E} \sigma_{kk} \delta_{ij} \tag{9}$$

where E is the elastic (Young's) modulus and ν is Poisson's ratio. By using Eq. (8) (for the special case of constant externally applied stresses), making Poisson's ratio time-dependent, and substituting into Eq. (9), the time-dependent constitutive equations (Eqs. 6) become

$$\varepsilon_{ij}(t) = \hat{D}[1 + \nu(t)]\sigma_{ij} - \hat{D}\nu(t)\sigma_{kk}\varepsilon_{ij} \tag{10}$$

Eqs. (10) are valid for any isotropic, time-dependent material subject to a constant externally applied load.

Method of Solution

In the present study, it was desired to model a unidirectional composite material by using a finite element micromechanics analysis. A

finite element grid of the internal structure of a composite is constructed, allowing the examination of the internal stresses in a composite due to a variety of external conditions. The cross-sectional arrangement of fibers in most unidirectional fibrous composites typically tends to be random. However, there is usually little loss of generality in the analysis if some periodicity is assumed, as shown in Figure 3.

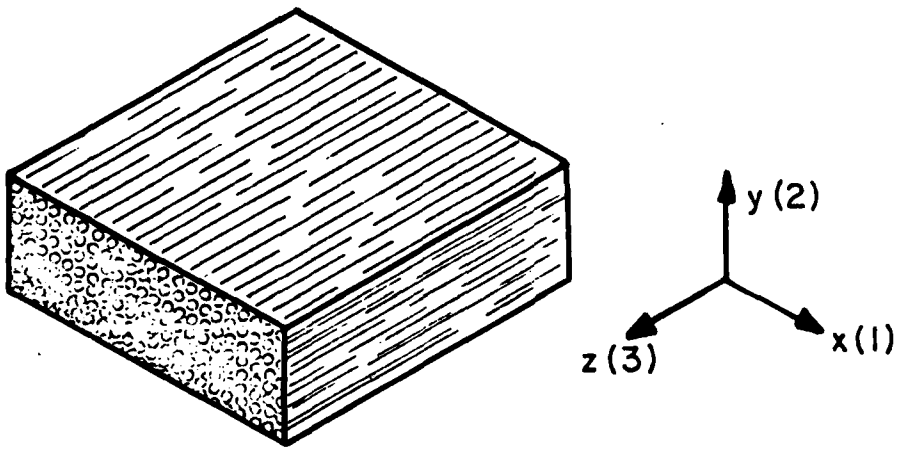

Figure 3. Fiber packing arrangement of a unidirectional composite

A detailed discussion of the various possible types of fiber packing, and the ramifications of assuming each type, are presented by Miller and Adams [14] and will not be repeated here. In the present analysis, the fibers are assumed to be arranged in a rectangular array, as shown in Figure 4a. Since this particular type of packing is assumed, symmetry arguments can be used [14], requiring only one quarter of a fiber to be modeled, as shown in Figure 4b.

In order to simulate a small continuum in a rectangular array of fibers in a composite, certain boundary conditions must be imposed.

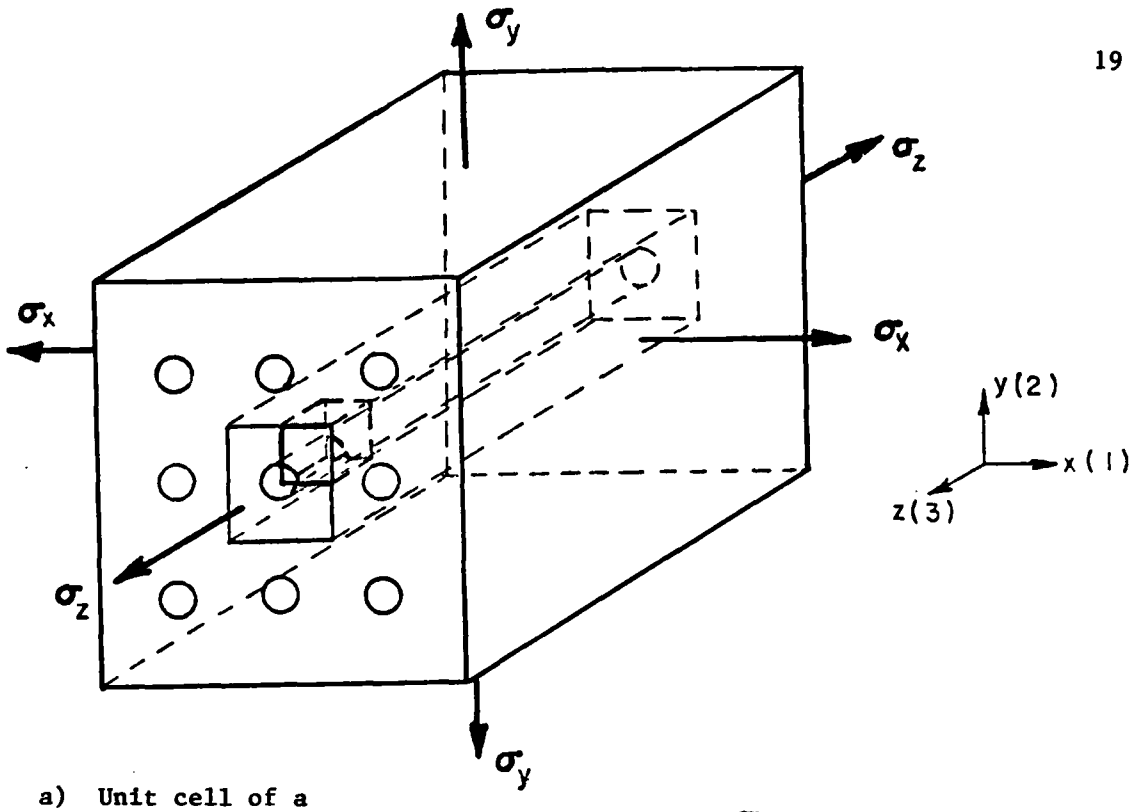

a) Unit cell of a rectangular fiber packing geometry

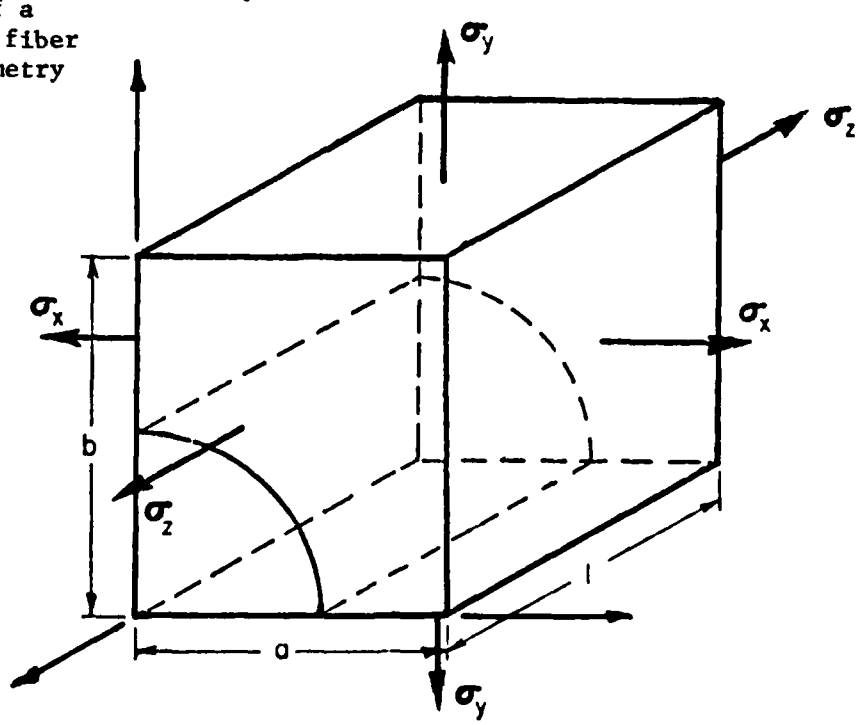

b) Quadrant to be analyzed

Figure 4. Unit cell for the finite element analysis

For descriptive purposes, a coordinate system has been set up in Figure 4b with the origin located in the lower left hand corner. The right hand boundary corresponding to x=a is assumed to displace parallel to the original boundary. That is, all displacements in the x-direction along the boundary x=a are equal in magnitude. Similarly, all displacements in the y-direction along the boundary y=b are considered to be equal. Both of these boundaries, x=a and y=b, are allowed to move freely in the y- and x-directions, respectively. The remaining two boundaries, x=0 and y=0, are assumed to be fixed in the x- and y-directions, respectively; yet they are free to move in the y- and x-directions, respectively. Under the conditions of generalized plane strain, which will be discussed shortly, all out-of-plane normal strains ε_z are assumed to be the same. In other words, all displacements in the z-direction are equal.

The finite element grid used in the present analysis is shown in Figure 5. A detailed description and flow chart of the computer program (including time-dependence) is presented in Appendix B.

In the present micromechanics analysis, thermal- and moisture-dilatational effects are included by means of initial strains [15]. In order for the creep formulation to be compatable with the current program, a scheme including creep strains as initital strains was adopted. The technique for accomplishing this will be briefly explained in the following paragraphs and illustrated in detail by mathematical equations after that.

First, however, it is appropriate to convert Eq. (10), which is in tensorial form, to the notation used by Miller and Adams [14]. The time-dependent constitutive equation for an isotropic material under a

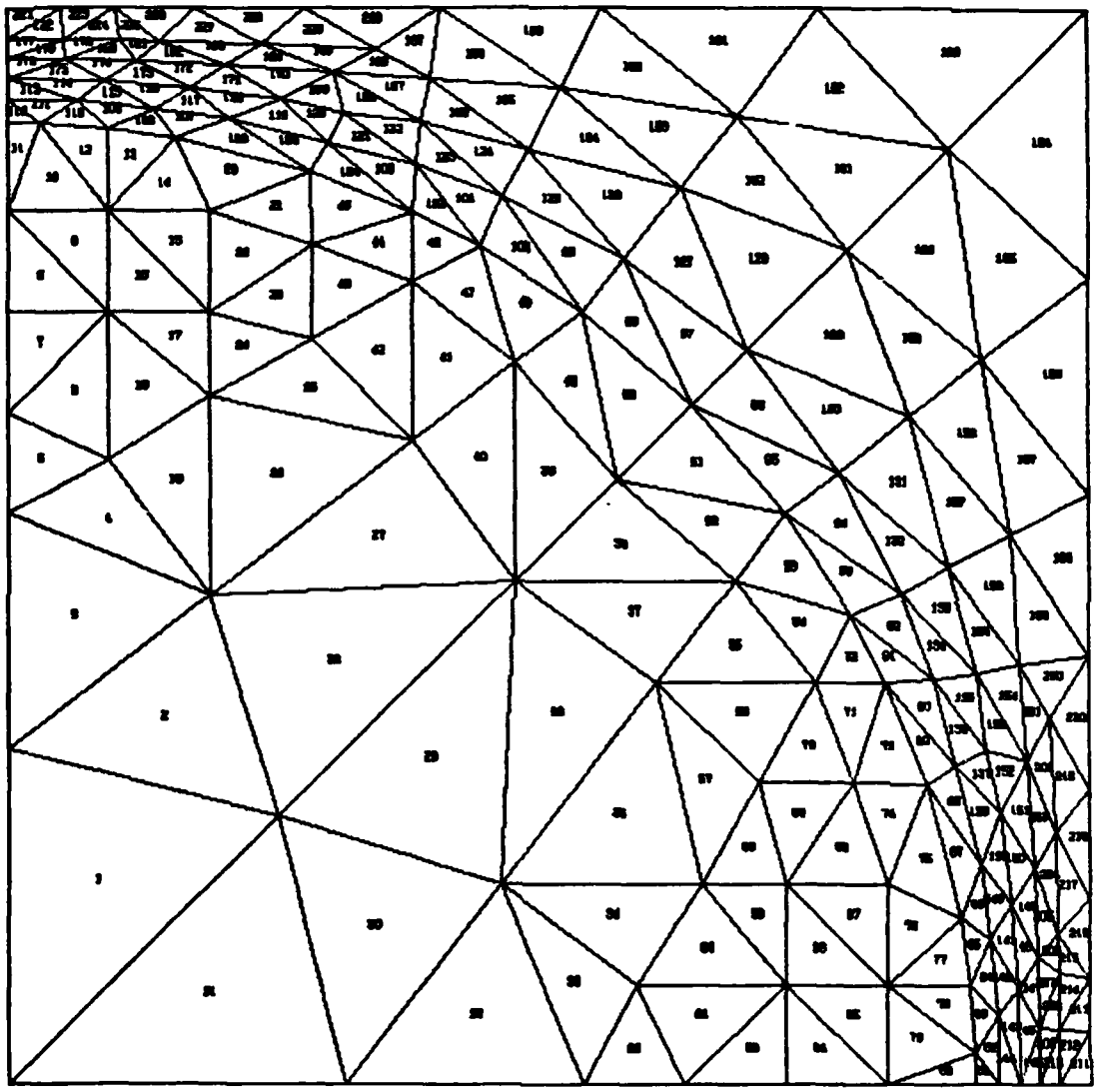

FINITE ELEMENT MESH

63.0 PERCENT FIBER BY VOLUME

Figure 5. The finite element grid used in the present analysis

generalized plane strain formulation for a constant stress state is

$$\begin{Bmatrix} \varepsilon_x(t) \\ \varepsilon_y(t) \\ \gamma_{xy}(t) \\ \varepsilon_z(t) \end{Bmatrix} = \hat{D} \begin{bmatrix} 1 & -\nu(t) & 0 & -\nu(t) \\ & 1 & 0 & -\nu(t) \\ & & 1+\nu(t) & 0 \\ \text{symmetric} & & & 1 \end{bmatrix} \begin{Bmatrix} \sigma_x \\ \sigma_y \\ \tau_{xy} \\ \sigma_z \end{Bmatrix} \quad (11)$$

Under conditions of generalized plane strain, the normal strain ε_z is a constant over the entire model (Figure 5), as previously mentioned, and the shear strains γ_{xz} and γ_{yz} are assumed zero. In Eq. (11), $\hat{D}$ is given by Eq. (8) and $\nu(t)$ is the time-dependent Poisson's ratio.

In the finite element analysis, nodal point forces are generated due to the creep strains. The magnitudes of these induced nodal forces are a function of the geometry of an element and the time-dependent material properties of that element. These node point forces are calculated using Eq. (11) and the elemental stresses at the beginning of the time increment. Since this is an incremental finite element program, care must be taken to insure that only the incremental and not the total creep strains are calculated. To accomplish this, Eq. (11) is differentiated with respect to time and evaluated at the time corresponding to the midpoint of the time increment. By assuming the elemental stresses to remain constant throughout the time interval, and multiplying through by the time increment Δt, a linear approximation of the incremental creep strain for that time increment is obtained. For this reason it is necessary to keep the time increments, which are input into the analysis, very small when the value of the creep compliance is changing rapidly. For a constant externally applied stress, this rapid change corresponds to the initial (or primary) part of the creep curve. Thus, it is

necessary to keep the time increments small just after a load has been applied or incremented. The magnitudes of these initial time increments will of course depend upon the viscoelastic properties or the type of material being modeled. Polymers may require many small increments (of minutes or fractions of minutes), while steels may require only a few increments (of minutes).

Details of the strain-displacement relations, shape functions, and basic finite element formulation for the time-independent formulation are given by Miller and Adams [14] and will not be repeated here. Rather, only the equations which deal with the time-dependent finite element formulation will be presented.

The equation which relates nodal forces to displacements can be written as [14]

$$\{\dot{F}\}_i = [K]_i\{\dot{\delta}\}_i + \{\dot{F}_{\varepsilon_0}\}_i \tag{12}$$

where $\{\dot{F}\}_i$ is the incremental nodal force vector of the ith element due to externally applied loads, $\{\dot{F}_{\varepsilon_0}\}_i$ is the incremental nodal force vector due to temperature, moisture, and time changes, $[K]_i$ is the element stiffness matrix, and $\{\dot{\delta}\}_i$ is the incremental element nodal displacement vector.

During a time increment, $\{\dot{F}\}_i$ must be zero since loads can only be applied during time-independent increments. Also, no changes in temperature or moisture content can occur. Thus, $\{\dot{F}_{\varepsilon_0}\}_i$ is the incremental nodal force due to incremental strain changes caused by creep or the time-dependent properties only.

The element stiffness matrix is defined as [14]

$$[K]_i^T = [B]_i^T[D]_i[B]_i t_i \Delta_i \tag{13}$$

where $[B]_i$, sometimes referred to as the shape matrix, relates the node point displacements and the element strains, t_i is the thickness of the element in the out-of-plane direction (which is unity in the present analysis), and Δ_i is the cross-sectional area of the element. The elemental material properties matrix $[D]_i$ is found by evaluating the time-dependent parameters such as $\hat{D}$ (see Eq. 8) and $\nu(t)$ at the time corresponding to the midpoint of the time increment, and then substituting into the following matrix for an isotropic material under generalized plane strain conditions:

$$[D] = \frac{(1-\nu^*)}{D^*(1+\nu^*)\ (1-2\nu^*)} \begin{bmatrix} 1 & \nu^*/(1-\nu^*) & 0 & \nu^*/(1-\nu^*) \\ & 1 & 0 & \nu^*/(1-\nu^*) \\ & & [(1-2\nu^*)/2(1-\nu^*)] & 0 \\ \text{symmetric} & & & 1 \end{bmatrix} \tag{14}$$

The terms D^* and ν^* are the creep compliance and the time-dependent Poisson's ratio, respectively, evaluated at the particular time defined above.

Using Eq. (12) and the finite element analysis, the incremental displacements can now be solved for if the incremental forces $\{\dot{F}_{\varepsilon_0}\}_i$ due to the creep strains are known. The expression for $\{\dot{F}_{\varepsilon_0}\}_i$ is [14]

$$\{\dot{F}_{\varepsilon_0}\}_i = [B]_i^T\ [D]\{\dot{\varepsilon}_0\}t_i\Delta_i \tag{15}$$

where $\{\dot{\varepsilon}_0\}$ is the incremental creep strain.

Evaluation of $\{\dot{\varepsilon}_0\}$ for an element is accomplished by the use of Eqs. (11) and the element stresses at the beginning of the increment. To get $\{\dot{\varepsilon}_0\}$, the derivative with respect to time is taken of Eqs. (11) and all of the time-dependent properties evaluated at the time corresponding to the midpoint of the time interval. Using the first of Eqs.

(11) as an example, i.e.,

$$\varepsilon_x = \hat{D}\sigma_x - \hat{D}\nu(t)\sigma_y - \hat{D}\nu(t)\sigma_z \tag{16}$$

its derivative with respect to time is

$$\begin{aligned}\frac{d}{dt}(\varepsilon_x) = \frac{d}{dt}(\hat{D})\sigma_x - \{[\frac{d}{dt}(\hat{D})]\nu(t) + \\ [\frac{d}{dt}\nu(t)]\hat{D}\}\sigma_y - \{[\frac{d}{dt}(\hat{D})]\nu(t) + [\frac{d}{dt}\nu(t)]\hat{D}\}\sigma_z\end{aligned} \tag{17}$$

It has been determined by several investigators [12,16,17] that Poisson's ratio is time-independent or a very weak function of time. For this reason, it was decided that certain terms in Eq. (17) could be considered higher order effects and therefore be dropped from the equations, viz., the terms involving time rates of change of Poisson's ratio. With this simplification, Eq. (17) becomes

$$\frac{d}{dt}(\varepsilon_x) = \frac{d}{dt}(\hat{D})\sigma_x - [\frac{d}{dt}(\hat{D})]\nu(t)\sigma_y - [\frac{d}{dt}(\hat{D})]\nu(t)\sigma_z. \tag{18}$$

The terms g_0, D_0, g_1, g_2, and a_σ in the nonlinear creep compliance $\hat{D}$ (Eq. 8), are functions of stress, temperature and moisture only, and are required to be constant throughout a time increment in this analysis. Thus, when Eq. (18) is evaluated at a time corresponding to the midpoint of the time increment and multiplied through by Δt, a linear approximation of the incremental creep strain ε_x is obtained.

A similar argument is applied to the relations for ε_y, ε_z, and γ_{xy}; the resulting equations are given below.

$$\begin{aligned}\frac{d}{dt}(\varepsilon_y) &= -[\frac{d}{dt}(\hat{D})]\nu(t)\sigma_x + \frac{d}{dt}(\hat{D})\sigma_y - [\frac{d}{dt}(\hat{D})]\nu(t)\sigma_z \\ \frac{d}{dt}(\varepsilon_z) &= -[\frac{d}{dt}(\hat{D})]\nu(t)\sigma_x - [\frac{d}{dt}(\hat{D})]\nu(t)\sigma_y + \frac{d}{dt}(\hat{D})\sigma_z \\ \frac{d}{dt}(\gamma_{xy}) &= [\frac{d}{dt}(\hat{D})][1+\nu(t)]\tau_{xy}\end{aligned} \tag{19}$$

Once these incremental values of strain are known, the program solves for the incremental node point displacements, which are later used to find the new values for elemental stress. When this has been accomplished, the program returns for the next increment of time, temperature, moisture, or load.

Multiple Step Loading

For a two-step loading, as shown in Figure 6, the

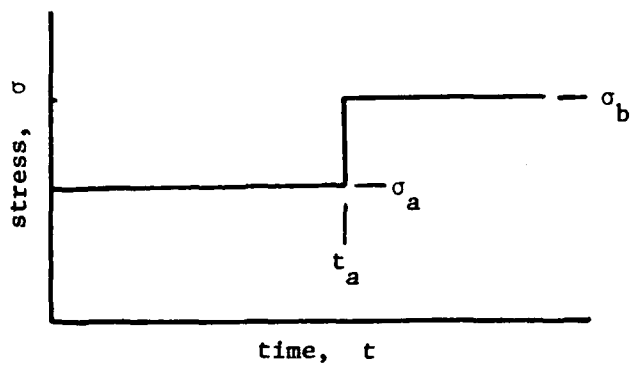

Figure 6. Plot of stress versus time for a two-step input

constitutive equation is given by

$$\varepsilon(t) = g_0^b D_0 \sigma_b + g_1^b g_2^b \Delta D\left(\frac{t-t_a}{a_\sigma^b}\right)\sigma_b - g_1^b g_2^a \Delta D\left(\frac{t-t_a}{a_\sigma^b}\right)\sigma_a + g_1^b g_2^a \Delta D\left(\frac{t_a}{a_\sigma^a} + \frac{t-t_a}{a_\sigma^b}\right)\sigma_a \tag{20}$$

for time $t>t_a$. Details of the derivation of Eq. (20) are presented by Schapery [18] and also in Appendix A. The superscripts and subscripts a and b are used to denote which constants, stresses, and times are

associated with each stress level. It is important to note the two additional terms which appear in Eq. (20), that did not appear in Eq. (7). These two terms represent the application of a $-\sigma_a$ stress and a $+\sigma_b$ stress, beginning at time $t=t_a$. It is necessary to include the two additional terms due to the nonlinear dependence of certain constants in Eq. (8) upon the applied stress level. If the material behavior were linearly viscoelastic, it would be necessary to add only one term to Eq. (7), viz., a term involving a stress increment of the difference between the two stress inputs $(\sigma_b-\sigma_a)$.

While other authors [19,20] have developed recursive relationships which require integration of the viscoelastic constitutive relations over the current time increment only, no feasable method of keeping track of the stress history was discovered which was compatable with the current finite element formulation. This means that individual histories for each load step had to be kept track of in the current analysis and the contribution of each history solved for separately. For example, a two-step loading shown in Figure 6 requires the program to solve for three contributions of the total creep strain for time $t>t_a$; the strain due to the initial application of $+\sigma_a$ at time $t=0$, the strain due to a pseudo application of $-\sigma_a$ at time $t=t_a$, and the strain due to a pseudo application of $+\sigma_b$ at time $t=t_a$. Each additional step in stress would require two extra solutions. While the program is capable of any number of step loadings, it can realistically model only a finite number of step loadings due to the increase of computer time necessary to solve additional increments. Using a CDC Cyber 760 computer, approximately 2-3 seconds of computer time are required to solve one stress increment using the

finite element mesh shown in Figure 5. (This mesh has a bandwidth of 75.) Thus, for times $t>t_a$, approximately 6-9 seconds of computer time are required for each time increment.

While the formulation by Haisler and Saunders [19,20] avoids this difficulty, it requires the use of an iterative scheme and hence cannot readily model materials with "flat" stress-strain curves such as aluminum [21]. Thus, the micromechanical modeling of a composite such as boron/aluminum would be very difficult. Also, iterative schemes can require large amounts of computer time to converge upon a solution.

The intent of the present study was not to analyze the relative advantages and disadvantages of a particular finite element method. Rather, the goal was to use an existing finite element micromechanics program and incorporate time-dependent effects. In this chapter, the viscoelastic constitutive equations were presented and a scheme for incorporating these equations into a finite element analysis was devised. However, numerical values for the time-dependent parameters must be known. In the following chapter, a brief experimental program is described which was conducted to determine these parameters.

CHAPTER IV

EXPERIMENTAL CHARACTERIZATION

In order to utilize the constitutive equations presented in the previous chapter, a series of creep-recovery tests is necessary. To include the dependence of the kernels in the equations upon temperature and moisture, a full experimental program of isothermal, constant humidity, and constant stress tests must be conducted. A method of evaluating all parameters given in Eqs. (4) and (5) has been developed by Lou and Schapery [11] and will be demonstrated in this chapter.

Test Method

In the present study, a brief experimental program was undertaken in order to evaluate the creep constants which were needed as input to the finite element program. This experimental program was not intended to completely evaluate the viscoelastic parameters necessary for the constitutive equations. Rather, the goal was to obtain approximations of the numerical values for the kernels to be used as input to the computer program. A series of compression creep-recovery tests were run on Hercules 3501-6 epoxy resin [22] test specimens. A compression test was selected to avoid the gripping problem usually associated with tensile tests of neat (unreinforced) resin materials [12].

For this program, a total of fifteen specimens were tested at five different stress levels (i.e., three specimens at each stress level

selected). All tests were conducted at room temperature (21°C) and ambient humidity.

The specimens were fabricated from ½-inch diameter rods cast in a split steel mold. The rods, molded in approximately 6-inch lengths, were cut into 1½-inch long test specimens. The ends were then ground flat using a surface grinder to insure that they were smooth and parallel to each other. Details of the fabrication and curing process may be found in Reference [23].

An Instron Model 1321 servohydraulic testing machine was used to apply and maintain a constant load on the rods. Strain was measured using a ½-inch gage length extensometer and all data were taken using a Hewlett-Packard 21MX Series E minicomputer. The values of load, strain, and time were taken just prior to and just after application of the load. The total time to apply load for all tests was about four seconds. After application of the load, values of load, strain, and time were recorded each minute for ten minutes. After that time, data were recorded every five minutes. The creep tests lasted for approximately one hour, after which time the computer automatically removed the load while continuing to record the load, strain, and time. At this point data were taken at one minute intervals for ten minutes. After ten minutes, data were taken every five minutes for another two hours.

This procedure was used for each of five different compressive stress levels, i.e., 2000, 6000, 8000, 16,000, and 20,000 psi. The tests conducted at 2000 psi were checked for linearity and found to satisfy the principle of superposition as discussed in Chapter III.

Experimental Results

Plots of the data taken are shown in Appendix C. These plots are actual unretouched data acquired by the minicomputer.

The technique developed by Lou and Schapery [11], which reduces the data presented in Appendix C, makes use of a power law representation to describe the nonlinear creep compliance expressed by Eq. (8). This method utilizes recovery data to determine the exponent used in the power law. A constitutive equation describing the recovery portion of the creep curve is derived in Appendix A and the equations are repeated here for convenience. For the stress history described in Figure 7, the recovery strain is

$$\varepsilon_r(t) = \frac{\Delta\varepsilon_a}{g_1}\left[(1 + a_\sigma\lambda)^n - (a_\sigma\lambda)^n\right] \tag{21}$$

where

$$\lambda \equiv \frac{t-t_a}{t_a} \tag{22}$$

and

$$\Delta\varepsilon_a = \varepsilon(t_a) - \varepsilon_0 = g_1 g_2 C t_a^n \sigma_a \tag{23}$$

for time $t>t_a$. The term C is a constant from the power law (see Appendix A) and the term ε_0 in Eq. (23) is the initial or time-independent value of strain which occurs at time t=0.

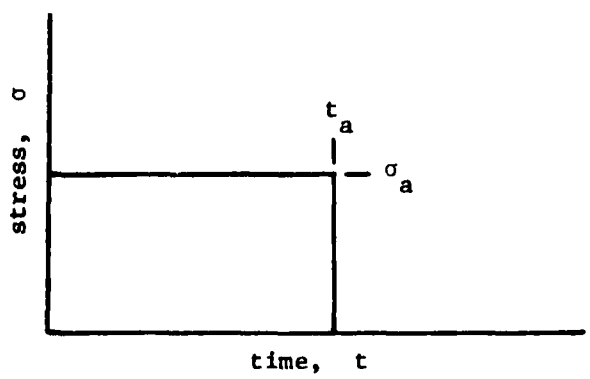

Figure 7. Plot of stress versus time for a creep-recovery test

The first step in the evaluation of the creep parameters is to determine the exponent n. This may be found by plotting the equation

$$\varepsilon_r(t) = (1 + \lambda)^n - (\lambda)^n \tag{24}$$

on log-log paper for several values of n (usually $0<n<0.5$) and overlaying these curves on the experimental recovery curves. Equation (24) is generated by setting $\Delta\varepsilon_a$, g_1, and a_σ equal to one in Eq. (21). This is done since only the exponent is being determined at this time. The best fit to all of the data will determine a value for n.

Since the tests run at 2000 psi satisfied the superposition principle, the response was linear viscoelastic and all of the terms g_0, g_1, g_2, and a_σ were equal to one. For this reascn, these particular curves were averaged and used as a reference curve for all other stress levels tested. By using a reference curve, the values of g_0, g_1, g_2, and a_σ as a function of stress were determined.

To make the recovery curves described by Eq. (21) match the reference curve (at 2000 psi), a certain amount of horizontal and vertical shifting is necessary. The amount of horizontal shifting required determines the value for a_σ. If $a_\sigma>1$ the data must be shifted to the right, and if $a_\sigma<1$ the data must be shifted to the left. The amount of vertical shifting determines the value of $\Delta\varepsilon_a/g_1$. If $\Delta\varepsilon_a/g_1>1$ the data must be shifted downward; if $\Delta\varepsilon_a/g_1<1$ the data must be shifted upward.

Once the values for a_σ and $\Delta\varepsilon_a/g_1$ have been determined, the value of g_1 may be calculated using the first part of Eq. (23) to get $\Delta\varepsilon_a$. Plots of a_σ and g_1 versus stress for Hercules 3501-6 epoxy resin are shown in Figures 8 and 9, respectively. Note that these plots show abrupt changes around 2000 psi. This was intentionally done to force these constants to

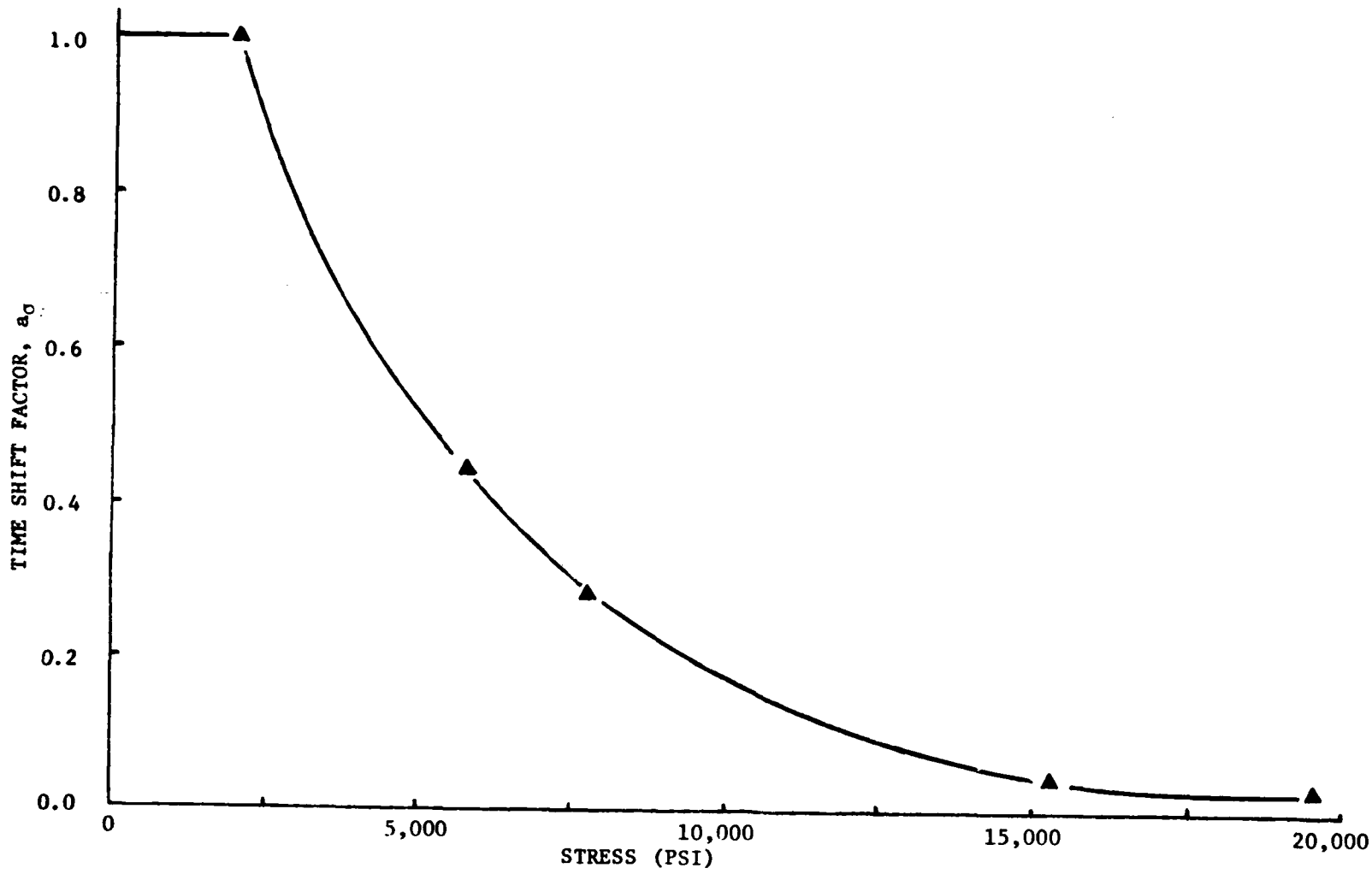

Figure 8. Plot of a_σ versus stress for Hercules 3501-6 epoxy resin

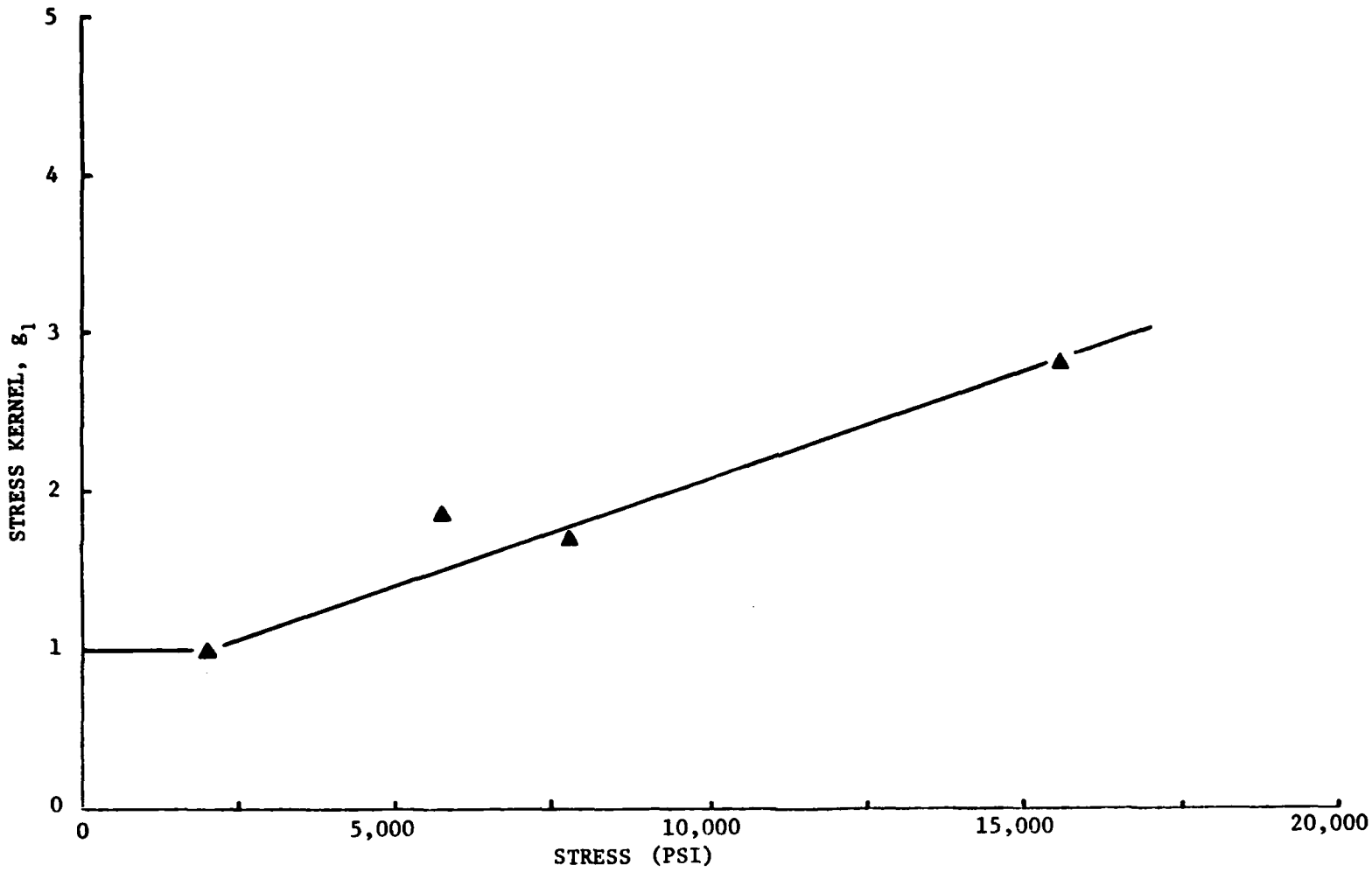

Figure 9. Plot of g_1 versus stress for Hercules 3501-6 epoxy resin

have a value of one, during the range of linear viscoelastic behavior. It would not be meaningful for these constants to have values other than one in this range. To determine exactly how the curves transition from linear to nonlinear viscoelasticity, more tests need to be run at these stress levels.

The only remaining creep constants which need to be determined are g_0 and g_2. Values of the product g_0D_0 in Eq. (8) are easily calculated since they are merely the ratio of initial strain to the applied stress (ε_0/σ_a). A plot of the relationship of the product g_0D_0 to stress is shown in Figure 10.

The functional relationship of g_2 with stress was determined by utilizing a power law in Eq. (7). Substitution of the power law Eq. (A-15) into Eq. (7) gives

$$\varepsilon(t) = g_0D_0\sigma_a + Cg_1g_2\left(\frac{t}{a_\sigma}\right)^n\sigma_a. \tag{25}$$

Using Eq. (25) and the parameters g_0D_0, g_1, and a_σ just determined from the creep data, the product Cg_2 may be determined for each value of stress. During the linear viscoelastic range (up to approximately 2000 psi in the present case), g_2 is equal to one and C is equal to the net time-dependent (transient) portion of the creep compliance at unit time. By dividing through by C for each product Cg_2 determined, the term g_2 as a function of stress is obtained. A plot of g_2 versus stress for Hercules 3501-6 epoxy resin is as shown in Figure 11.

In Appendix C, Figures C-11 through C-15 show actual data (indicated by the stars) plotted against the predicted creep response, using the creep parameters just calculated. There is excellent agreement between the data and the prediction, as expected.

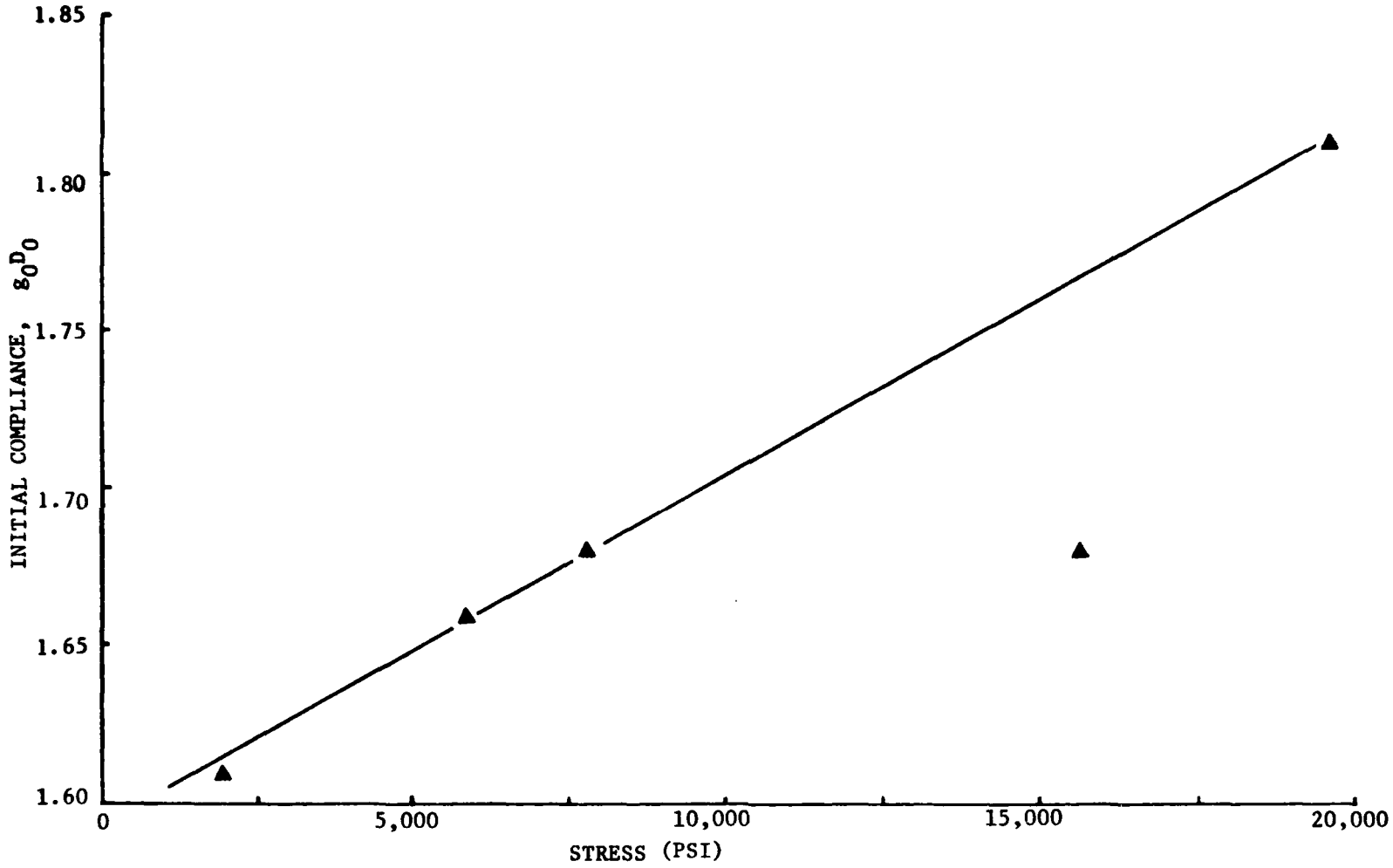

Figure 10. Plot of g_0D_0 versus stress for Hercules 3501-6 epoxy resin

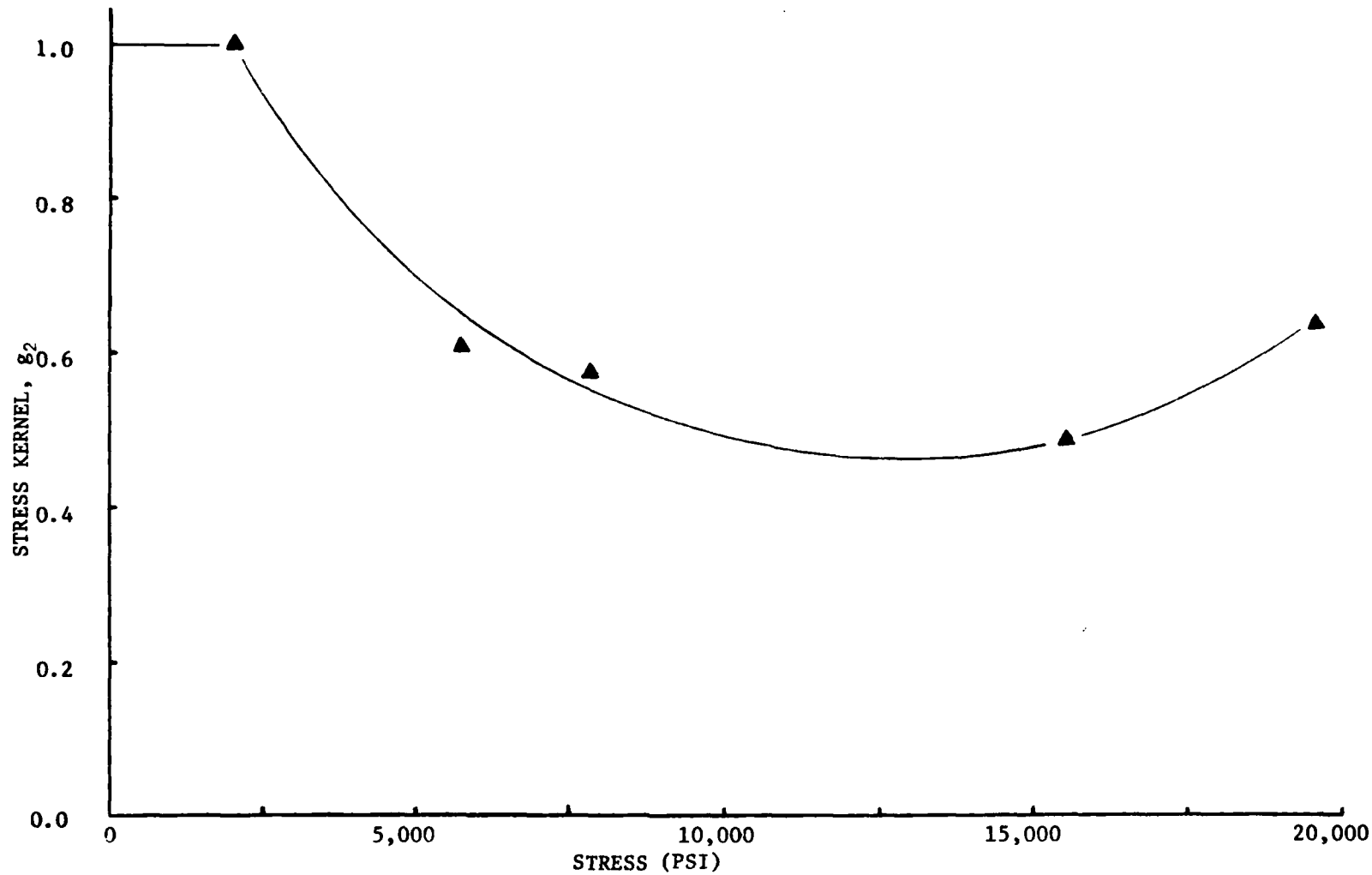

Figure 11. Plot of g_2 versus stress for Hercules 3501-6 epoxy resin

Some difficulty was encountered when shifting of the recovery data was done to obtain the terms a_σ and $\Delta\varepsilon_a/g_1$. For this reason, the data plotted in Figures 8 through 11 may be questionable. In particular, the amount of shifting done for each test was not always consistent. For some of the tests, a specific amount of horizontal and vertical shifting was done, while for others (subjected to the same stress level) only vertical shifting was necessary. Thus, the results plotted in Figures 8 and 9 have been obtained through a degree of estimation. Agreement between the data and the predictions presented in Appendix C for creep is good since the final parameter g_2 is found by using creep data and Eq. (25), with the values determined for D_0g_0, g_1, and a_σ. The problem of a poor fit of the predictions to the data would arise only when the kernels appear individually and not together as the product $g_1g_2/(a_\sigma)^n$ in Eq. (25). One such instance would be during recovery. In Eq. (21), the kernel g_1 cancels with g_1 contained in the term $\Delta\varepsilon_a$ and hence does not appear in the equation. This problem will be exemplified in the next chapter by recovery predictions made using these kernels. To avoid this difficulty, data should be sampled more often during both the creep and recovery tests. Also, it has been recommended in the literature [11,12] that a curve be drawn through the data points and used for shifting instead of using the actual data points as was done here. This helps to smooth out and also eliminate extaneous data points. By following these suggestions it is expected that more accurate values for g_0, g_1, g_2, and a_σ will be obtained.

CHAPTER V

NUMERICAL EXAMPLES

Several examples are presented in this chapter to demonstrate the capability of the analysis. A short description of each load case is presented, followed by a series of contour plots illustrating the internal stress state of the composite. All examples use the finite element mesh shown in Figure 5, which corresponds to a 63 percent fiber volume, except where noted.

The computer program was first checked out by applying a uniaxial tensile load to a model made up entirely of resin. Two independent sets of data, one generated in this study for Hercules 3501-6 epoxy resin and another generated by Beckwith [12] for Shell 58-68R epoxy resin, were used as input to the program. Temperature and moisture levels were held constant during each simulation so that the solution generated by the computer program could be compared to the input data.

The next check was performed by modeling an actual composite subjected to a uniaxial transverse normal load. The results predicted by the program were compared with actual data generated by Beckwith [12] and Irion [24] using the Shell and Hercules resin systems, respectively.

Once verifications with simple uniaxial creep tests were demonstrated, the effect of fiber volume was briefly examined. Next, several runs were made to demonstrate that the internal stress behavior of a composite during cooldown can be predicted. Finally, uniaxial cycling and multiaxial load tests were simulated and the internal stress states of each

composite as a function of time were examined.

The analysis is capable of handling the effects of moisture; however, no examples are presented in this chapter since there were no experimental data available concerning this effect. The absorption of moisture into a composite has the same general effect as a temperature increase, i.e., both have a similar influence on the time shift factor a_σ. Specifically, the absorption of moisture tends to make a composite creep more. As mentioned in Chapter IV, to include the effects of moisture, several creep-recovery tests at various moisture levels for several values of stress must be run.

Creep of Epoxy Resin

Using the data generated by Beckwith [12] for the Shell epoxy resin, a uniaxial load was applied to a neat epoxy resin model. This model was made by specifying all elements in the finite element mesh shown in Figure 5 to have neat resin properties. A stress of 1000 psi in the x-direction (see Figure 4b) was applied for 2.1 hours and then removed, after which recovery was determined for another 2.1 hours. This procedure was repeated for three separate constant temperature levels, i.e., -6.7°C (20°F), 23.9°C (75°F), and 60.0°C (140°F). During each simulation, the moisture content was assumed to be zero.

Results of the comparison are shown in Figures 12 and 13. The actual input response is represented by the solid lines while the predictions made using the finite element analysis are shown by the symbols. To obtain the solid lines or the input (expected) response, the constitutive equation for each test condition was written and then plotted for

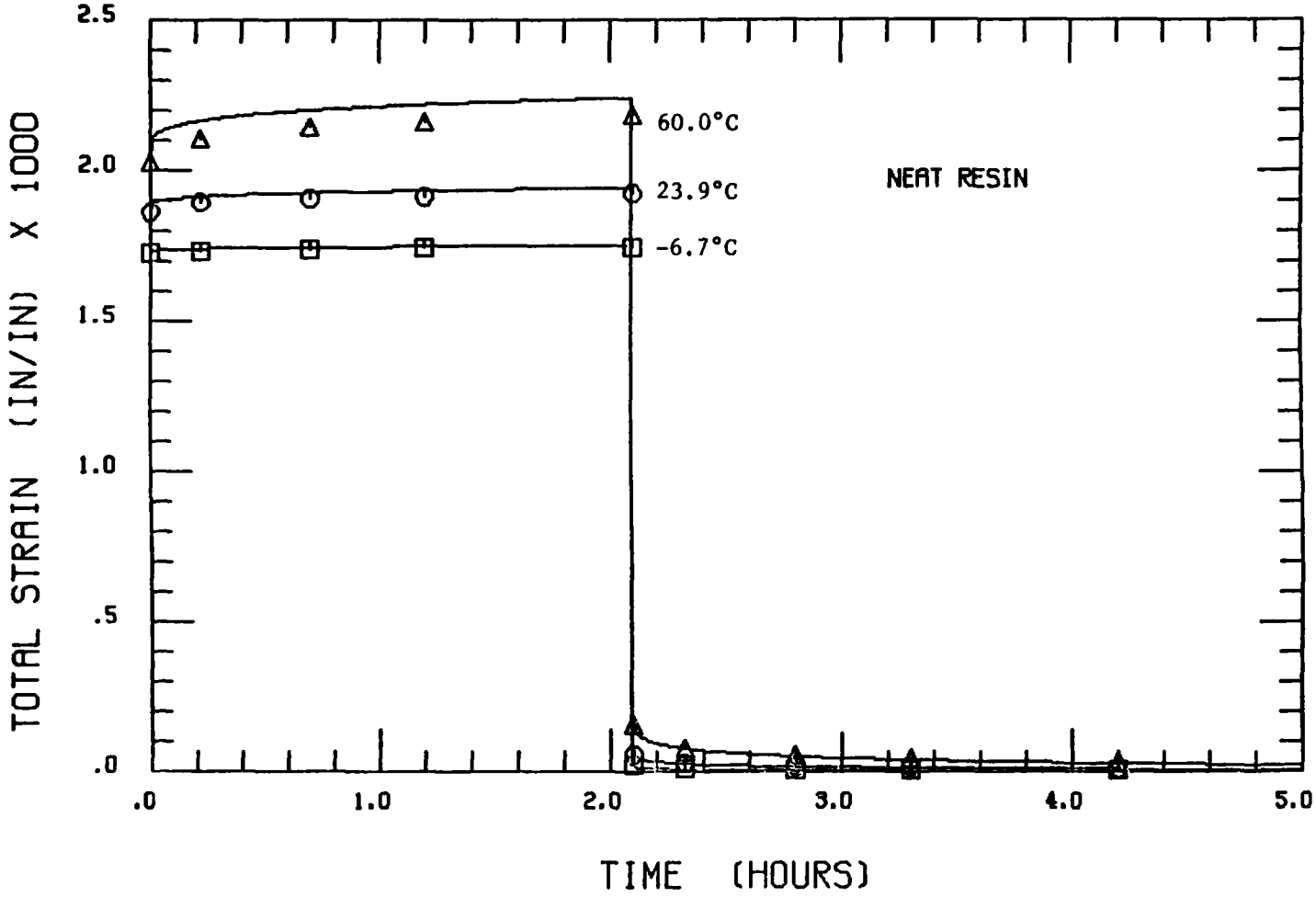

Figure 12. Plots of strain versus time for Shell 58-68R epoxy resin subject to a 2.1 hour creep and a 2.1 hour recovery test. Predicted values are shown by symbols while the solid lines represent the actual experimental response [12].

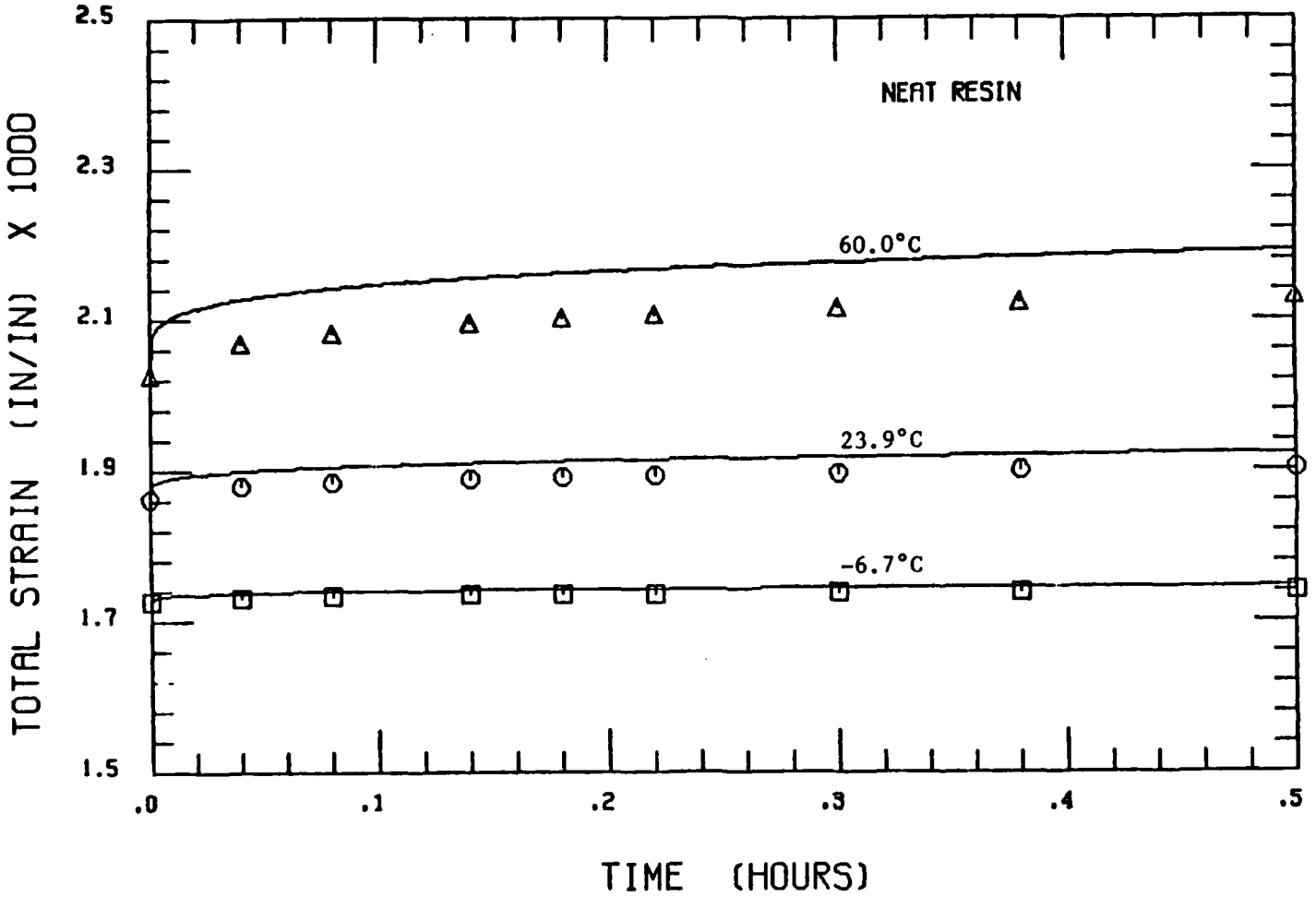

Figure 13. Expanded scale plots of strain versus time for Shell 58-68R epoxy resin subject to a 2.1 hour creep and a 2.1 hour recovery test. Predicted values are shown by symbols while the solid lines represent the actual experimental response [12].

a total time of five hours. This was easily done since the moisture, temperature, and stress levels were held constant throughout the tests (except during recovery, where the stress was removed). In Figure 13 the strain scale has been expanded, greatly exaggerating the error between the predictions (symbols) and the expected response (solid lines). By closely examining Figure 13, it can be seen that the agreement between the predictions and the expected response is excellent; the maximum error for the highest temperature (60.0°C) is less than 3 percent. To obtain this close agreement at the high temperature, several time increments of one minute were used at the beginning of the creep and recovery portions of the test. It was necessary to use these small increments since the effects of creep are magnified by higher temperature, moisture, or stress levels. In these cases, the initial or primary portion of the creep curve is changing very rapidly. Thus, it is necessary to keep the time increments small just after the load has been changed or incremented.

The time increments used in each test in this example were selected somewhat arbitrarily. It is clear that a certain amount of care is required when selecting the time increments. While the 60°C test required several one minute increments, the -6.7°C test did not. Of course it is always possible to use more and smaller time increments for any particular loading case. However, the additional accuracy achieved requires additional computer time and may or may not be cost effective. Finer increments than those used in Figure 12 were tried, but no significant improvement in accuracy was obtained.

Uniaxial creep-recovery tests were also simulated for the Hercules epoxy resin data generated in the present study. Since the effects of

temperature and the parameters necessary to describe such effects were not investigated, two-hour creep followed by two-hour recovery tests at various stress levels were modeled. Results for 2000 psi, 8000 psi, and 19,000 psi uniaxial tensile simulations at 21.0°C and zero moisture are shown in Figures D-1 through D-6 in Appendix D. Figures D-2, D-4, and D-6 show the creep portion of the curves with expanded strain scales. The predictions (symbols) compare well with the experimentally measured response (solid lines). For all cases, the error is less than 6 percent and the general shape of the predicted response matches the experimental response quite well. Closer examination of these figures reveals that the error present is essentially constant for all times, meaning that the error was generated during the first few time increments. Again, to keep this error small, as shown in these figures, the time increments were judiciously chosen for the primary stages of creep (when the load had just been changed), especially at higher stress levels. As expected, the error increases with higher applied stresses.

While the recovery predictions for all simulations (including the Beckwith data) matched the expected response quite well, there was considerable error for the recovery predictions for the Hercules resin subject to 19,000 psi (see Figure D-5). No reasonable explanation for this anomaly can be offered at this time.

Stress contour plots for the above simulation have not been presented since the resin is obviously in a uniform stress state. Element stresses were checked immediately after application of a load and at various times later to make certain that there were no changes. Also, the element stresses were checked to make certain they were zero upon removal of the

load and at various times following.

Creep of a Composite

Using the data for the Shell epoxy resin generated by Beckwith [12] and the properties for S2 glass given in Table I, two-hour creep and two-hour recovery tests for a 1000 psi transverse normal stress were simulated. The assumed properties of the fibers were based upon available experimental data as referenced. Since the transverse properties of the fibers (i.e., E_t, $\nu_{\ell t}$, ν_{tt}, α_t) are not well-characterized, their values are estimates based upon the existing literature. In all of the following composite models, the fibers are assumed to behave time-independently. That is, the fibers themselves do not show any viscoelastic behavior. Longitudinal creep data generated by Beckwith [12] and Irion [24] for unidirectional glass and graphite composites support this assumption.

The results of each simulation are compared with those for actual composite specimens [12] subject to three different constant temperatures of -6.7°C (20°F), 23.9°C (75°F), and 60°C (140°F). They are plotted in Figure 14. The moisture content was taken to be zero for all simulations since no data were available [12] to account for this effect. While Beckwith [12] used S-901 glass fibers instead of S2 glass, the difference between the fiber properties should not affect the results significantly, as will be explained shortly.

The agreement for low temperatures is excellent; however, there is considerable error at the high temperature of 60.0°C. The time increments were the same as the ones used previously for the epoxy resin modeling. While this could be responsible for some of the error (see

TABLE I

TIME-INDEPENDENT CONSTITUENT MATERIAL PROPERTIES

Material	Longitudinal Modulus (Msi) E_ℓ	Transverse Modulus (Msi) E_t	Major Poisson's Ratio* $\nu_{\ell t}$	In-Plane Poisson's Ratio* ν_{tt}	Coefficient of Thermal Expansion (10^{-6}/°C) Longitudinal α_ℓ	Coefficient of Thermal Expansion (10^{-6}/°C) Transverse α_t	Coefficient of Moisture Expansion (10^{-3}/%M) Longitudinal β_ℓ	Coefficient of Moisture Expansion (10^{-3}/%M) Transverse β_t
S2 Glass Fiber [25]	12.6	12.6	0.22	0.22	5	5	0	0
AS Graphite Fiber [26]	32.0	2.0*	0.20	0.25	-0.36	18	0	0
3501-6 Epoxy Resin [27]	0.6	0.6	0.34	0.34	40	40	2	2

*Estimated Values [28]

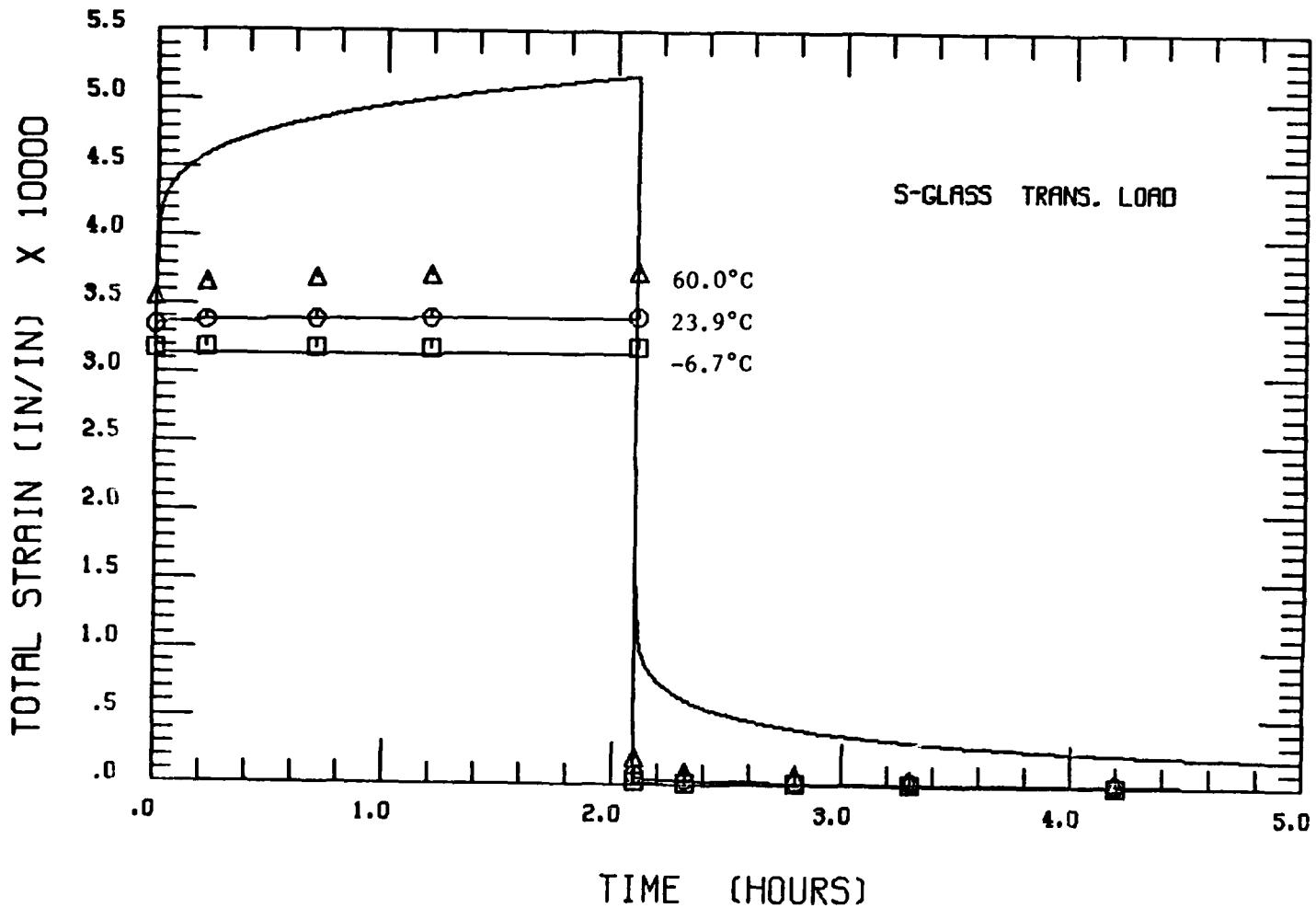

Figure 14. Plot of strain versus time for S2 glass composite (using Shell 58-68R epoxy resin) subject to a 2.1 hour creep and a 2.1 hour recovery test. Predicted values are shown by the symbols while the solid lines represent the experimental response [12].

Figure 13), it certainly is not the sole cause. Since there was reasonably good agreement for the neat resin at the high temperature, and since transverse normal loading is a matrix-dominated response, it would be reasonable to assume that the results presented in [12] for this particular temperature are questionable. That is, during a transverse loading, the fiber properties do not play a significant role in the strain response of the composite. While the fiber volume content does affect the response, as will be demonstrated later, the time-indpendent modulus and transverse strain are typically characteristic of the type of matrix material used (in this case epoxy resin). Thus, it is logical to assume that the transverse time-dependent (creep) response of a composite will also be characteristic of the type of matrix material used. Further examination of the value generated by Beckwith at this particular temperature reveals some discrepancy between it and the values for other fiber angles. The data in Reference [12] show the time-independent portion as well as the time-dependent portion of the creep compliance to be gradually increasing as the angle of orientation of the load (with respect to the fibers) increases. In the Beckwith data [12], however, there is a drop in the time-independent portion and a drastic increase in the time-dependent portion of the creep compliance for the angle of 90°. Thus, it is likely that the prediction made using the present analysis represents more closely the true material response than the reduced data presented in Reference [12].

The following comparisons with the data presented by Irion [24] tends to support this statement. Using data for Hercules 3501-6 epoxy resin determined in this study, and the properties for S2 glass and

Hercules AS graphite fibers given in Table I, creep tests were simulated. The S2 glass composites were subjected to -20 and -23 ksi (compressive) transverse stresses in the x-direction. The predictions are plotted along with actual experimental data in Figures 15 through 17. Similarly, an AS graphite/epoxy composite subjected to a -27 ksi (compressive) transverse stress was simulated and the comparison shown in Figure 18. In all four figures the scale has been expanded, magnifying the error between the predictions and the experiment. In Figures 15 through 18, predictions are shown by the symbols while the experimental results are represented by the solid lines. All simulations were made assuming the temperature to be 21°C and the moisture content to be zero. While actual test specimens may have contained some moisture due to the relative ambient humidity, no data were available to determine this influence upon the creep parameters used in the analysis. Therefore its effect was neglected.

For the comparisons mentioned above, two predictions were actually made, one including a cure simulation and one without a cure simulation. The predictions with a cure, represented by the * symbols in Figures 15 through 18, involved simulating a cooldown from the 177°C cure temperature to room temperature (21°C). This was done using six time-independent temperature increments to achieve 21°C, and was followed by a 140-hour relaxation period. The relaxation time was arbitrary and was included in order to simulate what would happen to the stresses in a composite after it had been cured and allowed to "stand" for several hours. It was discovered that longer relaxation times tend to produce lower and more uniform stress states. This will be demonstrated later using

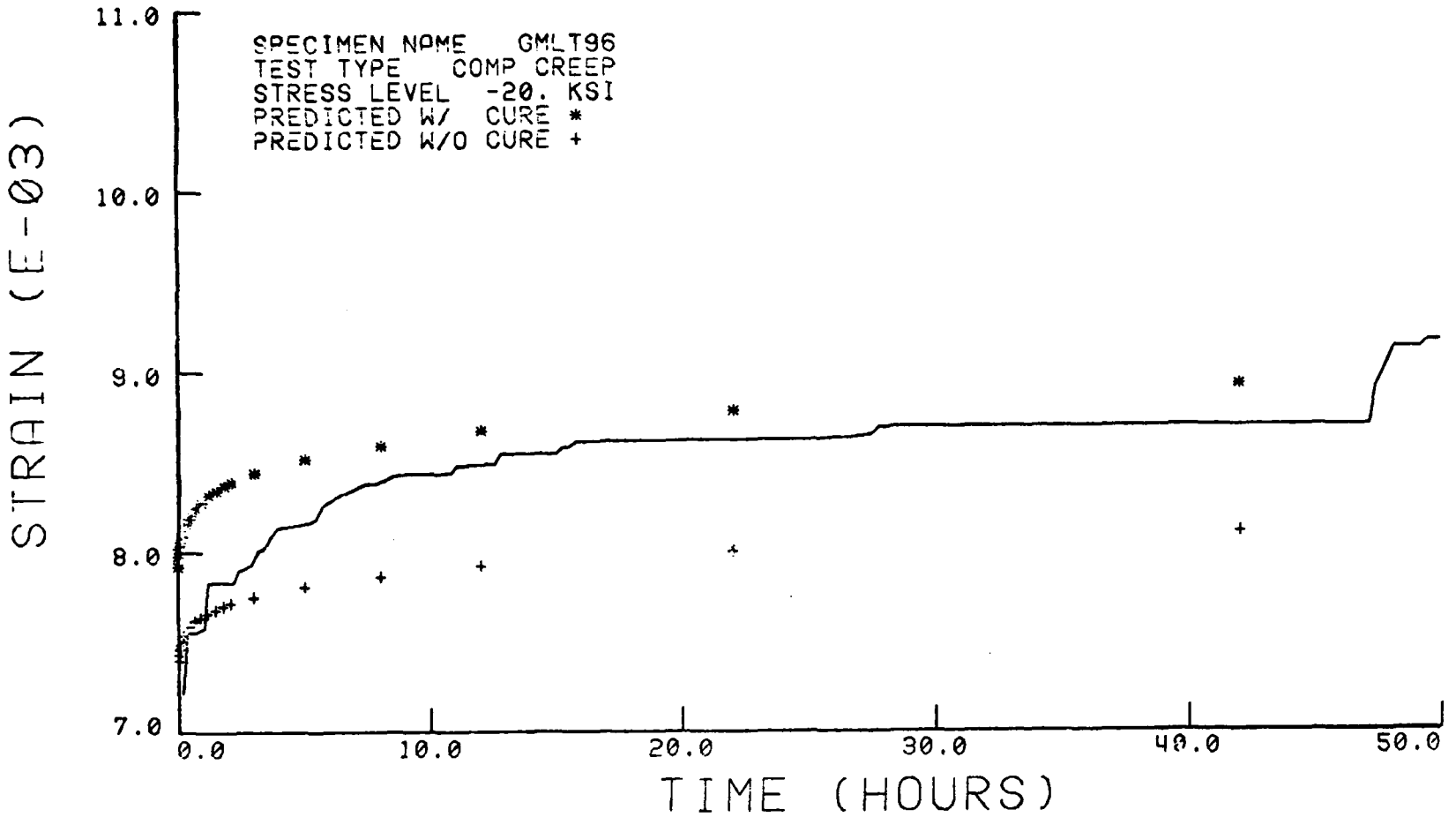

Figure 15. Plot of strain versus time for an S2 glass composite (using Hercules 3501-6 epoxy resin) subject to a 50 hour creep test. Predicted values are shown by the symbols while the solid line represents the experimental data [24].

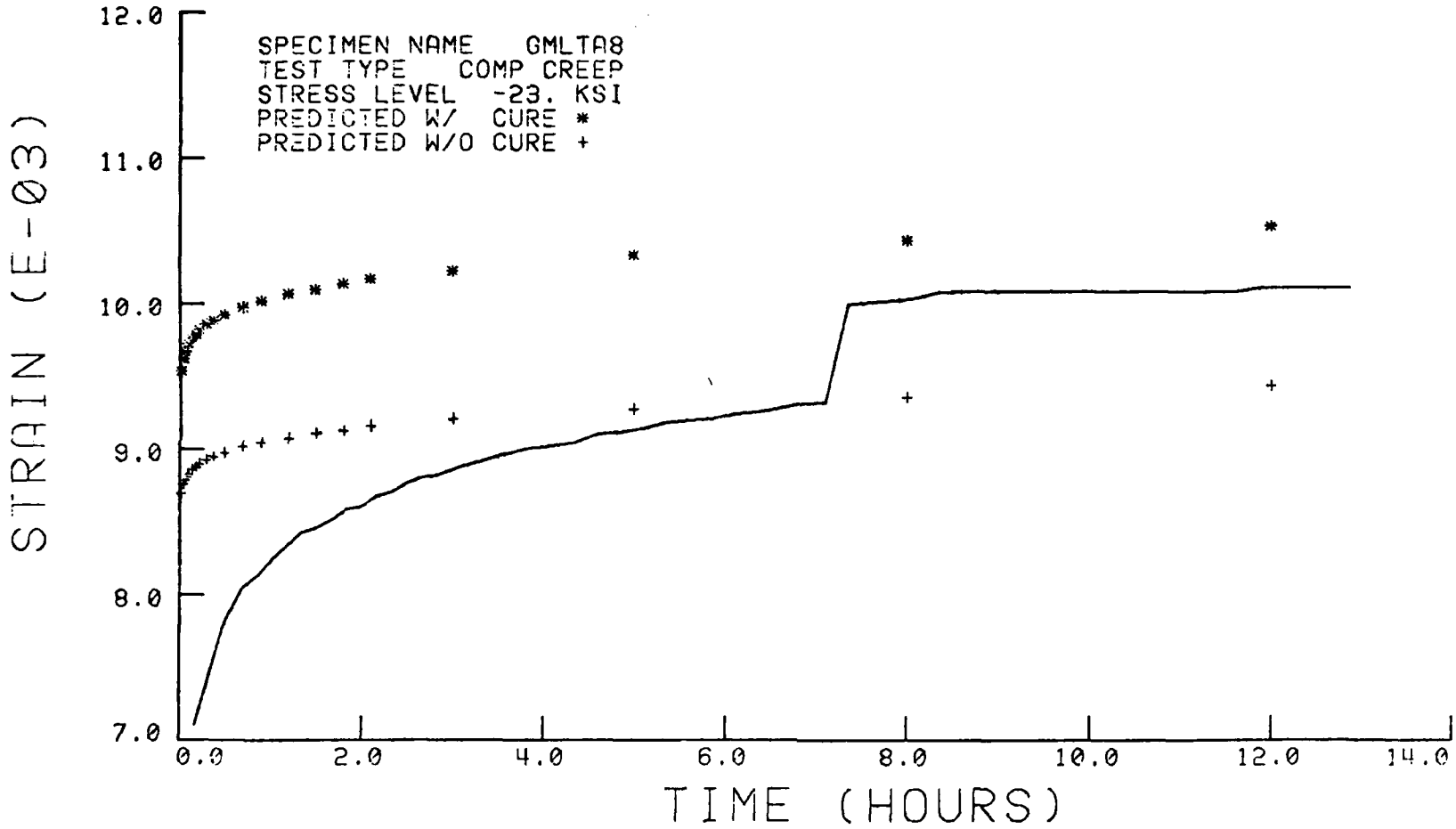

Figure 16. Plot of strain versus time for an S2 glass composite (using Hercules 3501-6 epoxy resin) subject to a 14 hour creep test. Predicted values are shown by the symbols while the solid line represents the experimental data [24].

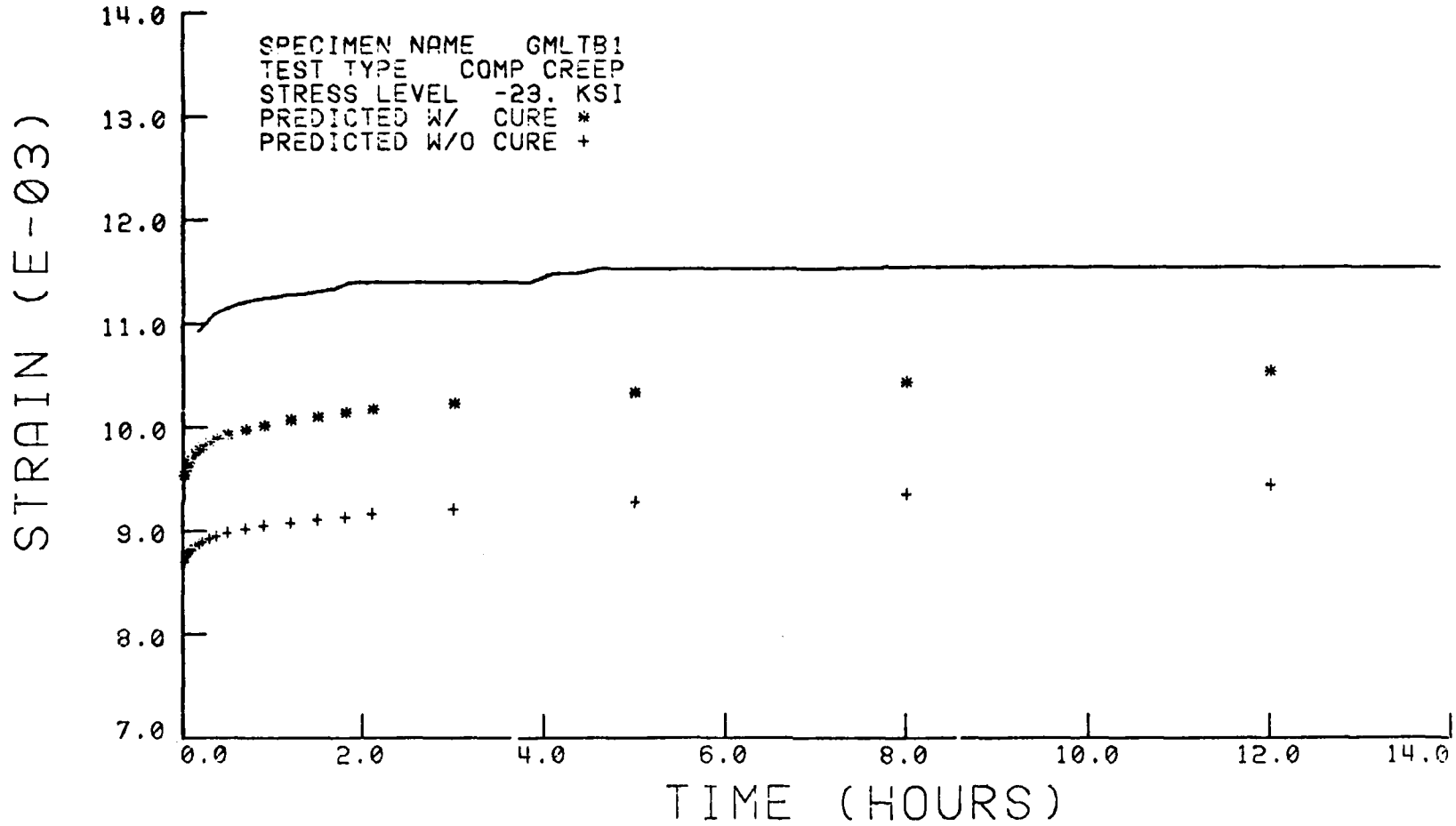

Figure 17. Plot of strain versus time for an S2 glass composite (using Hercules 3501-6 epoxy resin) subject to a 14 hour creep test. Predicted values are shown by the symbols while the solid line represents the experimental data [24].

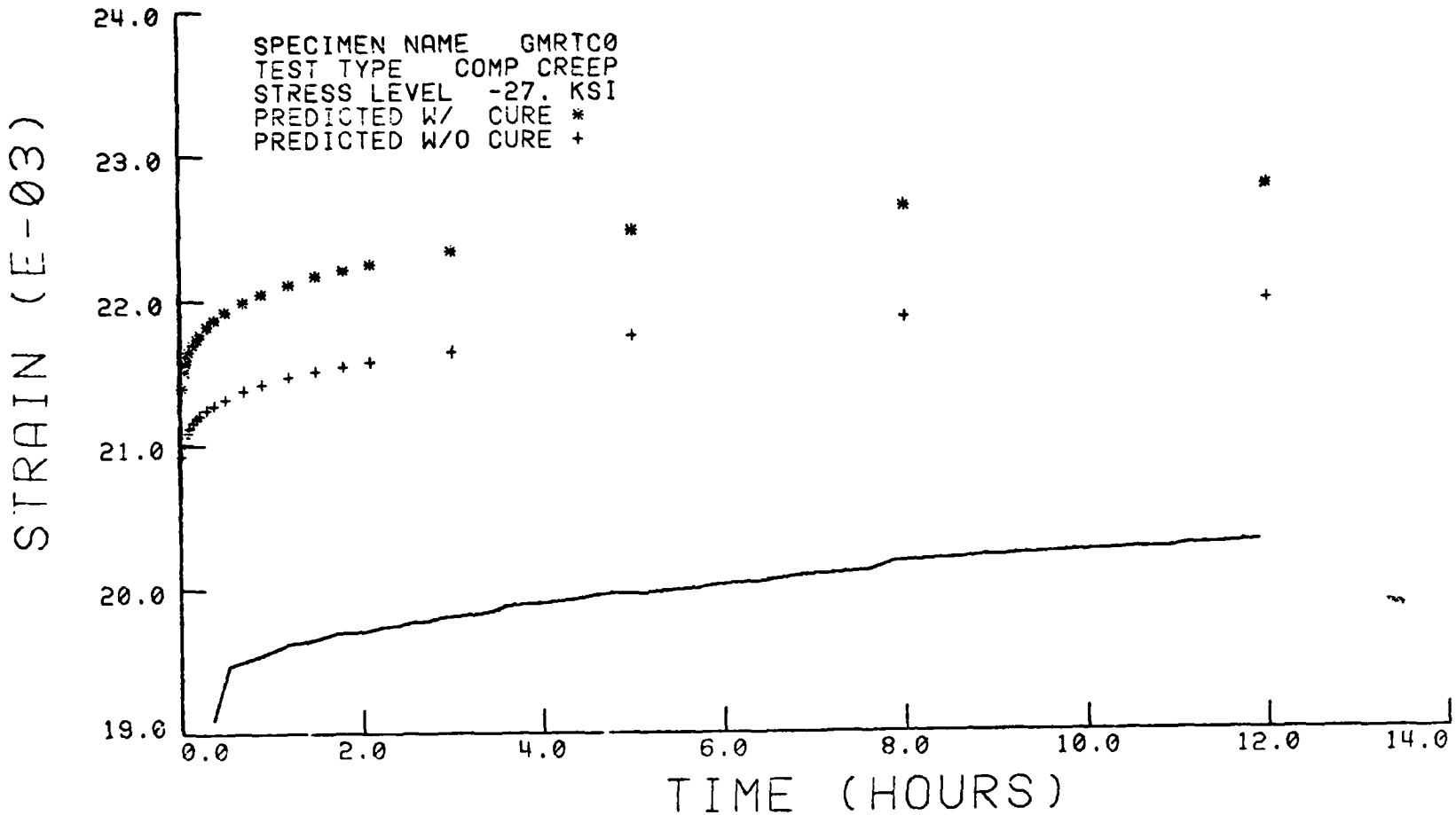

Figure 18. Plot of strain versus time for an AS graphite composite (using Hercules 3501-6 epoxy resin) subject to a 14 hour creep test. Predicted values are shown by the symbols while the solid line represents the experimental data [24].

contour plots of the composite model during a cure simulation.

After this relaxation period, the load was applied and the model allowed to creep. Creep strains plotted in Figures 15 through 18 for the "with cure" simulation were "zeroed" by subtracting the thermal strain prior to loading from the subsequent total strains. In examining these figures it will be noted that the creep strains for the simulation which involved a cure cycle are higher than those for the simulation which did not involve a cure cycle. The reason is that the ininital internal stresses in an uncured composite model are zero, while the internal stresses in the cured composite are very high. These initial stresses are mainly compressive and are caused by the difference in the coefficients of thermal expansion between the fiber and the matrix. In the transverse plane (see Figure 5), the fiber contracts during the cooling process, while the matrix contracts even more. With the presence of a fiber, however, this matrix contraction is restricted, producing compressive residual stresses in the matrix. Thus, the application of a compressive stress serves to raise the internal stress state, which tends to make the composite creep more. Actually, the cause of these residual stresses in the composite is more complicated than just described. The relative stiffnesses and Poisson's ratios of both the fiber and the matrix material also play a role in determining these stresses. Adams and Monib [29] have described the influence of these parameters in detail.

Both "with" and "without cure" predictions were made in order to obtain a "range" in which the experimental data might lie. In other words, the subsequent response of a composite is a function of how long it has been since the specimen was fabricated. In theory, the internal

stresses should be very small and uniform after a very long relaxation time. It is expected that the actual experimental data will lie somewhere within this range, and the predictions shown in Figures 15 through 18 seem to confirm this. In Figures 16 and 17, the predictions (for the -23 ksi stress) are over and under, respectively, the actual measured data for the glass/epoxy composite, while the experimental data for the -20 ksi stress (Figure 15) fall within the predicted range. In figure 18, the predictions for the graphite/epoxy composite overestimate the experimentally measured response. There is considerable scatter in the experimental data found in Reference [24]. The errors between the predictions and these experiments, as shown in Figures 15 through 18, are of the same magnitude as the experimental scatter. Thus, the agreement between the predictions and experiment is quite reasonable considering the limited abount of data available. It is important to note that in each of these figures the strain scale has been enlarged, magnifying the errors between the predictions and the experimental data. By picturing these plots with a full scale, the relative error is put into proper perspective.

While Irion [24] used a slightly lower cure temperature for a longer period of time, it is expected that the results using his cure would be very close to those actually modeled. In fact, the lower cure temperature would tend to induce lower initial residual stresses. Thus, such a cure simulation would fall within the range already predicted.

Contour plots for the glass/epoxy composite for both the "with" and "without cure" cycles are shown in Appendix D. Figures D-7a and D-7b show octahedral shear stress and strain contours immediately after cool-

down of the composite, while Figures D-7c through D-7h show the composite after 0.5, 2.1, and 140 hours of relaxation. Figures D-7i and D-7j show octahedral shear stress and strain contours, respectively, for the composite just after application of the load, and Figures D-7k and D-7ℓ show these two plots for the composite after the load has been applied for 140 hours.

It is important to note that the octahedral shear stress plots for all of the following examples have been "normalized". That is, all of the contour values shown in the plots have been divided by the yield value of the octahedral stress. The yield values for the epoxy resin were previously determined in Reference [27]. Thus, a contour value greater than one signifies that the region has yielded.

It is clear from Figures D-7a, D-7c, D-7e, and D-7g that the internal stresses are relaxing from the cure cycle, as expected. While the shapes of the contour lines appear to be the same, the magnitude of each contour line has been reduced with time. It is interesting to compare the contour values of the octahedral shear stresses in Figures D-7i and D-7k. After 140 hours of elapsed time after application of the load, the contours are seen to have shifted, relieving the high stress state in the lower right-hand corner. The concentration of stresses in this corner was induced by loading the composite in the x-direction (see Figure 4b).

The octahedral shear strain plots (Figures D-7b, D-7d, D-7f, and D-7h) reveal only minute changes of the internal strain during relaxation, as exhibited by both the shapes and magnitudes of the contour lines. This is reasonable since a change in temperature creates a symmetric

loading and the net force on the boundary due to this type of loading is zero. Figures D-7j and D-7ℓ illustrate the change in octahedral shear strain immediately after the load has been applied, and 140 hours later. During this time the strain in the lower right-hand corner is seen to substantially increase, while only moderate increases in strain are observed for the upper portions of the model. These changes in strain are responsible for the redistribution of stresses during this time period.

In Figure D-8, plots of the normal stress and tangential shear stress on the fiber-matrix interface are shown for the above simulation, immediately after cure, 140 hours later, immediately after application of the load, and 140 hours after that. Due to the required continuity of the normal and tangential shear stress at the interface, these figures represent the interface stress state in both fiber and matrix. Since a square fiber packing was assumed in this model, the interface stress plots must be symmetric. The normal stress (Figures D-8a and D-8c) is symmetric about the horizontal, vertical, and 45° axes, while the tangential shear stress (Figures D-8b and D-8d) is symmetric about the 22½° and 67½° axes. The shear stress is antisymmetric about the 45° axis, although the polar plots tend to distort this fact. These axes of symmetry will change, however, for a nonsymmetrical loading (see Figures D-8e through D-8h). Comparing Figures D-8a and D-8b with D-8c and D-8d, and D-8e and D-8f with D-8g and D-8h, it is seen that there is a reduction in both the normal and tangential shear stresses with time. For the symmetrical loading caused by the cooldown, the contour lines do not change in shape but only in magnitude, as expected. On the other hand, there is a slight change in shape as well as magnitude with time for the

loaded composite. These changes are in agreement with the upward redistribution of stress observed in Figures D-7i and D-7k.

Figure D-9 represents the glass/epoxy composite in which curing was not simulated. The first two plots are octahedral shear stress and octahedral shear strain contour plots for the instant immediately after application of the load, while the last two are for 140 hours after application of the load. Since the internal stresses are lower in this model than in the previous model (see Figures D-7i and D-7k), there is less redistribution of the stresses, as evidenced by Figures D-9a and D-9c.

The octahedral shear strain (Figures D-9b and D-9d) is again seen to increase significantly in the lower right-hand corner (where the stress is high), with only moderate increases in the upper portion of the model. This is also caused by the lower initial stress state present in this composite than in the composite with the cure. Thus, a higher stress state in a composite corresponds to a greater amount of creep strain, which in turn causes a greater redistribution of the stresses.

The normal and tangential shear stresses on the fiber-matrix interface were similar to those shown in Figures D-8e through D-8f. While the values were not as large in this case, the changes in shape and magnitude were very similar.

Effect of Fiber Volume

To demonstrate the effect of fiber volume, two identical computer runs were made, using 50 percent and 63 percent fiber volume. For this example, a glass/epoxy composite was subjected to a -20 ksi stress at 21°C and zero moisture for 140 hours. The composite strain response is

plotted in Figure 19 for the two fiber volumes. As expected, the lower fiber volume content composite showed more creep strain than did the higher fiber volume composite. This is due primarily to the fact that there is more matrix material in the 50 percent fiber volume composite. This is consistent with the results presented for the neat resin model (see Figure D-6), which showed even more creep than did the 50 percent fiber volume composite.

Contour plots of the 50 percent fiber volume composite are shown in Figure D-10 for times immediately after application of the load and 140 hours later. Comparison of these plots with those for the 63 percent fiber volume composite (Figure D-9) reveals the higher octahedral stress state just after load application and 140 hours later.

The octahedral shear strain plots for the 50 percent fiber volume composite show a significant change in the upper portion of the model, just as the higher fiber volume composite does. This indicates that a corresponding rearrangement of the stresses is occurring in this area. Figures D-10a and D-10c illustrate this fact.

The normal and tangential shear stresses along the fiber-matrix interface (Figure D-11) indicate a change in shape similar to that of the 63 percent fiber volume composite. The magnitude of this change is much smaller for the 50 percent fiber volume composite, however. This means that while there is a greater redistribution of stresses in this model, they are occurring away from the fiber-matrix interface.

Relaxation After Cure

Two runs were made in order to examine the change in internal stress

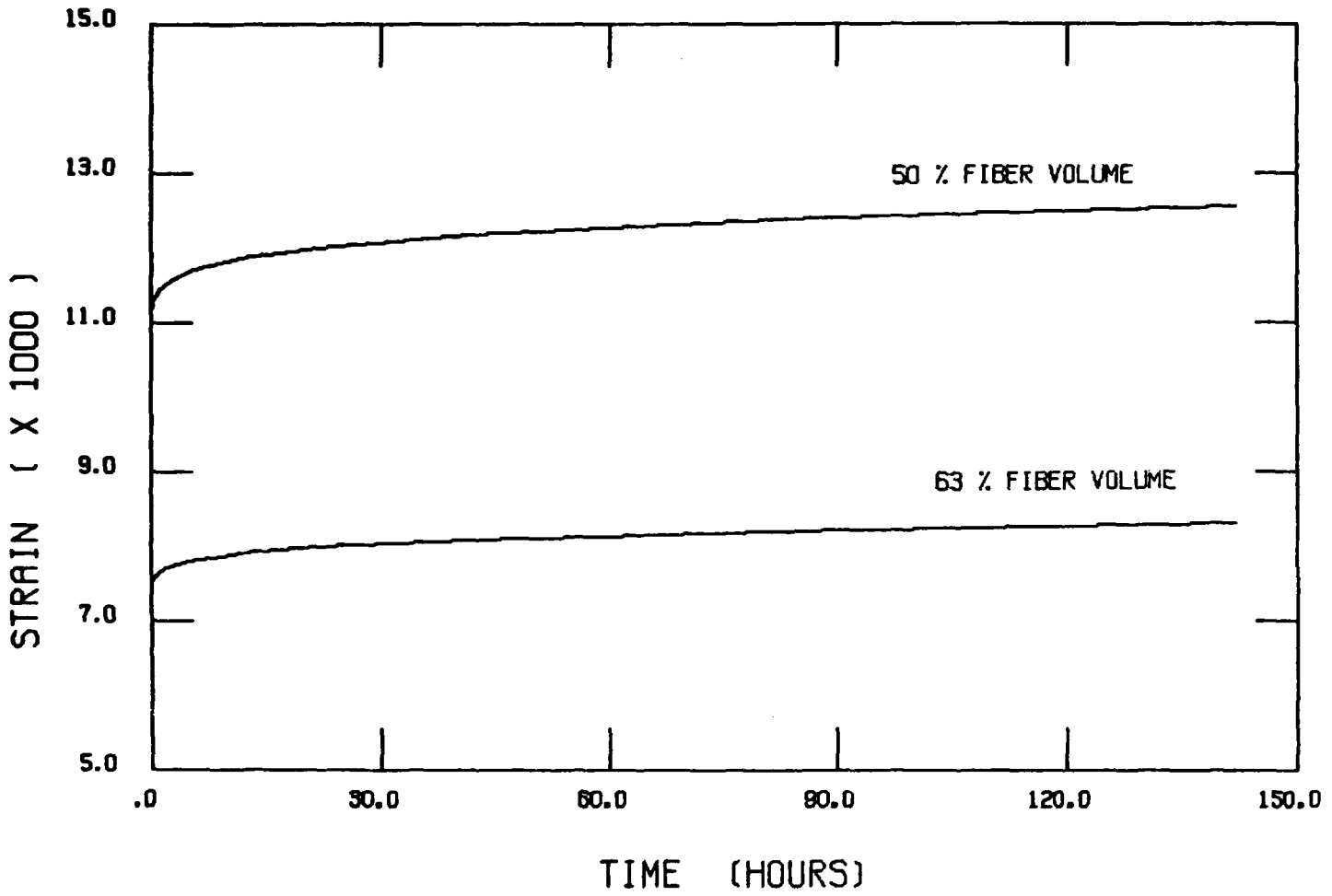

Figure 19. Plot of strain versus time for two different fiber volume glass/epoxy composites subject to the same -20 ksi stress for 140 hours.

state after curing the composite. Figures D-7a through D-7h demonstrate a symmetric distribution of the contour lines, and show that there are no changes in shape of these lines over a period of time. This is reasonable since the temperature, assumed to be uniform throughout the composite, would create a symmetrical stress state after the curing process. While the shape of the contour plots remained unchanged, the magnitudes of the lines decreased in the octahedral shear stress plots. This indicates that the relaxation continues to occur long after the cooldown process. The contour plots illustrate that the majority of relaxation takes place within a few hours, however.

The results of a modified cure cycle are presented in Figure D-12. A composite was cooled from 177°C to 99°C, held for 2.1 hours, then cooled to room temperature (21°C) and allowed to relax for another 2.1 hours. Figures D-12a and D-12b show contours for the time immediately following the cooldown to 99°C, while Figures D-12c and D-12d illustrate the stress state after 2.1 hours of relaxation. In Figures D-12e and D-12f, the contour plots are shown immediately after the cooldown to 21°C, and Figures D-12g and D-12h for 2.1 hours later.

A slight reduction in the octahedral shear stresses was observed in this case relative to those for the composite cured without the intermediate hold (see Figures D-7e and D-7f). This indicates that it is possible to "slow cool" a composite and achieve a lower internal stress state at the end of the cooldown. By changing the intermediate temperature and/or the length of time the composite is held at this temperature, an "ideal" curing cycle may be found using the current analysis. This can be extremely beneficial since it is usually

desirable to have a composite in the lowest stress state possible following a cure. This analysis could also be used to simulate the "annealing" of a unidirectional laminate. In other words, if the composite were reheated following a cooldown and slowly cooled again, this analysis could be used to determine a suitable cooling profile to reduce the residual stresses in the composite.

The octahedral shear strains in this example case did not change significantly with time, due to the symmetry and type of loading. As mentioned previously, a thermal loading produces a symmetric stress state with no net stresses on the boundary. Therefore, the total strain exhibited by the composite will be very small. The interface stresses changed very little throughout this curing cycle, and thus are not presented.

Cyclic Loading

To simulate a cyclic loading, a glass/epoxy composite was subjected to a plus and minus 5000 psi uniaxial, x-direction loading. No cure was simulated so that the effects of the cyclic loading could be isolated and studied independently. The stress was applied for 2.1 hours, then reversed for another 2.1 hours. About one and one-half cycles were modeled, and the total strain results are plotted in Figure 20. Here it is easily seen that the maximum absolute value of the strain just prior to the reversal of the stress is constant for each half cycle. At higher values of stress, it is expected that this value would not remain constant. To illustrate this point, the same composite was subjected to a plus and minus 20 ksi x-direction loading, a plot of strain versus time being

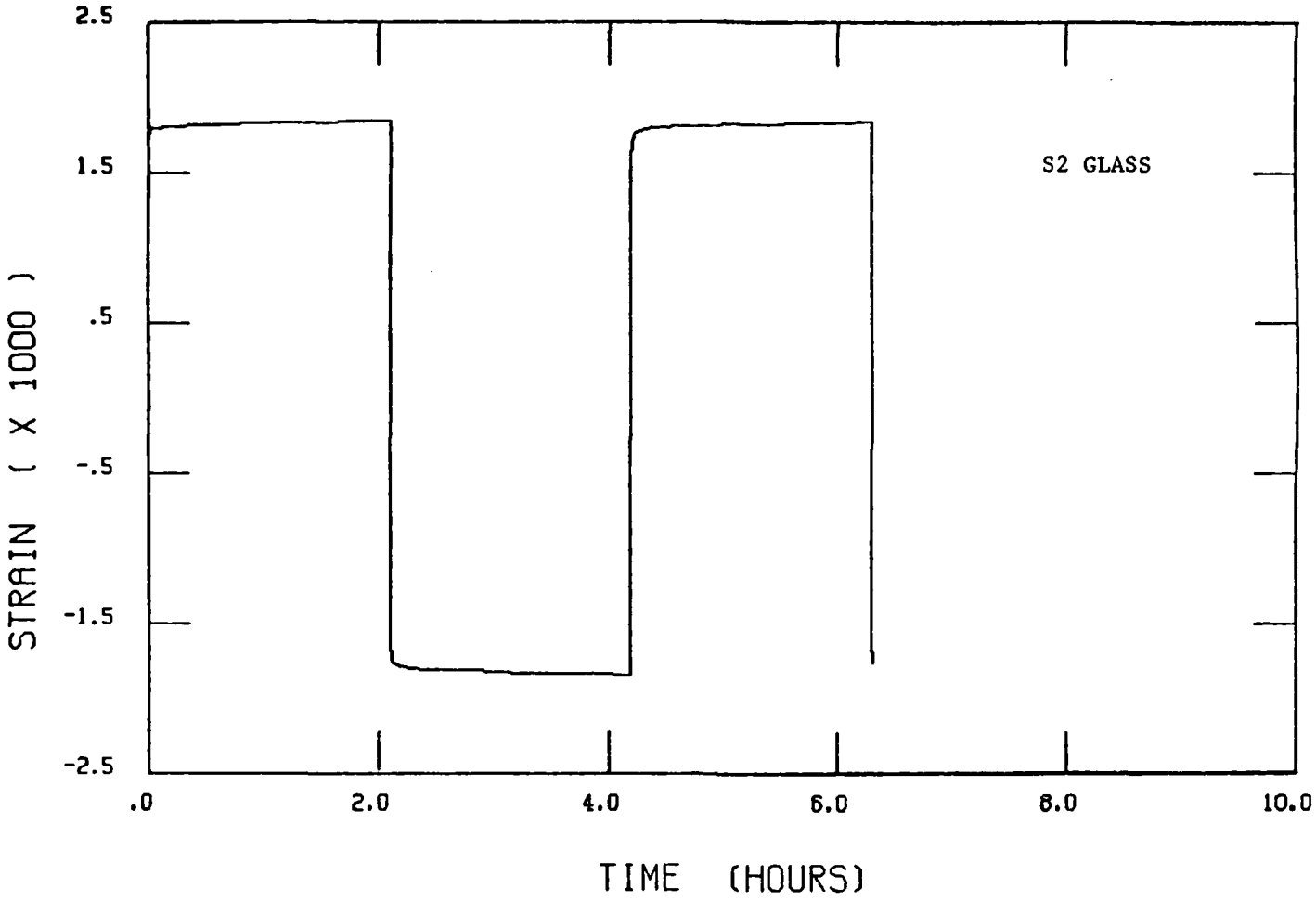

Figure 20. Plot of strain versus time for a glass/epoxy composite subject to a ±5000 psi stress for 2.1 hour intervals.

shown in Figure 21. Here the maximum absolute value of the strain just after each stress reversal actually increases with time. That is, the amount of time-independent strain produced by the first reversal of stress at 2.1 hours is greater than twice the amount of strain produced by the application of the initial 20,000 psi stress at zero hours. This is caused by the program using a different stiffness for the matrix material during the stress reversal. It would be expected that an increment of -40,000 psi would produce twice the amount of strain that the +20,000 psi stress did if the material behavior were elastic. However, the program which assumes the material behavior to be linear initially, now considers the matrix to be yielded. Since it cannot anticipate the next loading increment, it assumes the material to behave in a nonlinear (plastic) manner and hence calculates the corresponding tangent modulus. This modulus will be lower than the elastic modulus, which gives rise to the greater amount of strain. This problem could have been avoided by inputing a smaller increment of stress (-1000 psi for example) followed by a larger increment of stress (-39,000 psi). By doing this, the program would have unloaded the composite plastically during the first increment, sensed that the composite was being unloaded, and unloaded the composite elastically during the second increment. Actually, to accurately model stress reversal at this stress level, several increments are needed to apply and reverse the 20,000 psi stress during the time-independent increments. This was not done in this case since there was only a limited amount of epoxy matrix creep data available anyway. Rather, the idea here was to demonstrate the capability of the analysis.

It is also interesting to note that the strain due solely to creep

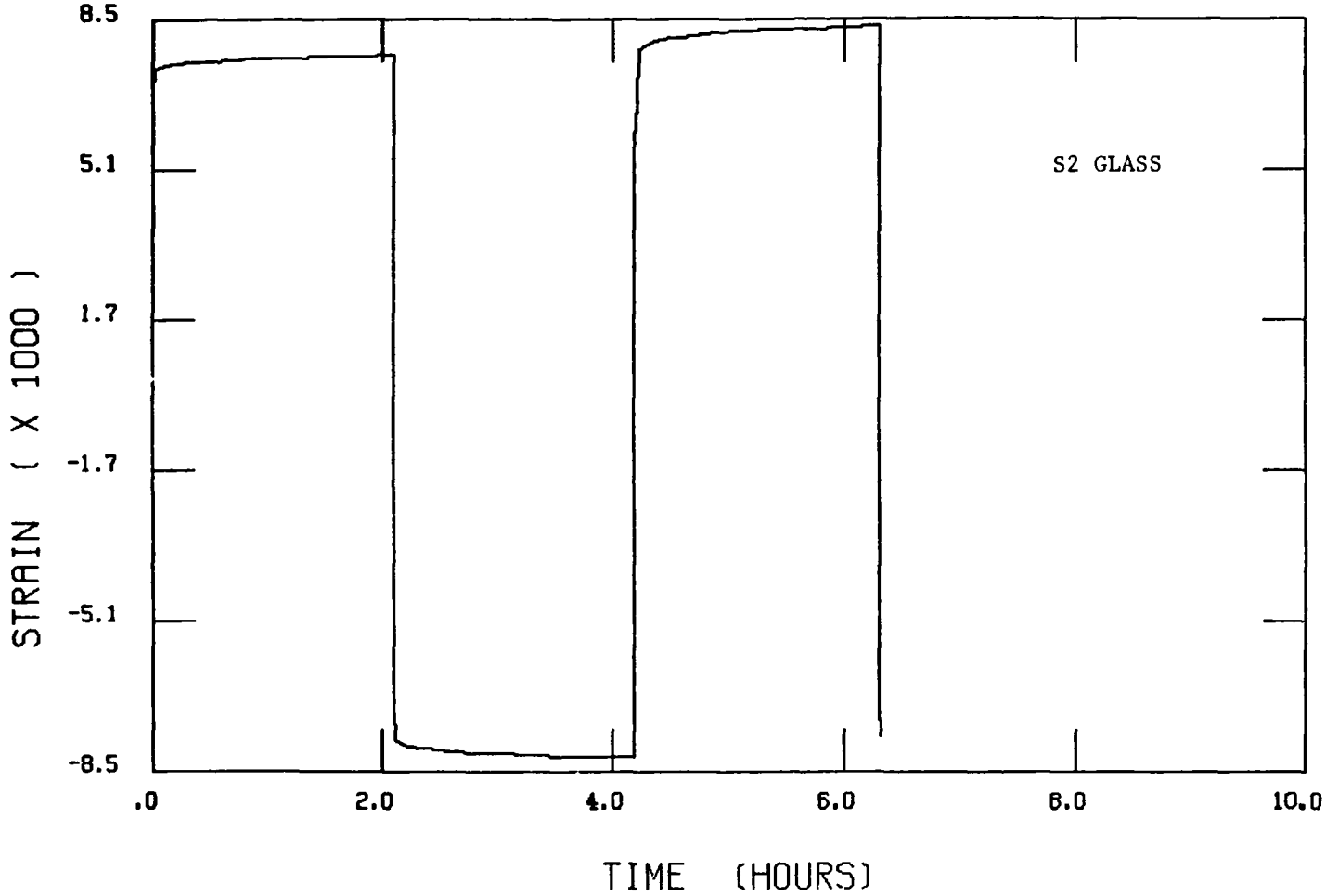

Figure 21. Plot of strain versus time for a glass/epoxy composite subject to a ±20,000 psi stress for 2.1 hour intervals.

actually increases with each half cycle. This is caused by the fact that there are two pseudo applied stresses immediately after a stress change which contribute to the total creep strain. Since these two stresses have just been applied, their (primary creep) contributions are much larger than those for stresses which have been applied for some time (secondary creep). As an example, for time $2.1<t<4.2$ hours, three contributions of strain are present (see Appendix B). These contributions are from the +20,000 psi stress applied at time t=0.0 hours and two -20,000 psi stresses applied at time t=2.1 hours. Examination of the data reveals that the creep strains due to the pseudo application of the two -20,000 psi stresses at 2.1 hours are much greater than those due to the +20,000 psi stress applied at the beginning of the test. The contributions of strain due to the +20,000 psi stress are secondary creep effects while those for recovery and the application of the -20,000 psi stress are primary creep effects (see Figure 1c). Thus, the composite shows more creep strain during the second half cycle than it did during the first. Likewise, the pseudo application of the two +20,000 psi stresses at 4.2 hours, plus the +20,000 psi stress applied at 0.0 hours, tends to negate the effects of the two -20,0 psi stresses applied at 2.1 hours.

Contour plots of the internal stress state immediately after application and just prior to the reversal of the stress for each half cycle are shown in Figure D-13. The contour plots, as before, indicate a lowering of the octahedral shear stress with time after the load has just been incremented. While both the octahedral shear stress and octahedral shear strain contour shapes changed very little, the magnitudes do indicate a leveling of the stresses, times 2.1 hours later being shown. It is

interesting to observe the difference in contour shapes for the two positive stress cycles during the test (Figures D-13a through D-13d and D-13i through D-13ℓ). Immediately after application of the second +20,000 psi stress, the contour values are higher than they were after application of the initial +20,000 psi stress. However, two hours after the second +20,000 psi stress is applied, the stresses rearrange themselves in Figure D-13k very much the same as they did two hours after application of the first +20,000 psi stress (Figure D-13c). In each case, the highly stressed region has moved upward (in the y-direction) from the lower right-hand corner. Thus, even after a stress reversal, the highly stressed regions tend to redistribute themselves in order to smooth or even out the stress gradients present. The octahedral shear strain plots show this redistribution by the large values of strain present in these areas.

In going from the +20,000 psi (Figure D-13c) to the -20,000 psi (Figure D-13e) value of stress (during the time-independent increment), the contour shapes also rearrange themselves so that the high stress concentration is moved upward. On the other hand, in going from the negative (Figure D-13g) to the posititve (Figure D-13i) value of stress, the high stress concentration area is pulled downward.

Contour plots for the plus and minus 5000 psi loading did not change much since the material behavior did not exceed the elastic limit. The contour shapes remained essentially the same and the only real indications of creep were the changes in the octahedral shear strain plots.

Plots of the normal and tangential shear interface stresses for the 20 ksi cycling case are shown in Figure D-14. Again, each plot corresponds to the stress state just before and after the load is incremented.

While the normal interface stresses are reduced with time during the tensile loads, they increase with time during the compressive loading. On the other hand, the tangential shear stresses behave in the opposite manner. It will also be noted that the signs of both interface stresses change when the load is reversed.

Multiaxial Loading

A 5000 psi stress was applied in both the x- and y-directions and the composite was allowed to creep for 140 hours. Again, no cure was simulated so that the effects of the multiaxial loading could be isolated and studied. A plot of x-direction strain versus time is shown in Figure 22. The y-direction strain versus time plot is not presented since it is identical to that for the x-direction. There is some irregularity in Figure 22 due to the limited number of points plotted. In this computer plot, the data points were connected with straight lines, giving the false illusion of a depression between 14 and 45 hours.

Contour plots of the internal stress state are shown in Figure D-15. As expected for a symmetrical loading, little redistribution of the octahedral shear stresses or strains occurred even after 140 hours. In fact, there were essentially no changes in the magnitudes of the octahedral shear stress at all. The plots of the octahedral shear strain did indicate that creep in the form of an overall expansion of the model was taking place, however.

A slightly different multiaxial loading case was also simulated. Here, a 15,000 psi and a 5000 psi stress were applied to the same model in the x- and y-directions, respectively, for 140 hours. Strain versus

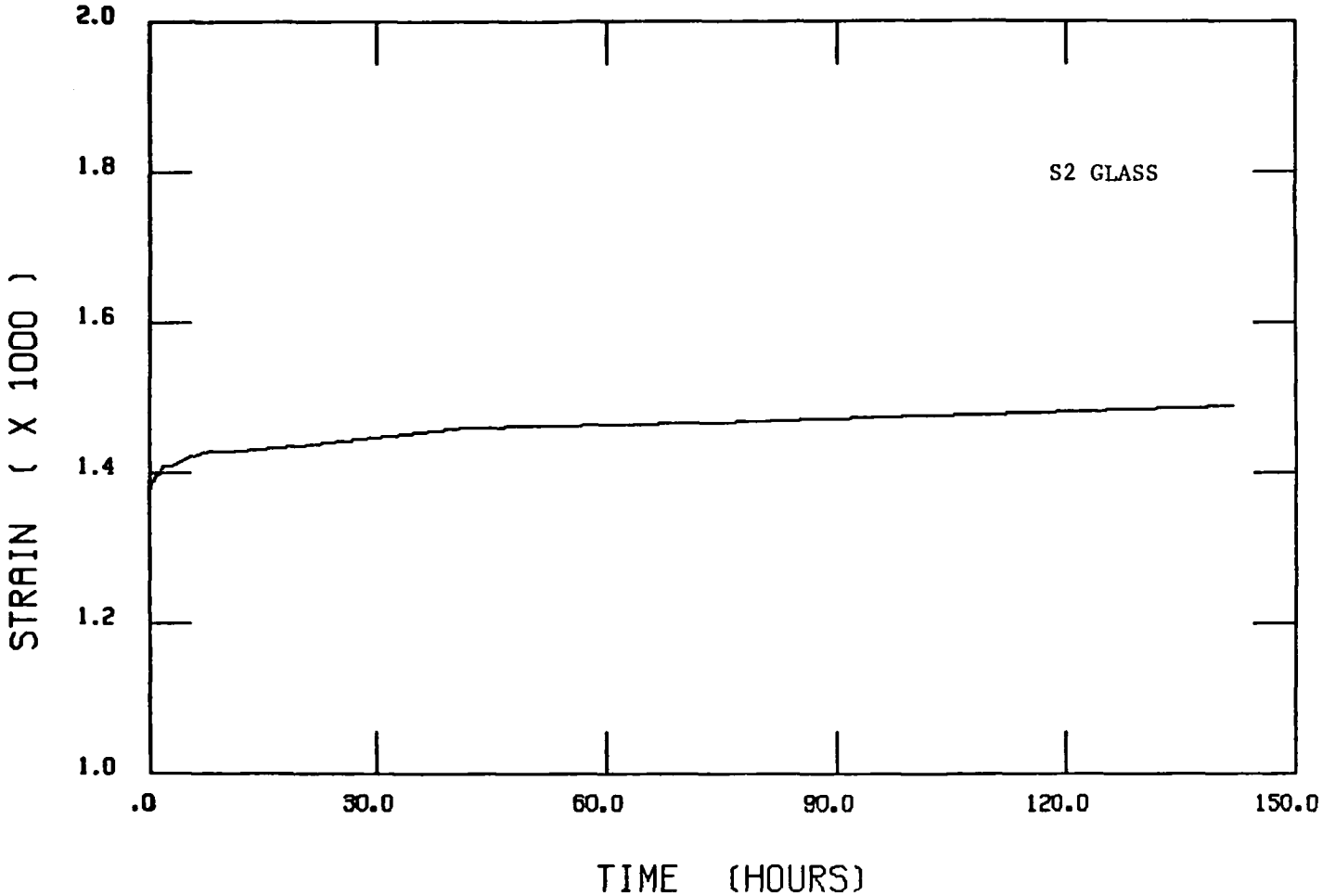

Figure 22. Plot of strain versus time (x-direction) for a glass/epoxy composite subjected to a 5000 psi stress in the x-direction and a 5000 psi stress in the y-direction.

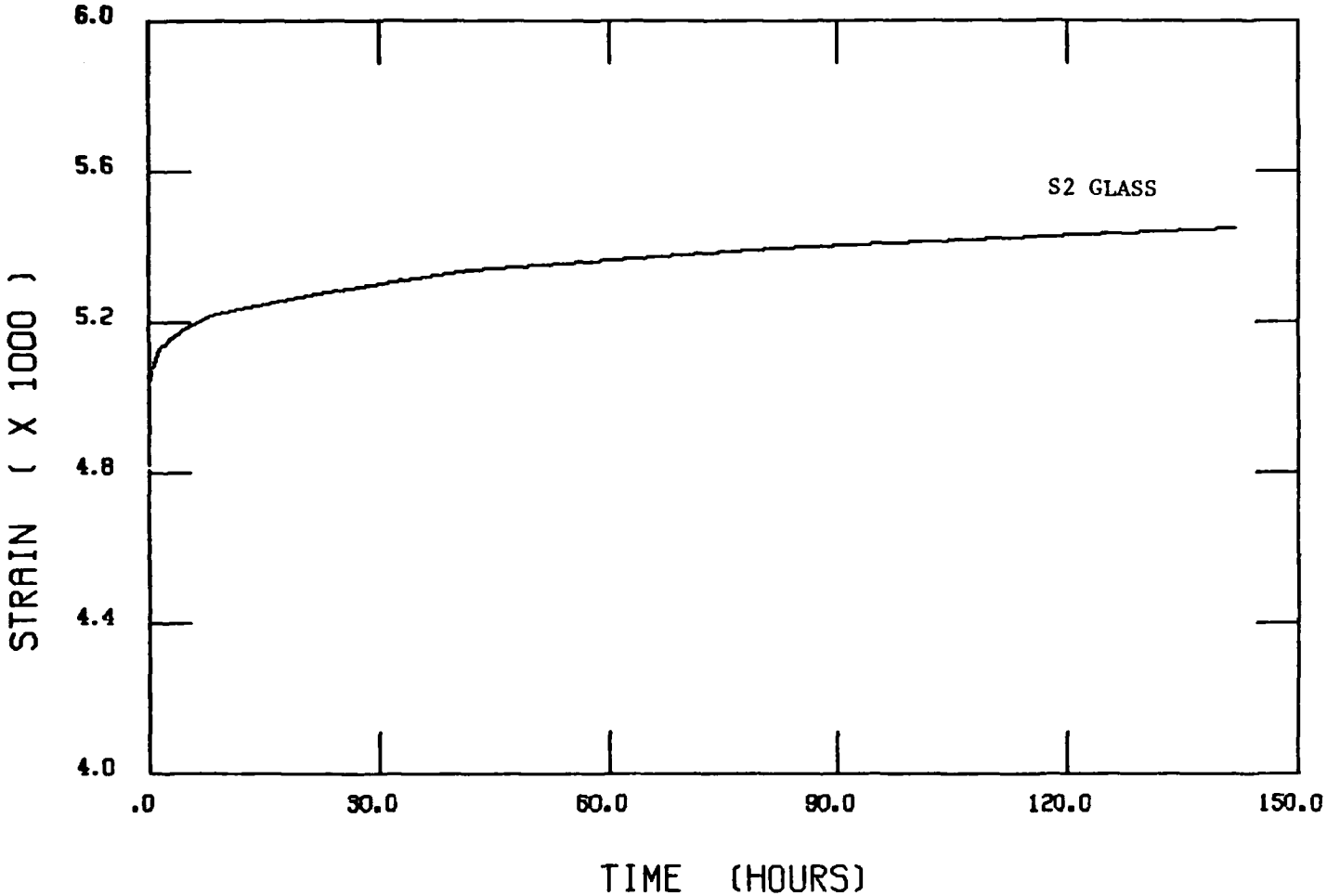

Figure 23. Plot of strain versus time (x-direction) for a glass/epoxy composite subjected to a 15,000 psi stress in the x-direction and a 5000 psi stress in the y-direction.

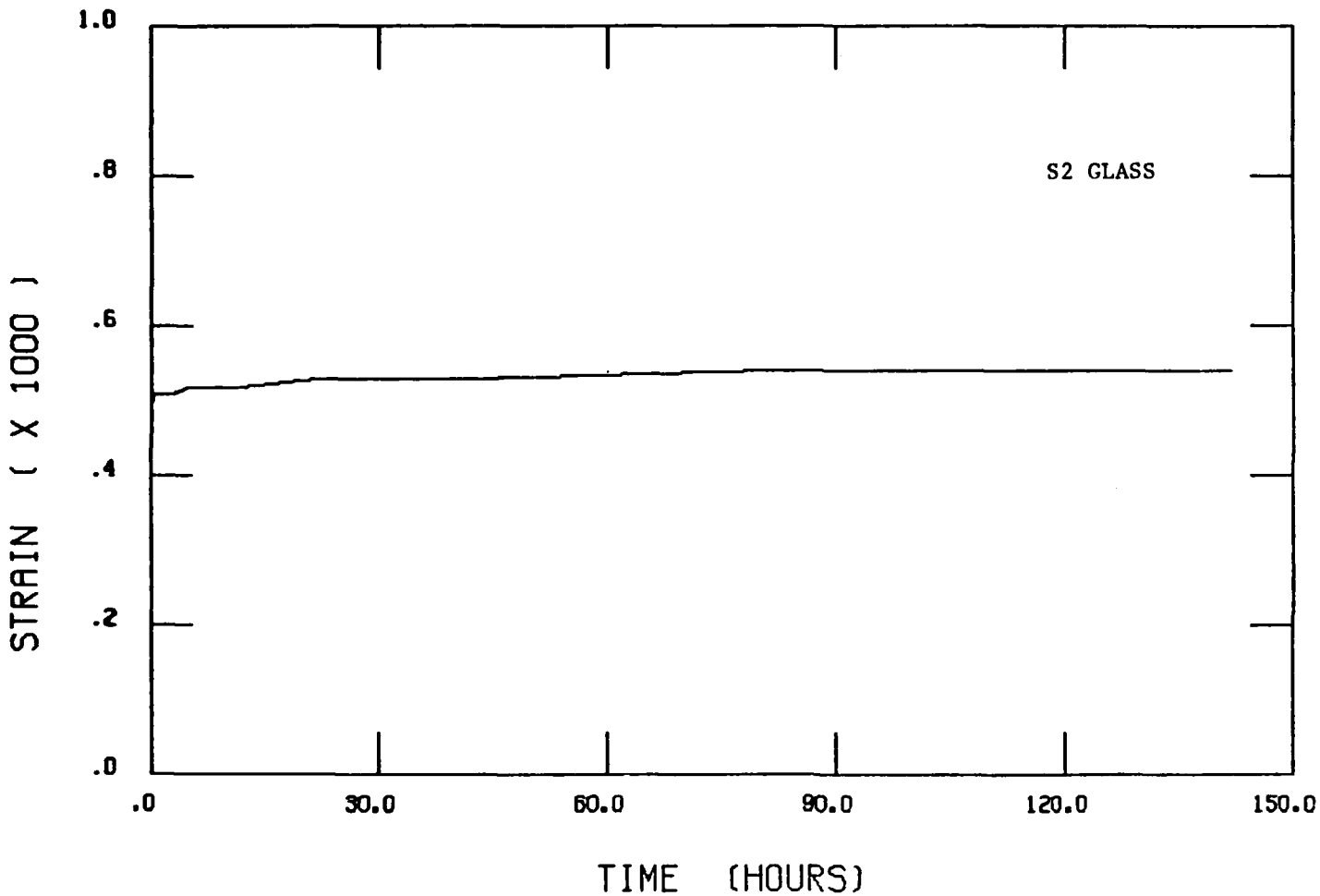

Figure 24. Plot of strain versus time (y-direction) for a glass/epoxy composite subjected to a 15,000 psi stress in the x-direction and a 5000 psi stress in the y-direction.

time plots are shown for the x- and y-directions in Figures 23 and 24. Note that while the x-direction displayed a reasonable amount of creep for the applied stress, the y-direction showed very little. It can be seen that this composite exhibited 10 to 15 times more creep in the x-direction than in the y-direction. By comparing the strain versus time plots for the direction in which the 5000 psi stress was applied in both multiaxial loading cases (Figures 22 and 24), it is seen that the specimen with the symmetric loading exhibited 3 to 4 times the amount of creep strain compared to the specimen which was not symmetrically loaded. This illustrates the time-dependent effect of a constant Poisson's ratio. If this ratio were assumed to change with time, the response would obviously be different.

Contour plots of octahedral shear stress for the nonsymmetrical loading case (Figure D-16) show a slight reduction in the internal stress state after 140 hours. On the other hand, the octahedral shear strain contour values are seen to increase with time. As in the symmetrical loading case, both the octahedral shear stress and strain contour shapes remain essentially unchanged.

Interface normal and tangential shear stress plots for the symmetric and nonsymmetric loading cases are presented in Figures D-17 and D-18, respectively. While no changes in the tangential shear stresses with time for either simulation were observed, the normal stresses on the interface increased slightly for the symmetric loading and decreased for the nonsymmetric loading. The reason for this is that the applied stresses are causing the matrix material to creep, while it is assumed that the fiber does not. For the symmetrical loading case, the stresses caused by the

creep strains in the matrix cannot redistribute themselves and therefore increase. This situation is analogous to placing a piece of material between two rigid supports and raising the temperature. As the material attempts to expand, the rigid supports restrict the expansion, inducing higher and higher stresses in the material. In the case of the non-symmetric loading, the stresses can redistribute themselves, as they did in the uniaxial loading cases, in order to relieve stress concentrations or highly stressed areas.

In general, it can be said that for the composite models subjected to a decrease in temperature, the octahedral shear strain plots showed only small changes with time, while the octahedral shear stress plots illustrated symmetrical decreases. On the other hand, models subjected to symmetrical external loadings showed balanced increases in octahedral shear strain with time, with only minute changes in octahedral shear stress. In all symmetric loading cases, only the magnitudes and not the shapes of the contours changed with time, as expected. For the nonsymmetric external loading cases, the contour lines for the octahedral shear stress plots were reduced in magnitude, and redistributed, in order to relieve highly stressed regions. At the same time, the octahedral shear strain plots illustrated this rearrangement of the stresses, by marked increases in strain in these areas.

Experimental data were not available for comparison for either the load cycling or the multiaxial creep tests. While the analysis is capable of predicting the composite response due to either of these loading histories, experimental verification would be useful. A series of uniaxial load cycling tests should be run at various stress levels in order to

confirm the behavior predicted by the analysis. It would be informative to compare the amount of creep strain increase per half cycle as predicted by the analysis (Figures 20 and 21) with that of experiment. Multiaxial creep tests, while being more difficult to run, could be used to confirm the amount of creep strain predicted (see Figures 22 through 24) by the analysis.

An assumption was made in the beginning of this study concerning the coupling between multiaxial applied stresses. Specifically, this assumption was that the only coupling between multiaxial stresses was due entirely to Poisson effects. By performing multiaxial creep tests, the validity of this assumption could be evaluated. It is felt that this was a good assumption due to the excellent correlation between the predictions and experiment obtained in the uniaxial loading cases. Although the composite is loaded uniaxially, the matrix is in a very complicated triaxial state of stress. Thus, the multiaxial stress response of the epoxy is actually being tested.

Verification of the changes in internal stress states for various cooldown cycles would also be helpful. Such changes are difficult to measure, however.

CHAPTER VI

SUMMARY AND CONCLUSIONS

The several examples presented in the previous chapter demonstrate only a few of the many potential applications of the analysis. It would be possible to combine several of these features, such as multiaxial cycling, thermal cycling, etc., to model many different situations. However, the purpose here is to give an indication of the possible uses and applications of the program. As mentioned previously, experimental verification of these capabilities would be helpful. Such verification would allow one to use the finite element program with assurance that predictions of complicated hygrothermal and/or loading histories were correct.

In summary, the analysis is capable of modeling any unidirectional composite subjected to longitudinal and/or transverse normal and/or hygrothermal loadings. A finite element computer program is used to model the composite. The constituent material parameters, which are functions of temperature, moisture, and time, are input to the program through two subroutines. Thus, material properties can readily be changed. The finite element analysis used in the computer program is based upon a displacement formulation, constant strain triangular elements with three degrees of freedom being used. The analysis is pseudo-three-dimensional in nature, utilizing the conditions for generalized plane strain. Nonlinear (elastoplastic) material behavior is included by means of the tangent modulus method. While this program is incremental in nature, and requires the use of several steps to load the composite into the non-

linear range, it can readily model matrix materials with "flat" stress-strain curves, such as aluminum. For example, the modeling of a boron/aluminum composite would present no difficulty.

Viscoelastic behavior is incorporated into the analysis by using nonlinear constitutive equations developed by Schapery [8]. Creep strains are treated as initial strains and are calculated by linearly approximating the value for the creep compliance over a time increment. Thus, it is necessary for these increments to be small when the value of the creep compliance is changing rapidly. While uniaxial loads produce complicated triaxial stress states in the composite, it is assumed that the only coupling between these multiaxial stresses in the material is due to Poisson effects. It is possible to include higher order coupling effects between multiaxial stresses; however, this complication has been neglected in the current analysis. Also, Poisson's ratio has been assumed to be time-independent or at most a very weak function of time. The validity of this assumption has been demonstrated by several investigators [12,16,17]. By making use of it, the constitutive equations are simplified immensely (see Appendix A).

The present analysis solves problems which involve changes of stress, temperature, and moisture content with time as a series of step loadings. That is, no increments of load, temperature, or moisture are permitted during a time increment. However, increments of load, temperature, and/or moisture may be applied simultaneously using a time-independent increment. Thus, a ramp loading must be simulated, for example, by a series of step loads. This could become inefficient as the number of steps grew large, due to the nature of the program. As explained before, each

successive step load requires two additional contributions of strain to be solved for. This is due to the nonlinear time-dependence which the matrix material displays.

In Chapter III, the conditions for linear viscoelastic behavior were discussed and a test for determining whether a material is linear or nonlinear was described. While most materials display some linear behavior at low stresses and temperatures, these same materials are usually quite nonlinear at higher values of stress and temperature. The transition values of stress and temperature (and for polymer-matrix composites, moisture) are different for each material and must be determined by experiment.

The nonlinear viscoelastic parameters for the matrix material which are input to the analysis can be determined by means of a series of creep-recovery tests at different stress levels, as demonstrated in Chapter IV. To include the effects of temperature and moisture, a series of creep-recovery tests at various temperatures and moisture contents must be run. Reduction of the experimental data can be achieved by means of simple graphical techniques.

In all of the examples presented in Chapter V, the failure criterion (present in the existing micromechanics computer program) was ignored. Since failure is an important criterion in many designs, this feature could prove very useful. First failure, as currently predicted by the analysis, does not always mean that a composite has failed, however. Many composites continue to carry load long after the matrix has experienced many microcracks. For this reason, crack propagation should be included in future analyses. The basic micromechanics program has been

modified by Murphy and Adams [30] to include crack propagation. Thus, this capability could easily be incorporated into the present analysis.

Other future considerations might include the addition of shear loading into the analysis. Currently, work is underway to include this capability [31] into a separate micromechanics program. By including this type of loading, all time-dependent parameters necessary for use in a laminate analysis may be determined.

A 3-D finite element laminate analysis has recently been developed by Monib [32]. The program uses advanced storage and computing techniques which make it ideal for use on most any computer system. While it does not include viscoelastic behavior at this time, it could easily be modified to handle such effects. This analysis could then be used to predict the viscoelastic response of any laminate desired, for ultimate use in the design of a specific component.

An important feature of the analysis and associated computer program developed in the present study is that only constituent material properties need to be evaluated. This avoids the difficulty of having to evaluate the time-dependent parameters of all fiber-matrix combinations. Usually only matrix materials need to be tested for time-dependence since most fibers do not show (or show very little) viscoelastic behavior. Thus, a designer can model the time-dependent behavior of many different types of composite systems with only a small amount of experimental data. This was demonstrated in Chapter V for glass/epoxy and graphite/epoxy composites. Here, only the epoxy had to be tested in order to determine the viscoelastic response of two different composites.

In general, the results obtained for uniaxial loading compare very well with the experimental data available. Comparisons with the data generated by Irion [24] proved the analysis to be within experimental error. While only a limited amount of data was available for comparison, it is felt that future comparisons will be equally accurate. The analysis is capable of modeling almost any type of loading history desired since all stress components are accounted for individually. Also, it has been shown that it is possible to determine an ideal curing cycle for a unidirectional composite, or the internal stress state of a composite after any curing cycle, using the present analysis. Any type of thermal or moisture history can be modeled to determine the effects of environmental exposure on a composite. This can be useful in determining whether a particular component has suffered any degradation during this period. Combinations of mechanical and environmental loadings can also be modeled using the program to determine if the environment intensifies or relieves the internal stresses in the composite. Thus, it is clear that the analysis and associated computer program of the present study are ideal for determining the time-dependent stress state and overall response of any unidirectional composite under many situations.

AD-A087 367 WYOMING UNIV LARAMIE DEPT OF MECHANICAL ENGINEERING F/G 11/4
NONLINEAR VISCOELASTIC BEHAVIOR OF A COMPOSITE MATERIAL USING A--ETC(U)
JUN 80 B G SCHAFFER, D F ADAMS DAAG29-79-C-0189
UNCLASSIFIED UWME-DR-001-101-1 ARO-16370.1-MS NL

2 OF 2
AD
A087367

END
DATE
FILMED
9-80
DTIC

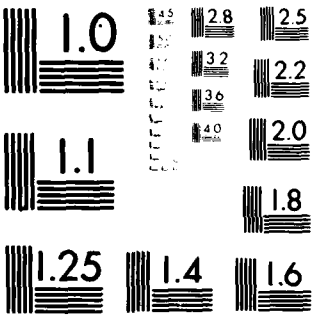

MICROCOPY RESOLUTION TEST CHART
NATIONAL BUREAU OF STANDARDS 1963-A

REFERENCES

1. Findley, W.M., and J.S. Lai, Creep and Relaxation of Nonlinear Viscoelastic Materials, North Holland Publishing Co., New York, New York, 1976.

2. Larke, E.C., and R.J. Parker, "Mathematical Relationships for Primary, Secondary and Tertiary Creep and Their Use in Extrapolation of Tensile Creep Data," Advances in Creep Design, Smith, A.I., and A.M. Nicholson, editors, Halsted Press Division, John Wiley and Sons, Inc., New York, New York, 1971, pp. 111-127.

3. Flügge, W., Viscoelasticity, Blaisdell Publishing Co., Waltham, Massachusetts, 1967, pp. 3-31.

4. Halpin, J.C., "Introduction to Viscoelasticity," Composite Materials Workshop, Progress in Materials Science Series, Vol. 1, Technomic Publishing Co., Westport, Connecticut, 1968, pp. 87-151.

5. Green, A.E., and R.S. Rivlin, "The Mechanics of Nonlinear Materials with Memory-Part I," Archive of Rational Mechanics Analysis, Springer-Verlag, Berlin, Germany, 1957, pp. 1-21.

6. Green, A.E., Rivlin, R.S., and A.J.M. Spencer, "The Mechanics of Nonlinear Materials with Memory-Part II," Archive of Rational Mechanics Analysis, Springer-Verlag, Berlin, Germany, 1959, pp. 387-404.

7. Schapery, R.A., "Application of Thermodynamics to Thermomechanical, Fracture, and Birefringent Phenomenon in Viscoelastic Media," Journal of Applied Physics, Vol. 35, No. 5, May 1964, pp. 1451-1465.

8. Schapery, R.A., "Further Development of a Thermodynamic Constitutive Theory: Stress Formulation," Report No. 69-2, School of Aeronautics, Astronautics, and Engineering Sciences, Purdue University, Lafayette, Indiana, February 1969.

9. Leaderman, H., "Elastic and Creep Properties of Filamentous Materials and Other High Polymers," The Textile Foundation, Washington, D.C., 1943.

10. Lai, J.S. and W.M. Findley, "Creep of 2618 Aluminum Under Step Stress Changes Predicted by a Viscous-Viscoelastic Model," Journal of Applied Mechanics, Vol. 47, March 1980, pp. 21-26.

11. Schapery, R.A., and Y.C. Lou, "Viscoelastic Characterization of a Nonlinear Fiber Reinforced Plastic," Journal of Composite Materials, Vol. 5, April 1971, pp. 208-234.

12. Beckwith, S.W., "Viscoelastic Characterization of a Nonlinear, Glass/Epoxy Composite Including the Effects of Damage," Ph.D. Dissertation, Mechanics and Materials Research Center, Texas A&M University, College Station, Texas, October 1974.

13. Fung, Y.C., A First Course in Continuum Mechanics, Prentice-Hall, Inc., Engelwood Cliffs, New Jersey, 1977.

14. Miller, A.K., and D.F. Adams, "Micromechanical Aspects of the Environmental Behavior of Composite Materials," Department Report UWME-DR-7011111, Department of Mechanical Engineering, University of Wyoming, Laramie, Wyoming, January 1977.

15. Zienkiewicz, O.C., The Finite Element Method, Third Edition, McGraw-Hill Book Co., New York, New York, 1977, pp. 471-478.

16. Altoulami, S.A.A., "Theoretical and Experimental Studies on the Creep Behavior of a Graphite/Epoxy Composite Material," Ph.D. Dissertation, Engineering Mechanics Dept., Drexel University, Philadelphia, Pennsylvania, June 1975.

17. Yeow, Y.T., "The Time-Temperature Behavior of Graphite/Epoxy Laminates," Ph.D. Dissertation, Engineering Mechanics Dept., Virginia Polytech Institute and State University, Blacksburg, Virginia, May 1978.

18. Schapery, R.A., "On the Characterization of Nonlinear Viscoelastic Materials," Polymer Engineering and Science, Vol. 9, No. 4, July 1969, pp. 295-310.

19. Saunders, D.R. and W.E. Haisler, "An Incremental Form of the Single-Integral Nonlinear Viscoelastic Theory for Elastic-Plastic-Creep Finite Element Analysis," Publication No. 79-PVP-114, American Society of Mechanical Engineers, New York, New York, 1979, pp. 1-12.

20. Haisler, W.E., and D.R. Saunders, "Elastic-Plastic-Creep-Large Strain Analysis at Elevated Temperature by the Finite Element Method," Computers and Structures, Vol. 10, 1979, pp. 375-381.

21. Cook, R.D., Concepts and Applications of Finite Element Analysis, John Wiley and Sons, Inc., New York, New York, 1974, pp. 293-304.

22. "Hercules Resin Systems," Hercules Incorporated, Bacchus Works, Magna, Utah, 1979.

23. Walrath, D.E., and D.F. Adams, "Fatigue Behavior of Hercules 3501-6 Epoxy Resin," Report No. NADC-78139-60, Naval Air Development Center, Warminster, Pennsylvania, January 1980.

24. Irion, M.N., "Compression Creep Testing of Composite Materials," M.S. Thesis, Department of Mechanical Engineering, University of Wyoming, Laramie, Wyoming, May 1980.

25. "Textile Fibers for Industry," Owens-Corning Fiberglas Corporation, Toledo, Ohio, 1971.

26. "Hercules Magnamite Graphite Fibers," Hercules Incorporated, Wilmington, Delaware, 1978.

27. Unpublished experimental data for Hercules 3501-6 epoxy resin, Mechanical Engineering Dept., University of Wyoming, Laramie, Wyoming, 1978.

28. Ishikawa, T., Koyama, K., and S. Kobayashi, "Elastic Moduli of Carbon/Epoxy Composites and Carbon Fibers," Journal of Composite Materials, Vol. 11, July 1977, pp. 332-344.

29. Adams, D.F., and M. Monib, "Moisture Expansion and Thermal Expansion Coefficients of a Polymer-Matrix Composite Material," Proceedings of the Fourth Conference on Fibrous Composites in Structural Design, Plenum Publishing Corporation, New York, New York, 1980.

30. Murphy, D.P., and D.F. Adams, "Energy Absorption Mechanisms During Crack Propagation in Metal Matrix Composites," Department Report UWME-DR-901-103-1, Department of Mechanical Engineering, University of Wyoming, Laramie, Wyoming, October 1979.

31. Crane, D.A., "Finite Element Micromechanics Analysis of a Composite Material Including Longitudinal Shear Loading," Department of Mechanical Engineering, University of Wyoming, Laramie, Wyoming, December 1980.

32. Monib, M., "Nonlinear Three-Dimensional Finite Element Analysis of Composite Laminates," Ph.D. Dissertation, Department of Mechanical Engineering, University of Wyoming, Laramie, Wyoming, August 1980.

33. Meirovitch, L., Analytical Methods in Vibrations, The Macmillan Company, New York, New York, 1967, pp. 13-14.

APPENDIX A

EVALUATION OF THE CONSTITUTIVE EQUATIONS

Single Step Input

For an isotropic material under isothermal conditions and loaded uniaxially, the constitutive equation is given by Eq. (4) of Chapter III as

$$\varepsilon(t) = g_0 D_0 \sigma(t) + g_1 \int_{0^-}^{t} \Delta D(\Psi-\Psi') \frac{d[g_2\sigma(t)]}{d\tau'} d\tau' \tag{4}$$

where reduced time is defined by Eqs. (5)

$$\Psi \equiv \int_0^t \frac{dt'}{a_\sigma} \qquad \text{and} \qquad \Psi' \equiv \int_0^{\tau'} \frac{dt'}{a_\sigma} . \tag{5}$$

Since the term a_σ is a function of stress (and possibly of temperature and moisture also), and since this parameter is required to be constant throughout the time increment, it may be brought outside of the integral.

First consider the term $\frac{d[g_2\sigma(t)]}{d\tau'}$ in Eq. (4). If a body is subjected to the loading shown in Figure A-1, the stress history may be written in terms of the unit step function [33].

Let

$$\sigma(t) = \sigma_a U(\tau'-a) \tag{A-1}$$

where τ' is the variable of integration, a is the time at which the load is applied, and the unit step function is defined as [33]

$$U(\tau'-a) = \begin{cases} 0 \text{ for } \tau'<a \\ 1 \text{ for } \tau'>a . \end{cases} \tag{A-2}$$

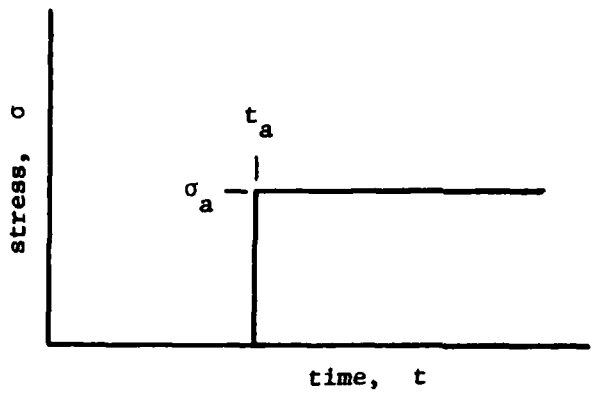

Figure A-1. Plot of stress versus time for a single-step input

Remembering that g_2 is constant over time, and substituting Eq. (A-1), we can write

$$\frac{d[g_2\sigma(t)]}{d\tau'} = g_2 \frac{d[\sigma_a U(\tau'-a)]}{d\tau'} \tag{A-3}$$

Since σ_a is also constant over time, and recognizing that the derivative of the unit step function is the Dirac delta function [33], Eq. (A-3) becomes

$$\frac{d[g_2\sigma(t)]}{d\tau'} = g_2\sigma_a\delta(\tau'-a) \tag{A-4}$$

Evaluating the reduced time terms (Eqs. 5) we get

$$\psi \equiv \int_0^t \frac{dt'}{a_\sigma} = \frac{t'}{a_\sigma}\bigg|_0^t = \frac{t}{a_\sigma} \quad \text{and} \quad \psi' \equiv \int_0^{\tau'} \frac{dt'}{a_\sigma} = \frac{t'}{a_\sigma}\bigg|_0^{\tau} = \frac{\tau'}{a_\sigma} \tag{A-5}$$

Substituting Eqs. (A-4) and (A-5) into Eq. (4) we get

$$\varepsilon(t) = g_0 D_0 \sigma_a U(\tau'-a) + g_1 \int_{0^-}^{t} \Delta D\left(\frac{t-\tau'}{a_\sigma}\right) g_2\sigma_a\delta(\tau'-a)d\tau' \tag{A-6}$$

Upon integration, the constitutive equation becomes

$$\varepsilon(t) = g_0 D_0 \sigma_a + g_1 g_2 \Delta D\left(\frac{t-t_a}{a_\sigma}\right)\sigma_a \tag{A-7}$$

for all $t>t_a$. Note that the time-dependent portion of the compliance is a function of the ratio of $(t-t_a)$ and a_σ, which is reduced time.

Multiple Step Inputs

A slightly more complicated case than that just presented is the two-step input shown in Figure A-2.

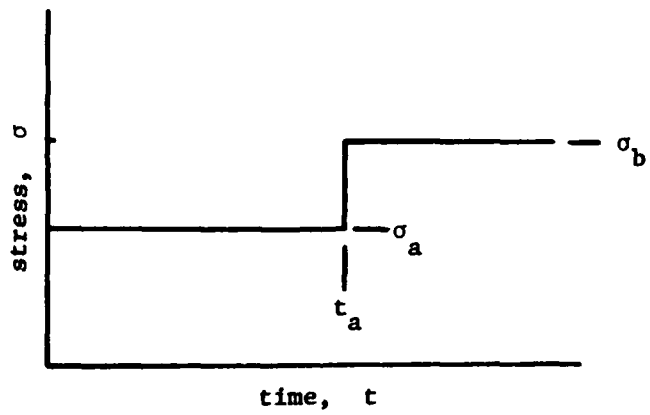

Figure A-2. Plot of stress versus time for a two-step input

In order to write a constitutive equation for $t>t_a$, we must consider the loading as consisting of three parts: $+\sigma_a$ applied at time $t=0$ and remaining unchanged, $-\sigma_a$ applied at time $t=t_a$ and remaining unchanged thereafter throughout the remaining lifetime, and $+\sigma_b$ applied at time $t=t_a$ and also remaining unchanged thereafter throughout the remaining lifetime. The corresponding constitutive equation using Eq. (4) is

$$\varepsilon(t) = g_0^a D_0(\sigma_a) + g_1^b \int_{0^-}^{t} \Delta D(\Psi-\Psi') g_2^a(\sigma_a)\delta(\tau')d\tau' +$$

$$g_0^a D_0(-\sigma_a) + g_1^b \int_{0^-}^{t} \Delta D(\Psi-\Psi') g_2^a(-\sigma_a)\delta(\tau'-a)d\tau' + \qquad \text{(A-8)}$$

$$g_0^b D_0(\sigma_b) + g_1^b \int_{0^-}^{t} \Delta D(\Psi-\Psi') g_2^b(\sigma_b)\delta(\tau'-a)d\tau'$$

where the substitution defined by Eq. (A-4) has been made. Note that the superscripts on the terms g_0, g_1, and g_2 denote which stress level they are associated with. Upon integration and cancelling terms, Eq. (A-8) becomes

$$\varepsilon(t) = g_1^b \Delta D(\Psi-\Psi_1') g_2^a \sigma_a - g_1^b \Delta D(\Psi-\Psi_2') g_2^a \sigma_a + \qquad \text{(A-9)}$$

$$g_0^b D_0 \sigma_b + g_1^b g_2^b \Delta D(\Psi-\Psi_2')\sigma_b$$

where the reduced time Ψ is

$$\Psi = \int_0^{t_a} \frac{dt'}{a_\sigma^a} + \int_{t_a}^{t} \frac{dt'}{a_\sigma^b} = \frac{t_a}{a_\sigma^a} + \frac{t-t_a}{a_\sigma^b} \qquad \text{(A-10a)}$$

$$\Psi_1' = \int_0^{\tau'} \frac{dt'}{a_\sigma^a} = \frac{\tau'}{a_\sigma^a} = 0 \qquad \text{(A-10b)}$$

$$\Psi_2' = \int_0^{t_a} \frac{dt'}{a_\sigma^a} + \int_{t_a}^{\tau'} \frac{dt'}{a_\sigma^b} =$$

$$\frac{t_a}{a_\sigma^a} + \frac{\tau'-t_a}{a_\sigma^b} = \frac{t_a}{a_\sigma^a} \qquad \text{(A-10c)}$$

The equations (A-10b) and (A-10c) have been evaluated at $\tau'=0$ and $\tau'=t_a$ respectively, corresponding to the times at which each load was applied. This is because the delta function in the intergrand in Eq. (A-8) is zero everywhere except at values of τ' corresponding to the load application.

Substituting Eqs. (A-10) into Eq. (A-9) we get

$$\varepsilon(t) = g_1^b g_2^a \Delta D\left(\frac{t_a}{a_\sigma^a} + \frac{t-t_a}{a_\sigma^b}\right)\sigma_a - g_1^b g_2^a \Delta D\left(\frac{t-t_a}{a_\sigma^b}\right)\sigma_a + g_0^b D_0 \sigma_b + g_1^b g_2^b \Delta D\left(\frac{t-t_a}{a_\sigma^b}\right)\sigma_b \tag{A-11}$$

After rearranging terms, Eq. (A-11) becomes

$$\varepsilon(t) = g_0^b D_0 \sigma_b + g_1^b g_2^b \Delta D\left(\frac{t-t_a}{a_\sigma^b}\right)\sigma_b - g_1^b g_2^a \Delta D\left(\frac{t-t_a}{a_\sigma^b}\right)\sigma_a + g_1^b g_2^a \Delta D\left(\frac{t_a}{a_\sigma^a} + \frac{t-t_a}{a_\sigma^b}\right)\sigma_a. \tag{A-12}$$

<u>Recovery</u>

If Eq. (A-12) is used where σ_b is equal to zero, as shown by Figure A-3, then the constitutive equation for the recovery portion of the creep curve can be written as

$$\varepsilon_r(t) = g_1^b g_2^a \Delta D\left(\frac{t_a}{a_\sigma^a} + \frac{t-t_a}{a_\sigma^b}\right)\sigma_a - g_1^b g_2^a \Delta D\left(\frac{t-t_a}{a_\sigma^b}\right)\sigma_a. \tag{A-13}$$

When stresses are zero during the recovery portion of the creep curve, the constants g_1^b, g_2^b, and a_σ^b are all equal to one, indicating that the material behavior is linear viscoelastic. With these substitutions,

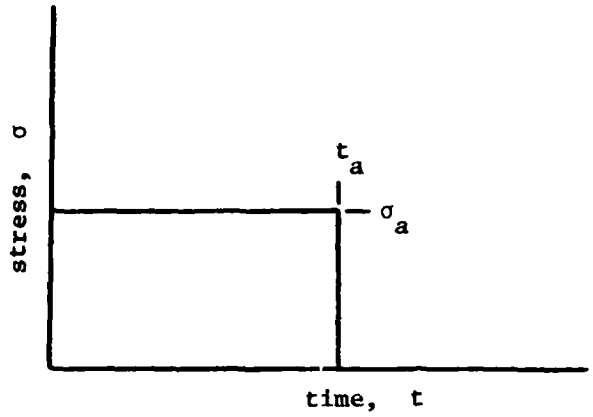

Figure A-3. Plot of stress versus time for a creep-recovery input

Eq. (A-13) becomes

$$\varepsilon_r(t) = g_2^a[\Delta D(\frac{t_a}{a_\sigma^a} + t-t_a) - \Delta D(t-t_a)]\sigma_a. \qquad \text{(A-14)}$$

While it is possible to represent the transient creep compliance $\Delta D()$ by almost any function, it is convenient to use a power law in time,

$$\Delta D(\Psi) \equiv C\Psi^n \ . \qquad \text{(A-15)}$$

Substitution of Eq. (A-15) into Eq. (A-14) gives

$$\varepsilon_r(t) = g_2^a \ C \ [(\frac{t_a}{a_\sigma^a} + t-t_a)^n - (t-t_a)^n] \ . \qquad \text{(A-16)}$$

Letting

$$\lambda = \frac{t-t_a}{t_a} \ , \qquad \text{(A-17)}$$

dropping the superscript a, substituting Eq. (A-17) into Eq. (A-16), and rearranging we get

$$\varepsilon_r(t) = Cg_2 t_a^n \ [(1+a_\sigma\lambda)^n - (a_\sigma\lambda)^n]\sigma_a \ . \qquad \text{(A-18)}$$

The amount of transient or creep strain just prior to the removal of the load at time t_a is defined as

$$\Delta\varepsilon_a = \varepsilon(t_a) - \varepsilon_0 = g_1 g_2 C(t_a)^n \sigma_a \tag{A-19}$$

where ε_0 is the initial or time-independent strain. Substituting Eq. (A-19) into Eq. (A-18) we get

$$\varepsilon_r(t) = \frac{\Delta\varepsilon_a}{g_1} [(1+a_\sigma\lambda)^n - (a_\sigma\lambda)^n]. \tag{A-20}$$

APPENDIX B

COMPUTER PROGRAM

The computer program, originally developed by Miller and Adams [14], uses simplex triangular elements and is based upon generalized plane strain conditions, which permit a pseudo-three-dimensional analysis. Nonlinear (elastoplastic) material behavior, modeled by Von Mises yield criterion and the Prandtl-Reuss flow rule, is incorporated by means of the tangent modulus method. This technique allows for the modeling of matrix materials which have "flat" or "nearly flat" stress-strain curves, such as aluminum.

Temperature- and moisture-induced strains are included as are material properties which are a function of temperature and moisture. The efficiency of the current micromechanics computer program lies within a method which allows all external tractions to be applied and solved for simultaneously. This method also permits changes in temperature and moisture to be applied simultaneously with changes in load during the same increment. This avoids the problem of having to solve for each loading component independently and using superposition to obtain the total solution.

Time-dependence, incorporated by means of initial strains [15], uses the constitutive equations presented in Chapter III. Application of any load, temperature, or moisture increments must occur in the time-independent steps. That is, no changes in load, temperature, or moisture are allowed to occur during a time increment.

A block diagram of the computer program is shown in Figure B-1. When this diagram is compared to the one in Reference [14], the only significant difference is the additional subroutine which contains the viscoelastic parameters. This feature allows the user to merely substitute a modified subroutine in order to simulate a different viscoelastic matrix material.

The program previously required the modification of another subroutine in order to model a different matrix and/or fiber in a composite. With the addition of time-dependence, there are now two subroutines which require modification in order to model a different composite material.

A typical computer run involves initialization of several parameters in the subroutine MAIN. Next, mesh data which includes node point coordinates, element numbers, element material types, and the node boundary conditions, are read into the program by subroutine GDATA. The grid used in the program is set up for 40 percent fiber volume; however, subroutine MADJ automatically recalculates the node point coordinates for any fiber volume desired. Subroutine MAIN then calls subroutine LOAD, which reads the first increment of temperature, moisture, or load. This subroutine in turn calls FORMK, which assembles the global stiffness matrix using the elastic material properties subroutine ELPROP if the element is in the linear range, or the plastic material properties subroutine PLPROP if the element is in the nonlinear (elastoplastic) range. For the first increment, the behavior is automatically assumed to be linear. Should a succeeding increment be a time increment, the elastic material properties subroutine ELPROP is called (to get certain time-

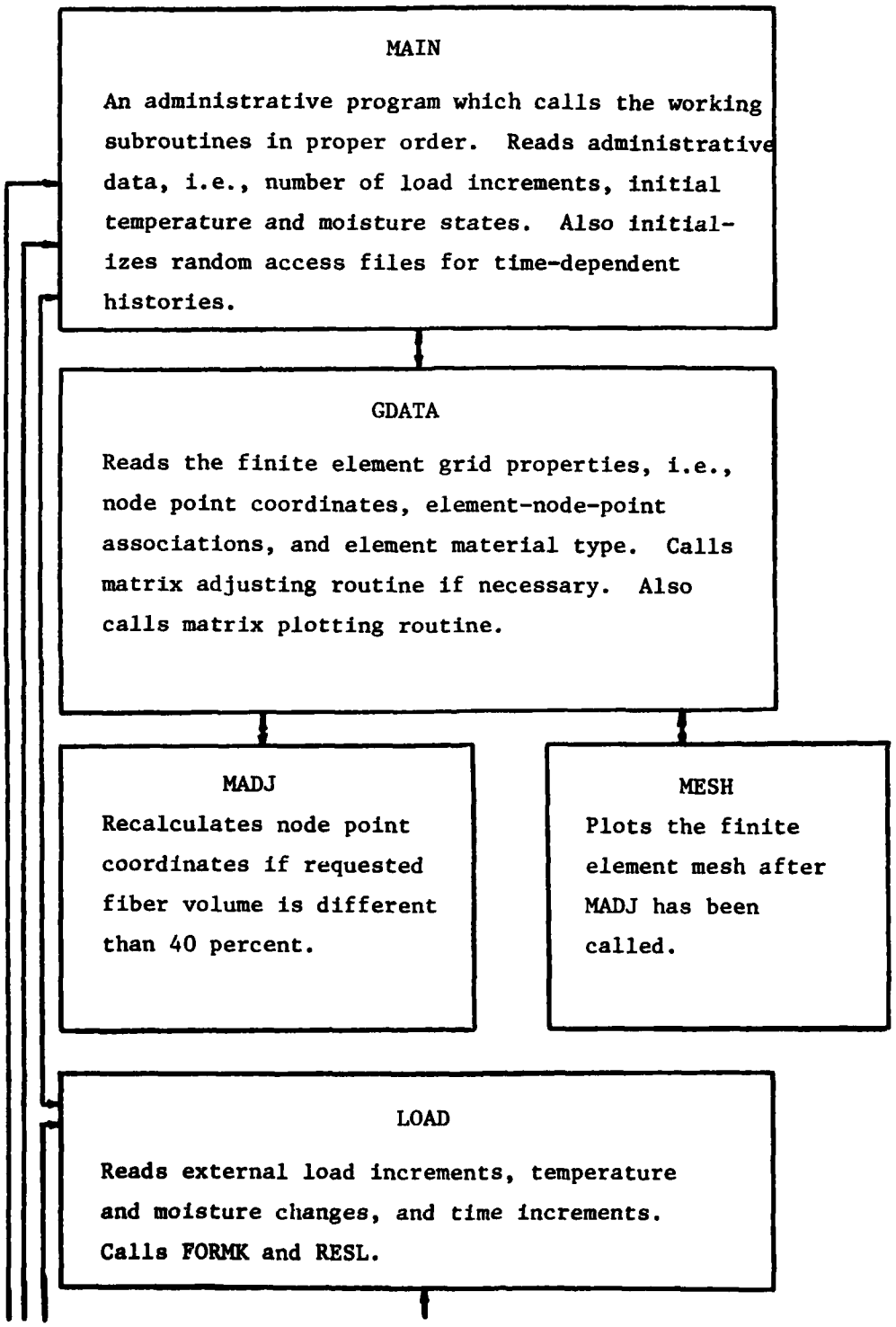

Figure B-1. Analysis Procedure Flowchart
(continued on the following page)

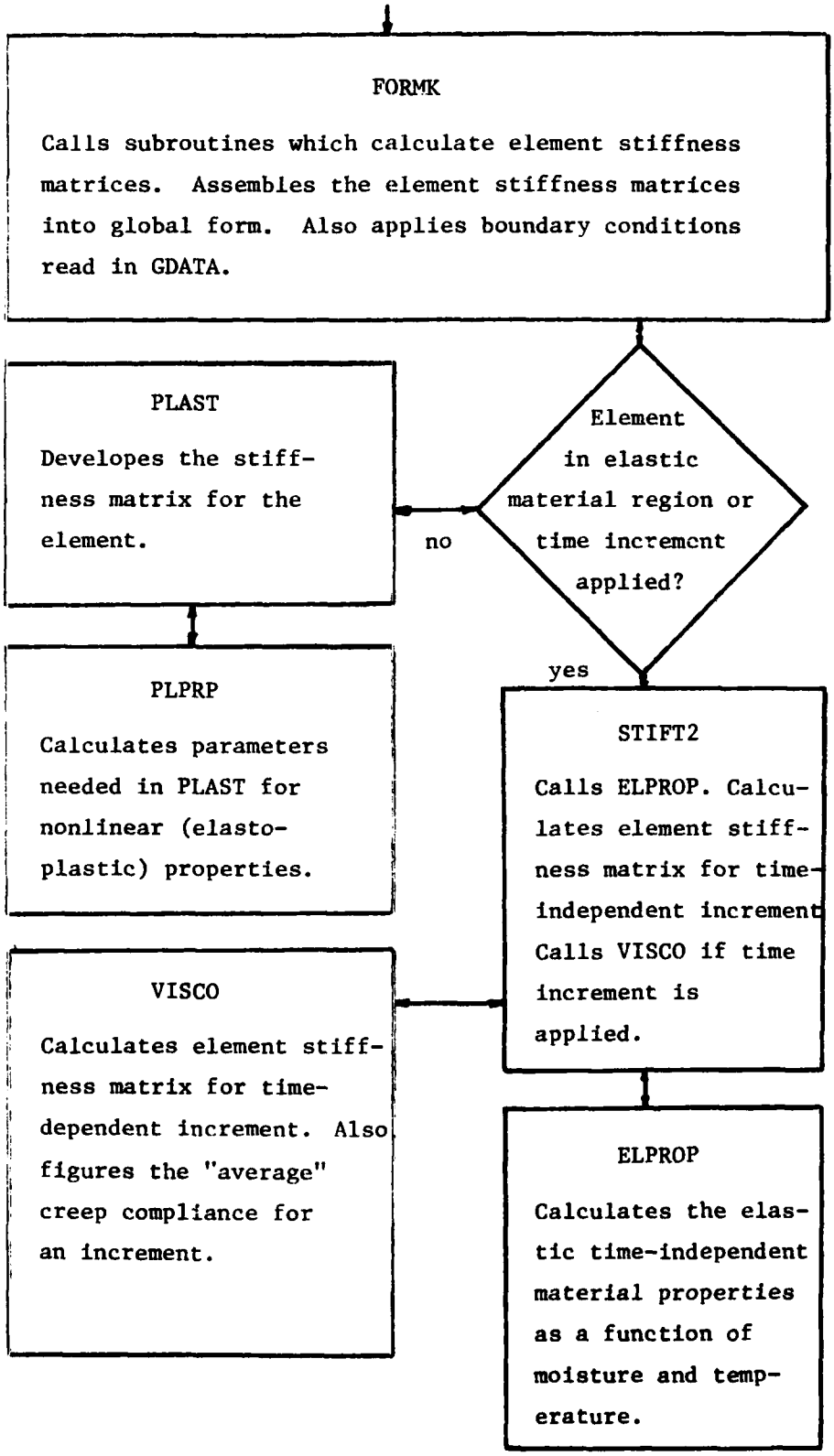

Figure B-1. (continued) Analysis Procedure Flowchart

(continued on the following page)

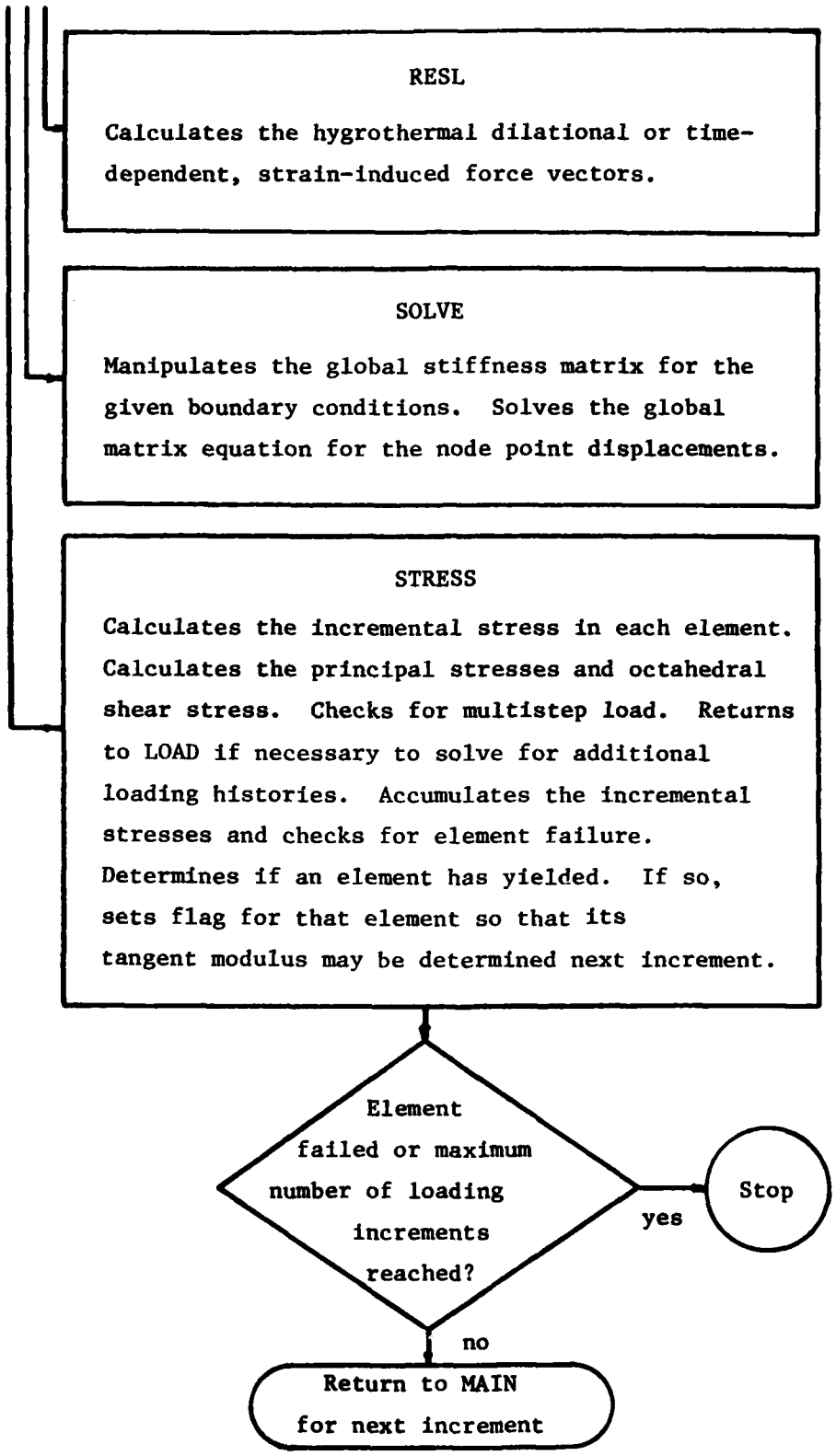

Figure B-1. (continued) Analysis Procedure Flowchart

independent parameters) and then the time-dependent materials property subroutine VISCO is called. This subroutine calculates the elemental stiffness matrix (Eq. 14) and the incremental creep compliance.

When formulation of the global stiffness matrix is complete, subroutine RESL calculates incremental node point forces (Eq. 15) for temperature, moisture or time increments. Inversion of the global stiffness matrix and solution for the node displacements occurs in subroutine SOLVE. The incremental stresses are then calculated in subroutine STRESS. This subroutine also calculates the octahedral shear stress and strain and checks for yielding and/or failure of an element. If no elements have failed, the program returns to MAIN for another increment. This process is repeated until all increments are exhausted, or an element fails, at which time the program automatically terminates.

In order to model a multistep input such as shown in Figure 6, the history of each load step must be kept track of independently. A scheme using a random access file technique was developed for this purpose. By using this method, large arrays necessary for storage of each stress history were not needed. Thus, it was only necessary to increase the core requirements of the previous micromechanics program in Reference [14] by some two percent.

An example of this scheme is as follows. Initial load, temperature, and moisture changes which occur in several time-independent increments produce certain stresses in each element. As these increments are applied, the elemental stresses are accumulated and stored in a file called FILE ONE. When the first time increment is applied, the contents of FILE ONE are copied into another file called FILE FIFTY. This file

is saved for later use when the load, temperature or moisture is again incremented. As succeeding time increments are applied, incremental stresses due to creep (if any) are accumulated in FILE ONE. At this point, the stresses in FILE ONE are the total stresses in each element. When more increments of load, temperature or moisture are applied, simulating a step input, the stresses which are contained in FILE FIFTY are copied into another file called FILE TWO, with a change of sign on each stress. This serves to simulate the pseudo application of a $-\sigma_a$ stress, as discussed relative to multistep loadings in Chapter III. At the same time, the contents of FILE FIFTY are copied into another file called FILE THREE. As the time-independent increments of load, temperature, or moisture are applied, the stresses are accumulated in FILE THREE. When the next time increment is applied, the contents of FILE THREE are copied over the contents of FILE FIFTY. Thus, for each element an initial "$+\sigma_a$ stress history" beginning at time $t=0$ corresponding to FILE ONE, a "$-\sigma_a$ stress history" beginning at time $t=t_a$ corresponding to FILE TWO, and a "$+\sigma_b$ stress history" beginning at time $t=t_a$ corresponding to FILE THREE is recorded. A third step load in time similar to that shown in Figure 6 at say, time $t=t_b$ would require two more files, FILE FOUR for a "$-\sigma_b$ stress history" occuring at time $t=t_b$, and FILE FIVE for a "$+\sigma_c$ stress history" occuring at time $t=t_b$. Similarly, extra step loads would require the addition of two files per step.

The solution for a time increment for times $t_a<t<t_b$ in Figure 6 requires incremental creep stresses to be calculated for each stress history; in this case there are three. These incremental stresses are accumulated in their respective files and all files, i.e., ONE, TWO, and

THREE are summed at the end of an inrement to give the total stress for each element. This procedure is then repeated for additional increments.

APPENDIX C

EXPERIMENTAL RESULTS

The following Figures (C-1 through C-10) are actual computer plots of creep-recovery data for Hercules 3501-6 epoxy resin. All plots at each stress level were similar and for brevity only two of the three plots for each stress level tested are shown. While the data are relatively smooth for the higher stress levels, they are quite irregular for the lower values of applied stress. This is due primarily to the lower output of strain shown by the specimens subjected to a lower stress. A smaller output requires the extensometer to be set on a more sensitive scale and consequently, the extensometer is also more sensitive to voltage fluctuations, noise levels, etc. The plots also appear quite irregular due to the limited number of data points taken. In these plots, a straight line was used to connect the data points. During the data reduction described in Chapter IV, a smooth curve should be drawn between these points.

Figures C-11 through C-15 are plots of the constitutive equations using the parameters g_0, g_1, g_2, and a_σ calculated from the creep-recovery data. The experimental creep data sampled by the computer for all three tests are indicated by the stars. The stress level given in the upper right-hand corner is the average of the applied stress for all three tests. There is excellent agreement between experiment and the constitutive equations except at the 15,000 psi stress level. By

examining Figure 10 in Chapter IV, the reason for this discrepancy is evident. The value for g_0D_0 obtained through data reduction and the value predicted by the curve in this plot are not the same, and since the constitutive equation plotted here uses the value predicted by the curve, there will obviously be some disagreement. The reason for this discrepancy in Figure 10 is not known at this time; however, the experimental data are suspect, as discussed in Chapter IV.

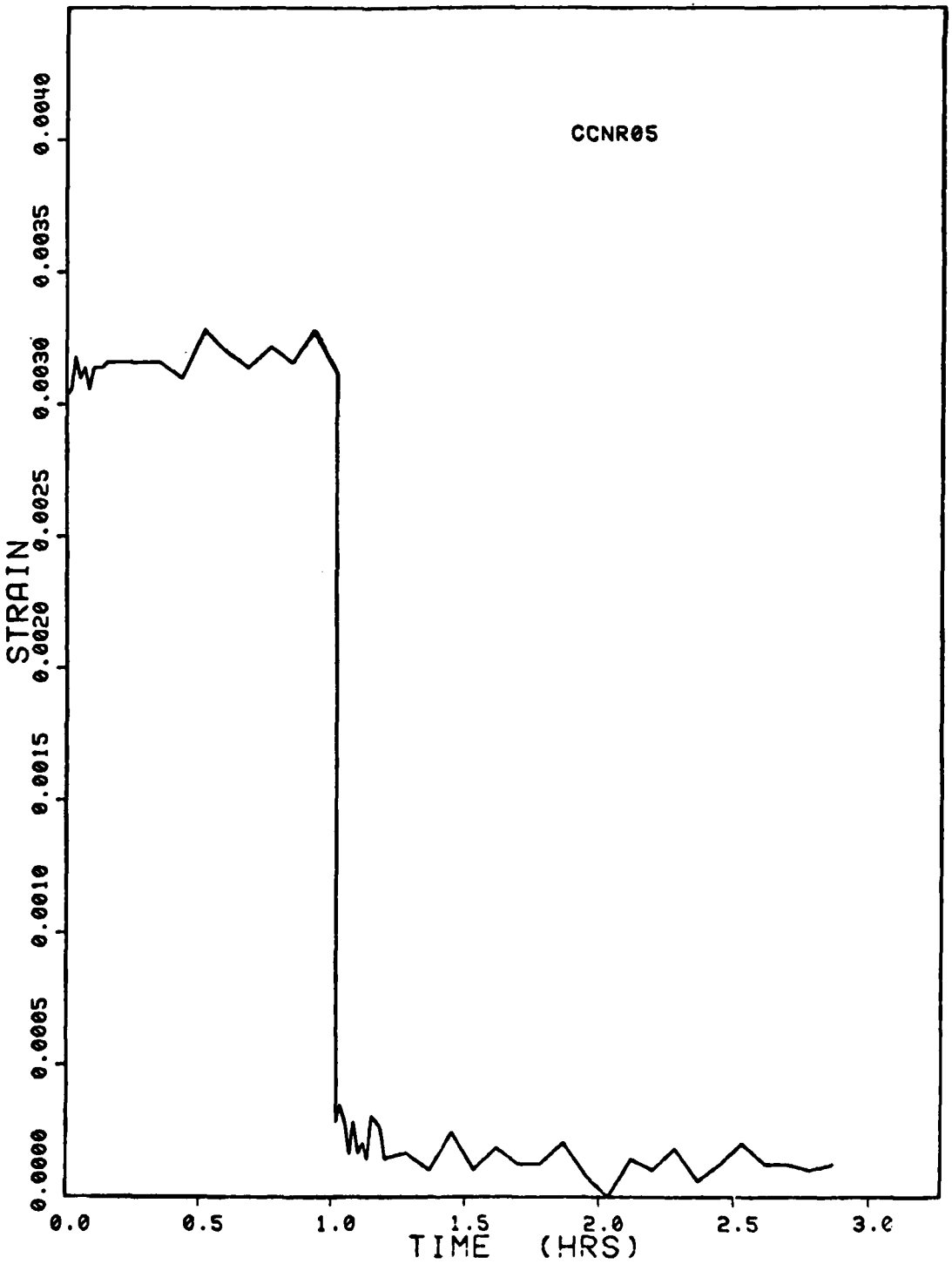

Figure C-1. Experimental creep-recovery data for Hercules 3501-6 epoxy resin subject to a 2000 psi uniaxial compressive stress.

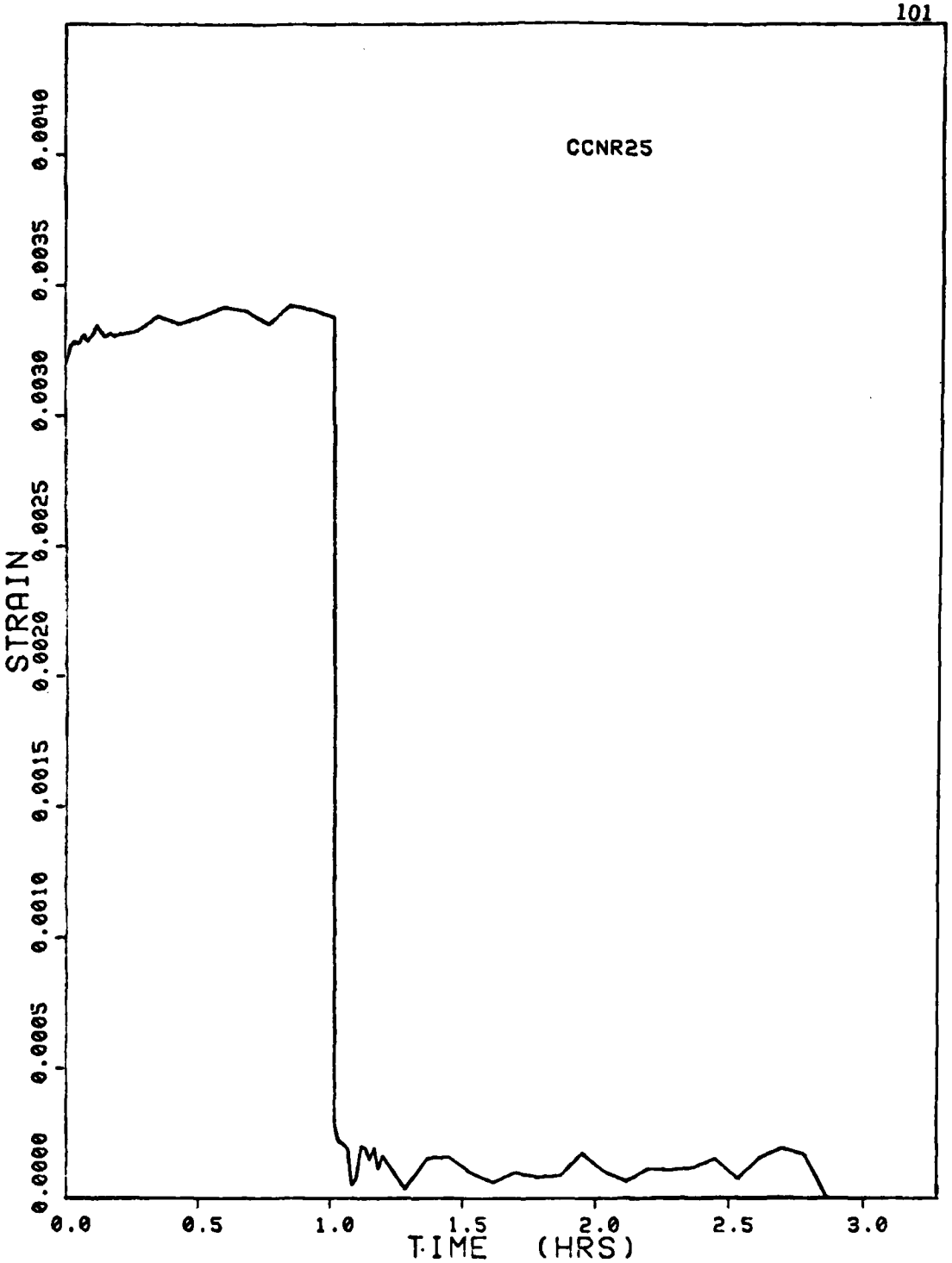

Figure C-2. Experimental creep-recovery data for Hercules 3501-6 epoxy resin subject to a 2000 psi uniaxial compressive stress.

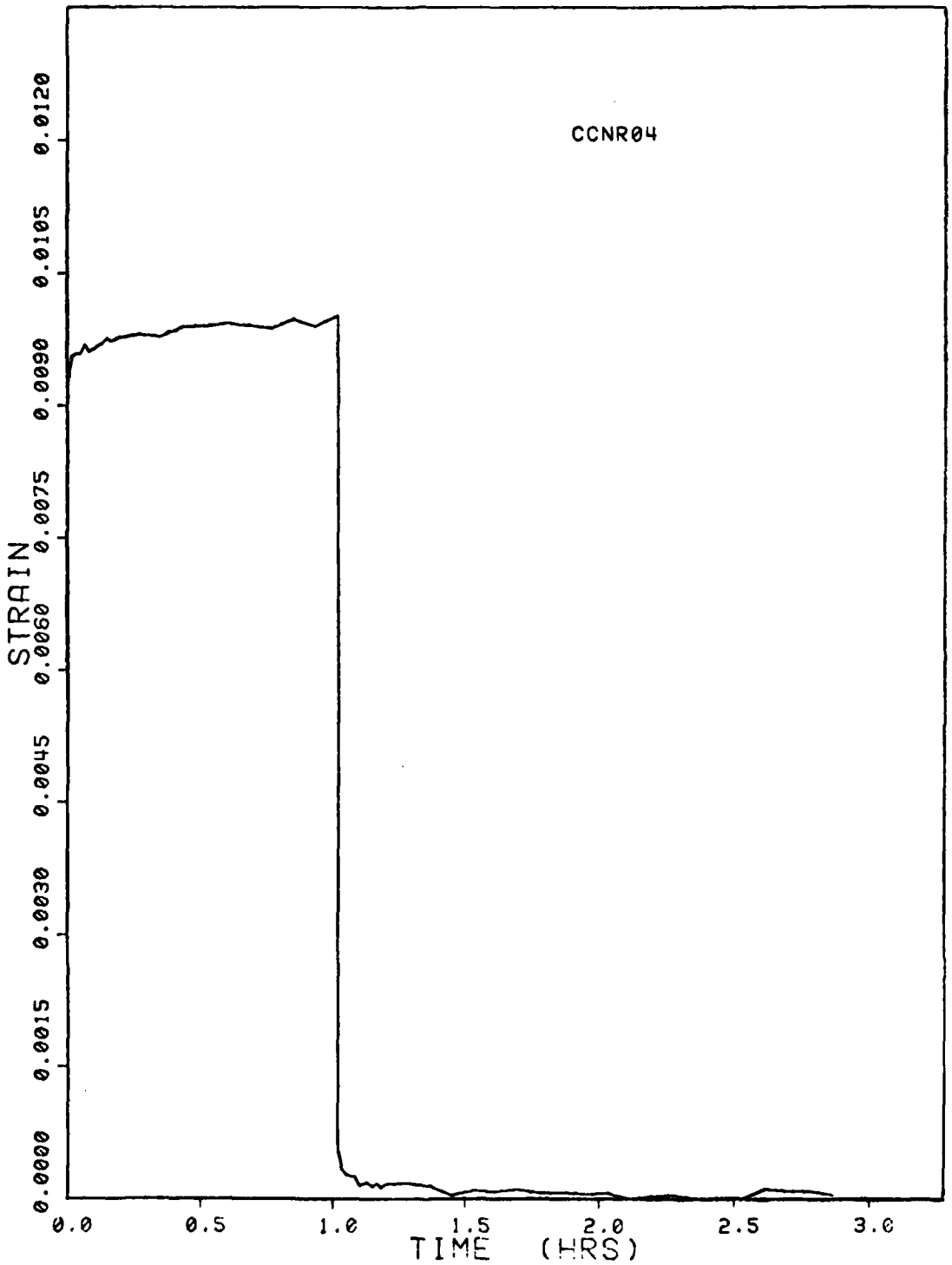

Figure C-3. Experimental creep-recovery data for Hercules 3501-6 epoxy resin subject to a 6000 psi uniaxial compressive stress.

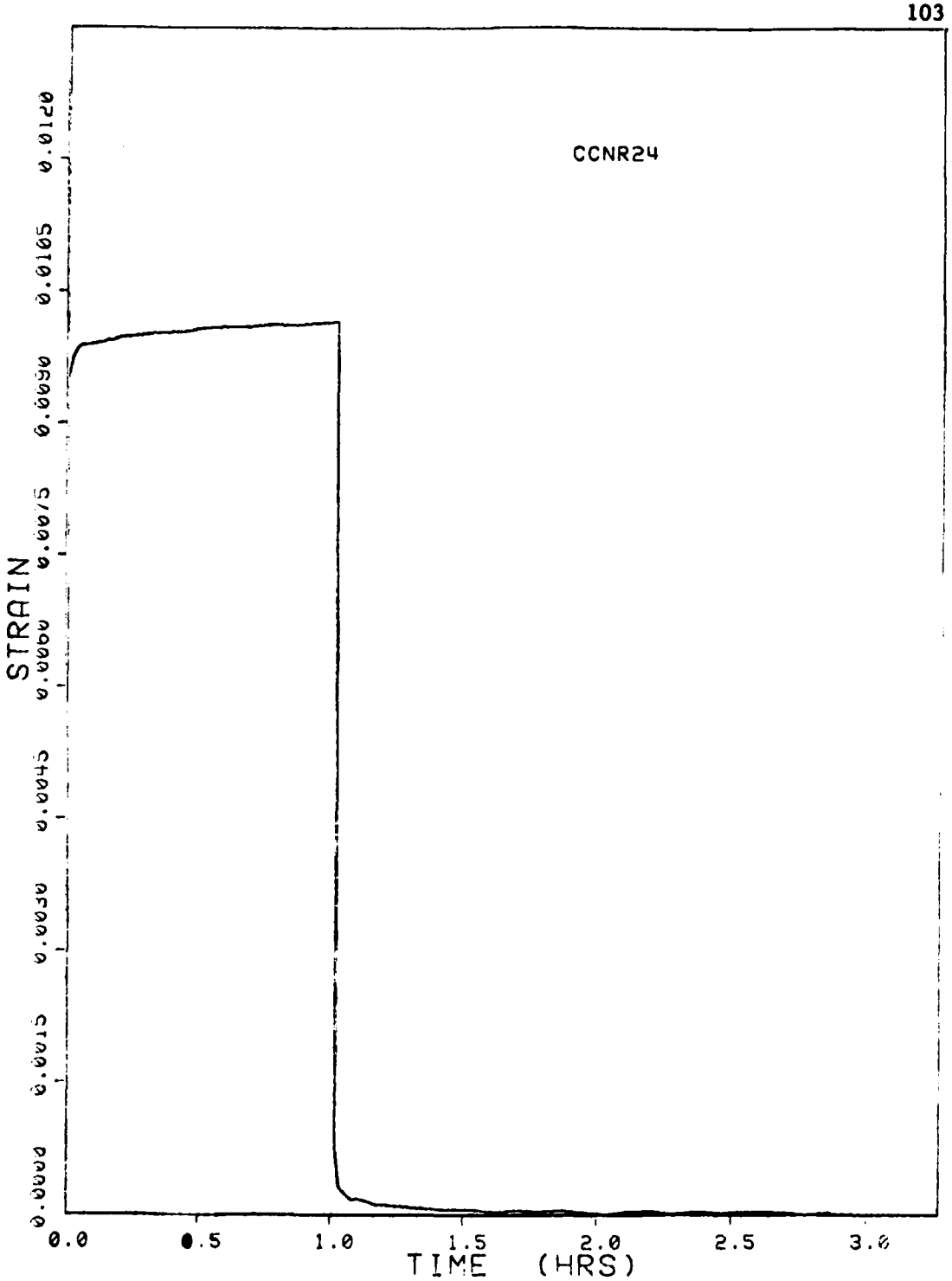

Figure C-4. Experimental creep-recovery data for Hercules 3501-6 epoxy resin subject to a 6000 psi uniaxial compressive stress.

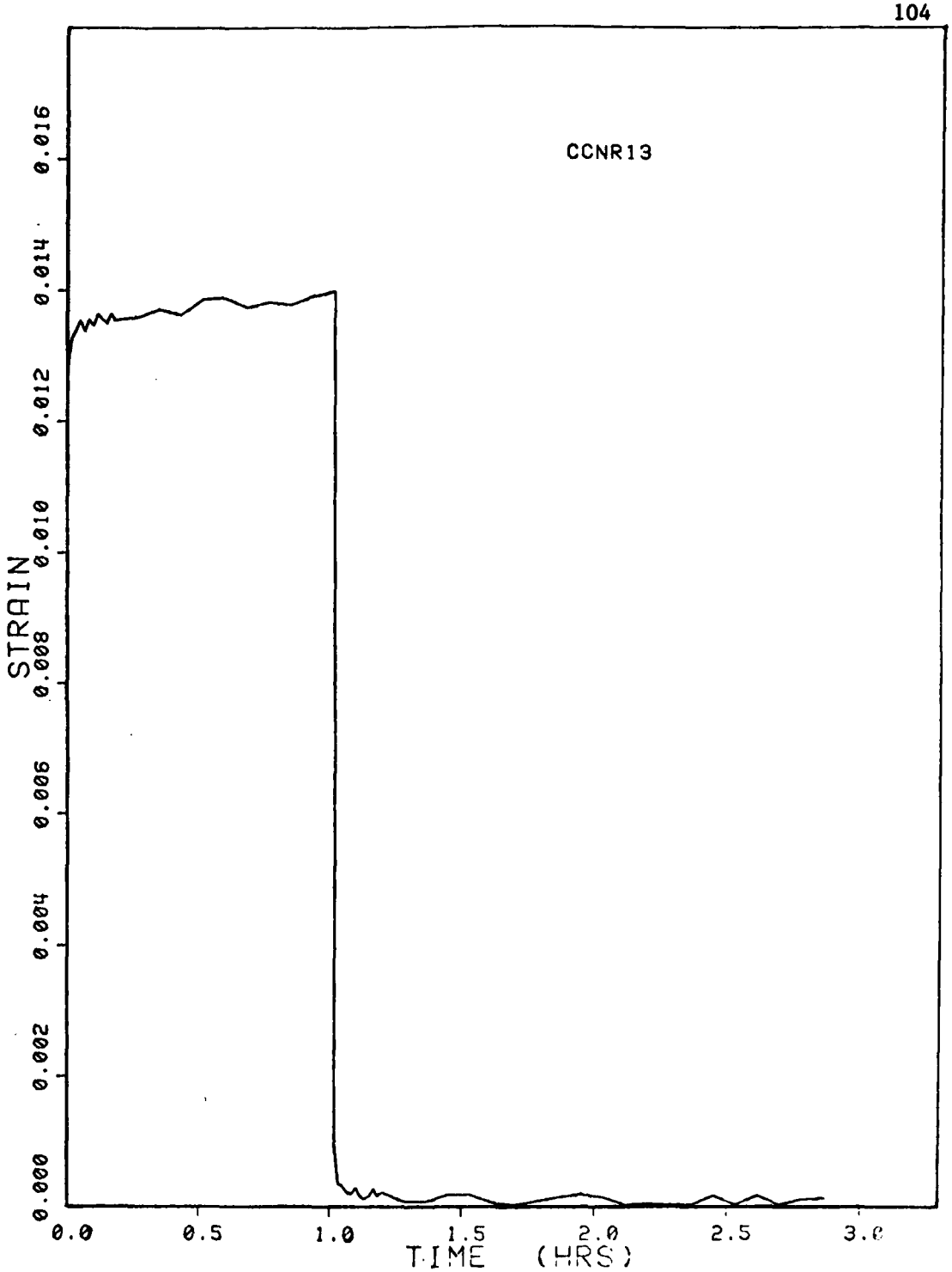

Figure C-5. Experimental creep-recovery data for Hercules 3501-6 epoxy resin subject to an 8000 psi uniaxial compressive stress.

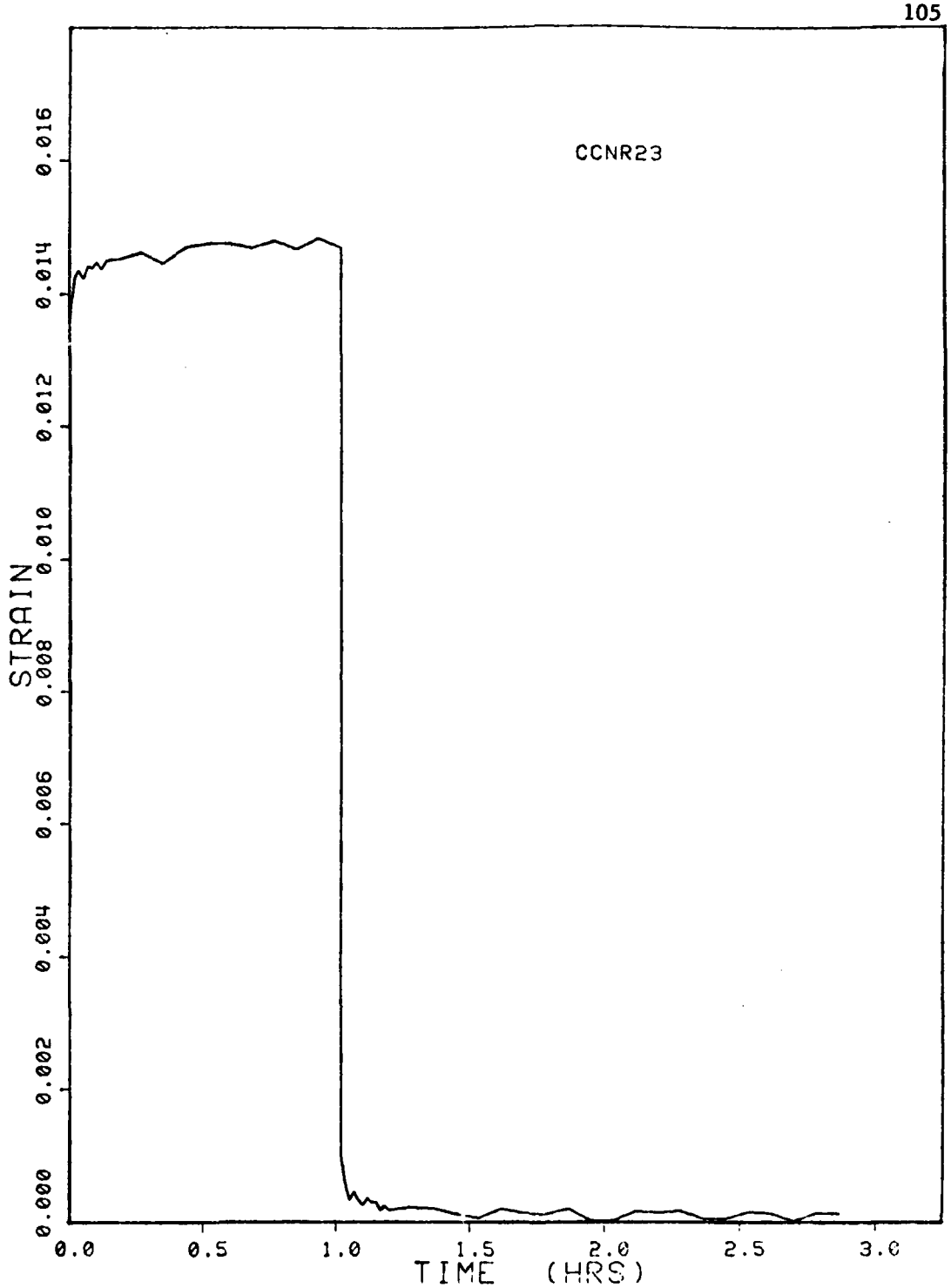

Figure C-6. Experimental creep-recovery data for Hercules 3501-6 epoxy resin subject to an 8000 psi uniaxial compressive stress.

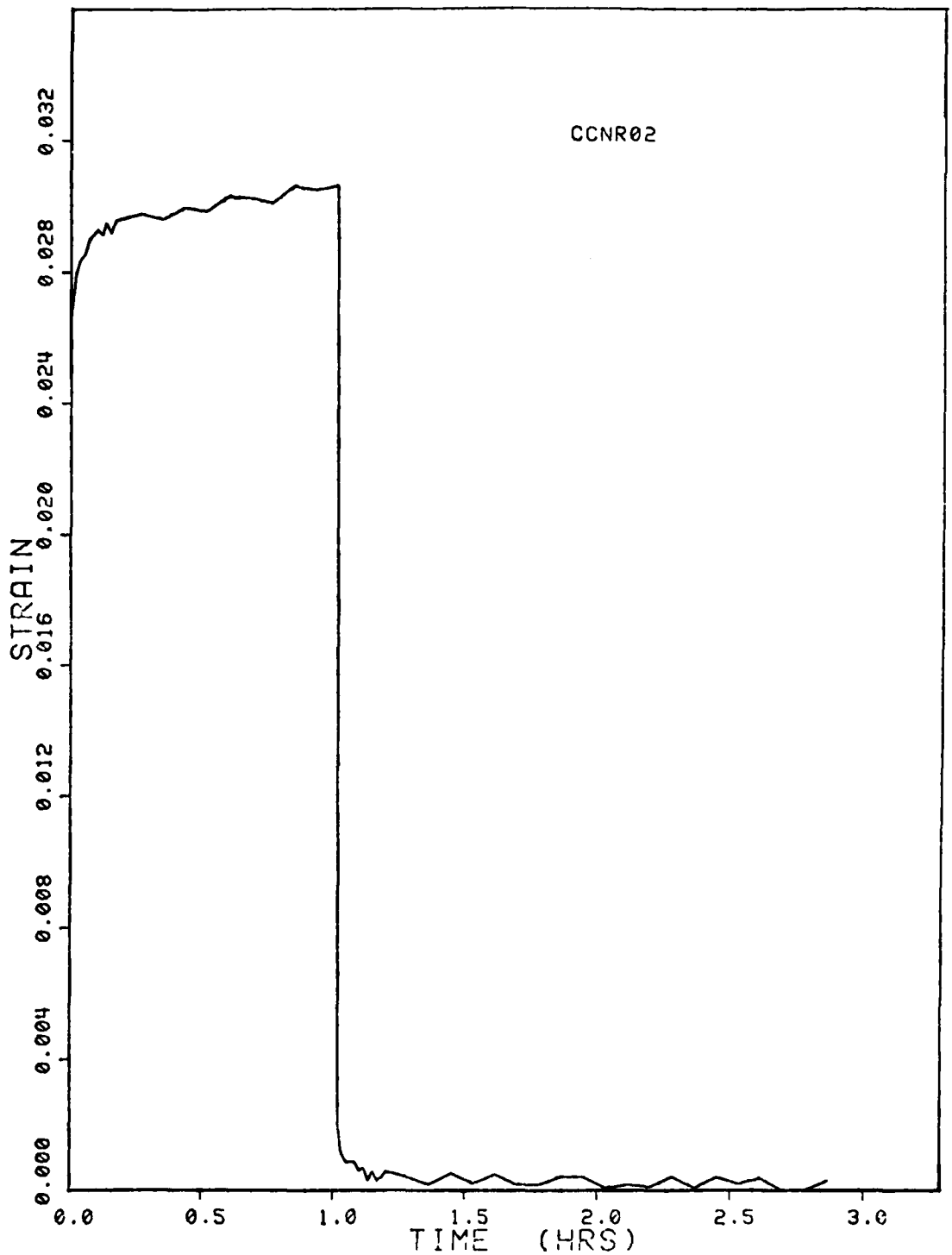

Figure C-7. Experimental creep-recovery data for Hercules 3501-6 epoxy resin subject to a 16,000 psi uniaxial compressive stress.

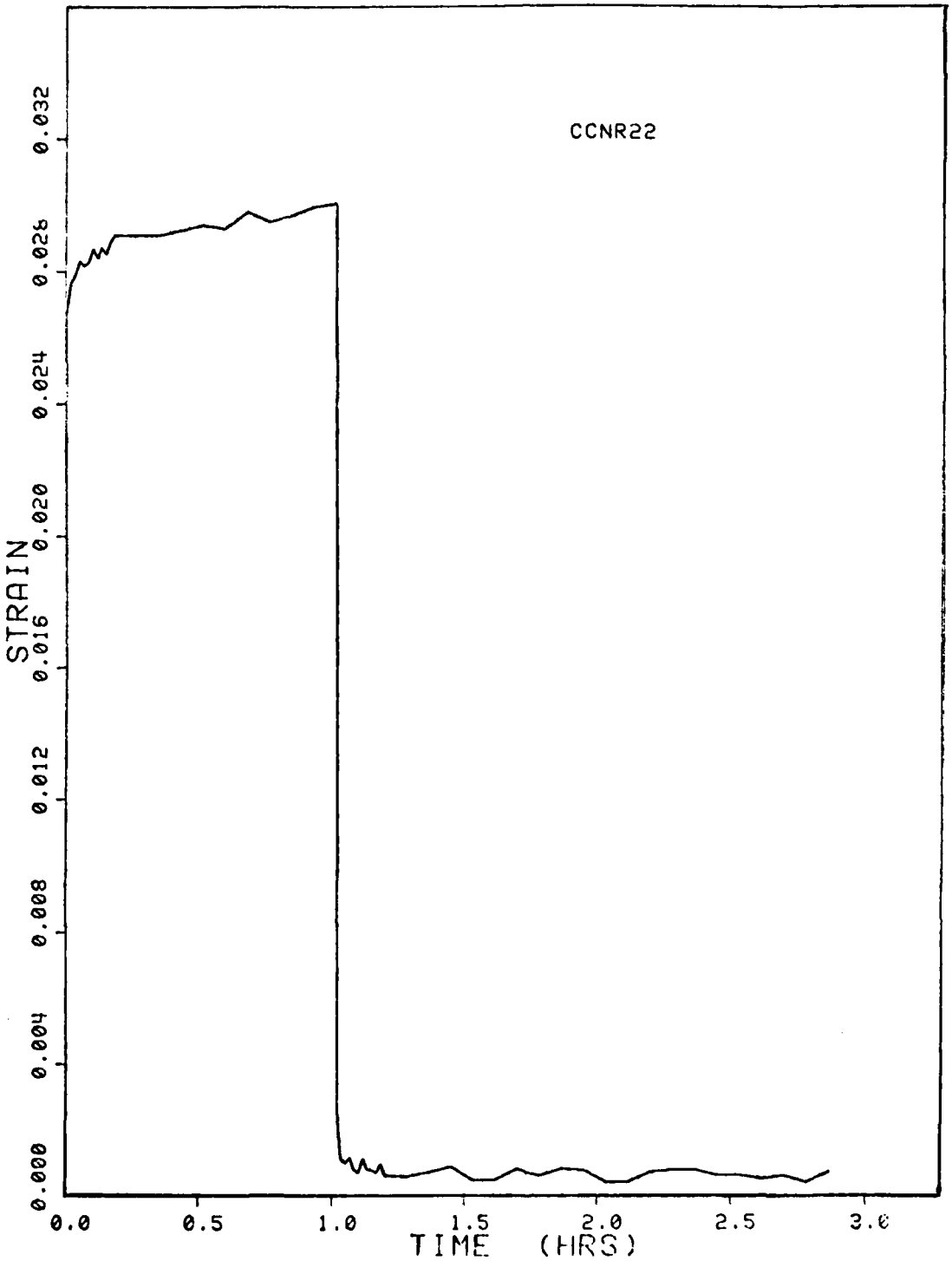

Figure C-8. Experimental creep-recovery data for Hercules 3501-6 epoxy resin subject to a 16,000 psi uniaxial compressive stress.

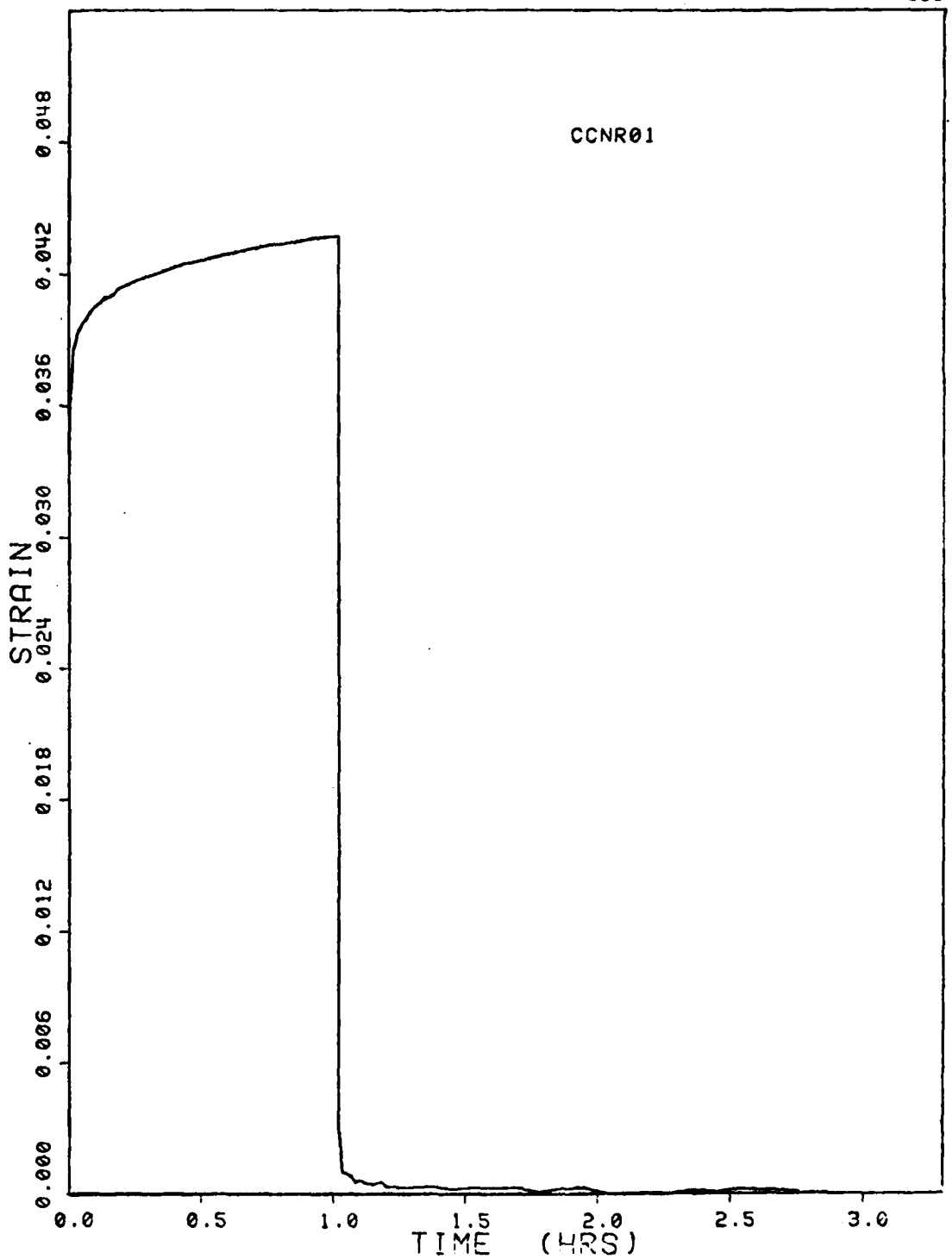

Figure C-9. Experimental creep-recovery data for Hercules 3501-6 epoxy resin subject to a 19,000 psi uniaxial compressive stress.

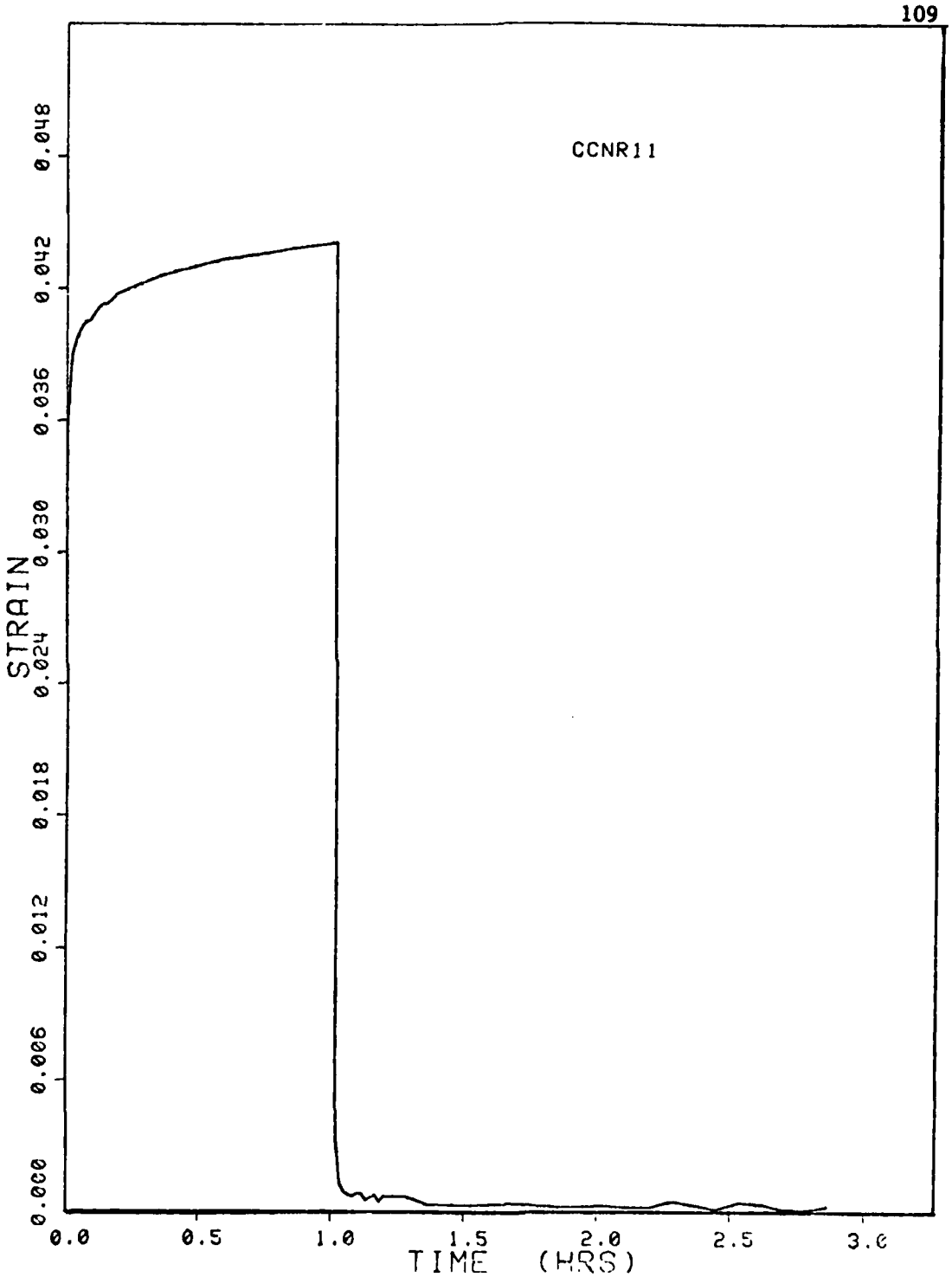

Figure C-10. Experimental creep-recovery data for Hercules 3501-6 epoxy resin subject to a 19,000 psi uniaxial compressive stress.

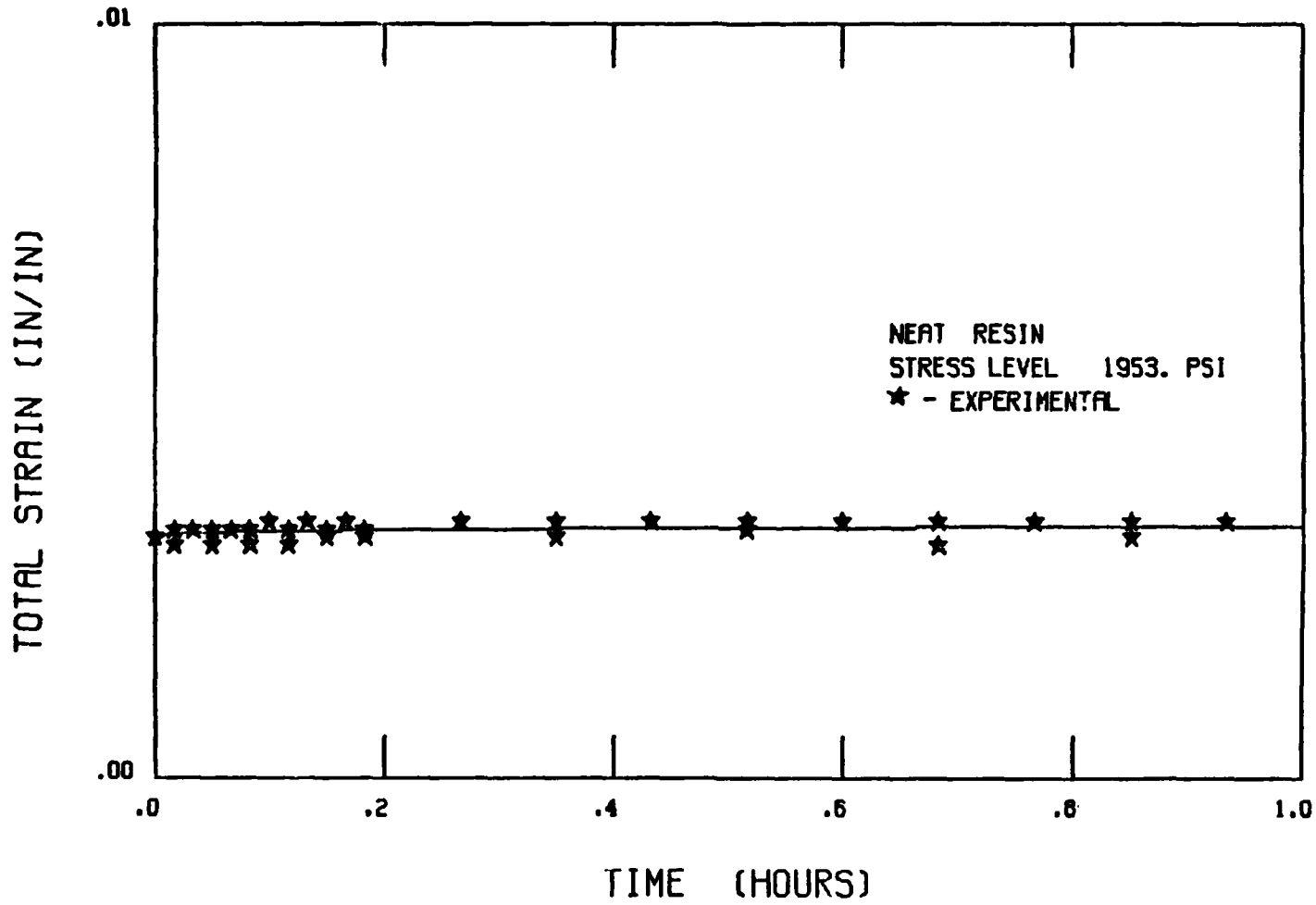

Figure C-11. Plot of strain versus time for Hercules 3501-6 epoxy resin subjected to a one hour creep test. Experimental values are shown by the stars while the solid line represents the constitutive equation.

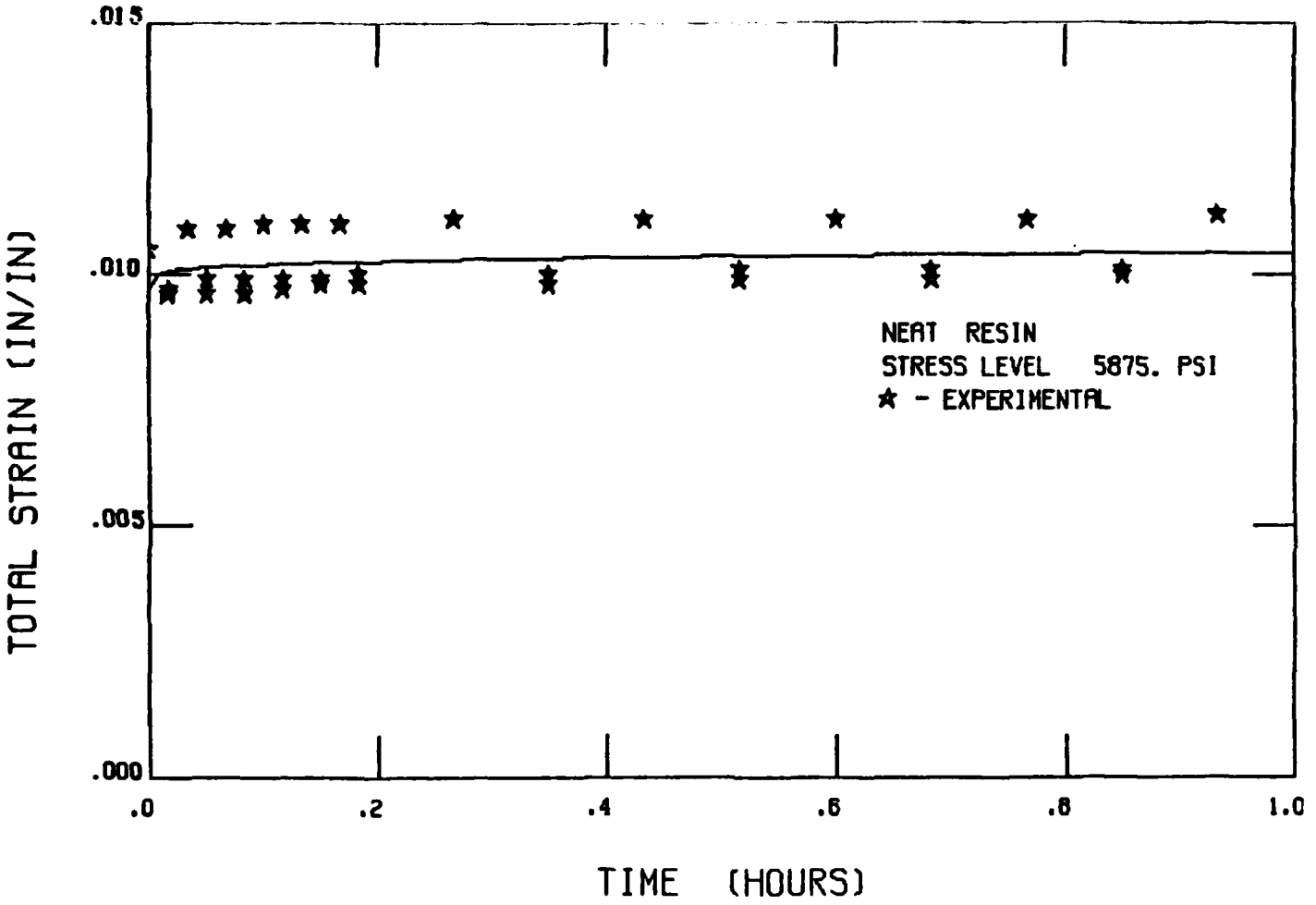

Figure C-12. Plot of strain versus time for Hercules 3501-6 epoxy resin subjected to a one hour creep test. Experimental values are shown by the stars while the solid line represents the constitutive equation.

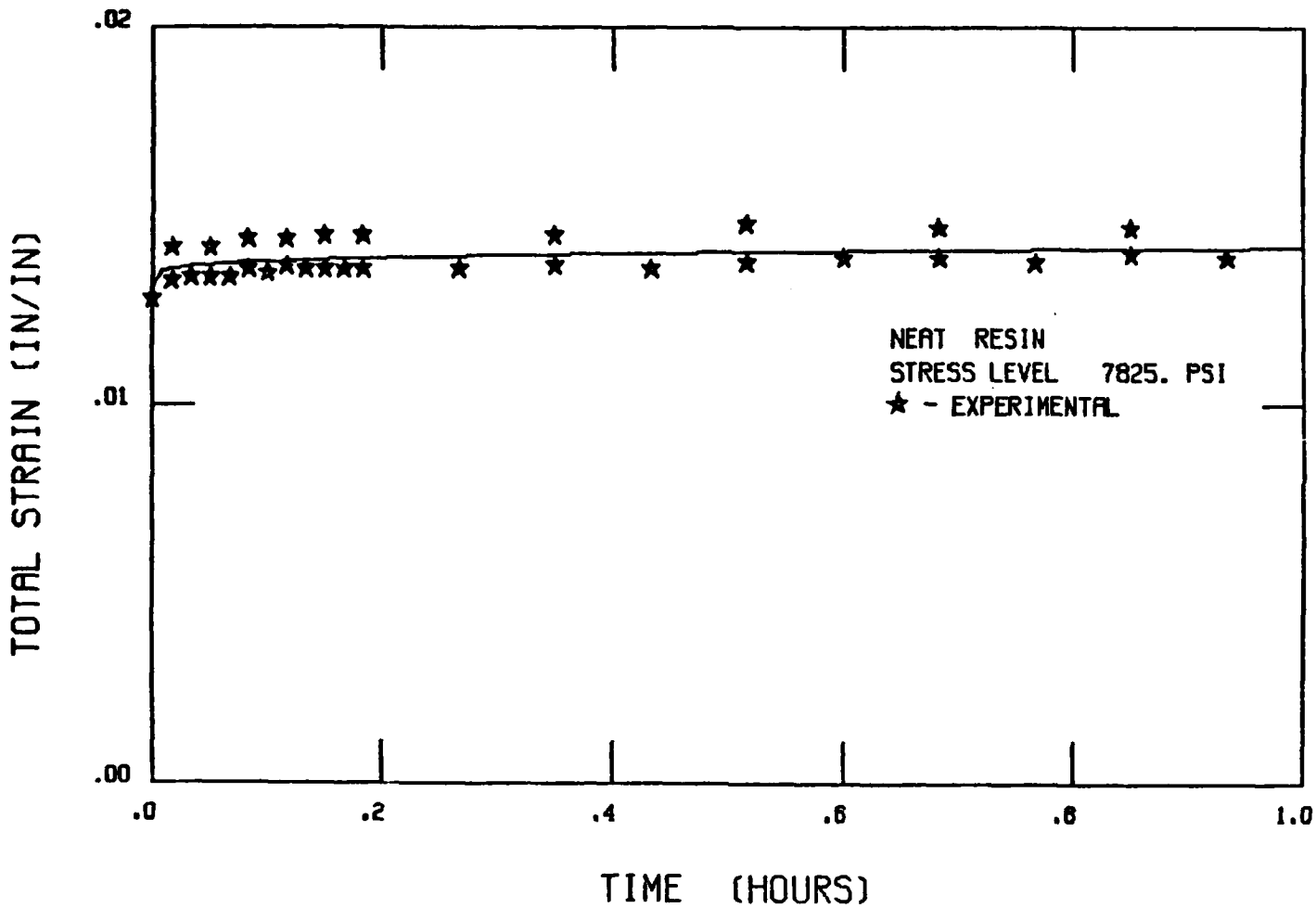

Figure C-13. Plot of strain versus time for Hercules 3501-6 epoxy resin subjected to a one hour creep test. Experimental values are shown by the stars while the solid line represents the constitutive equation.

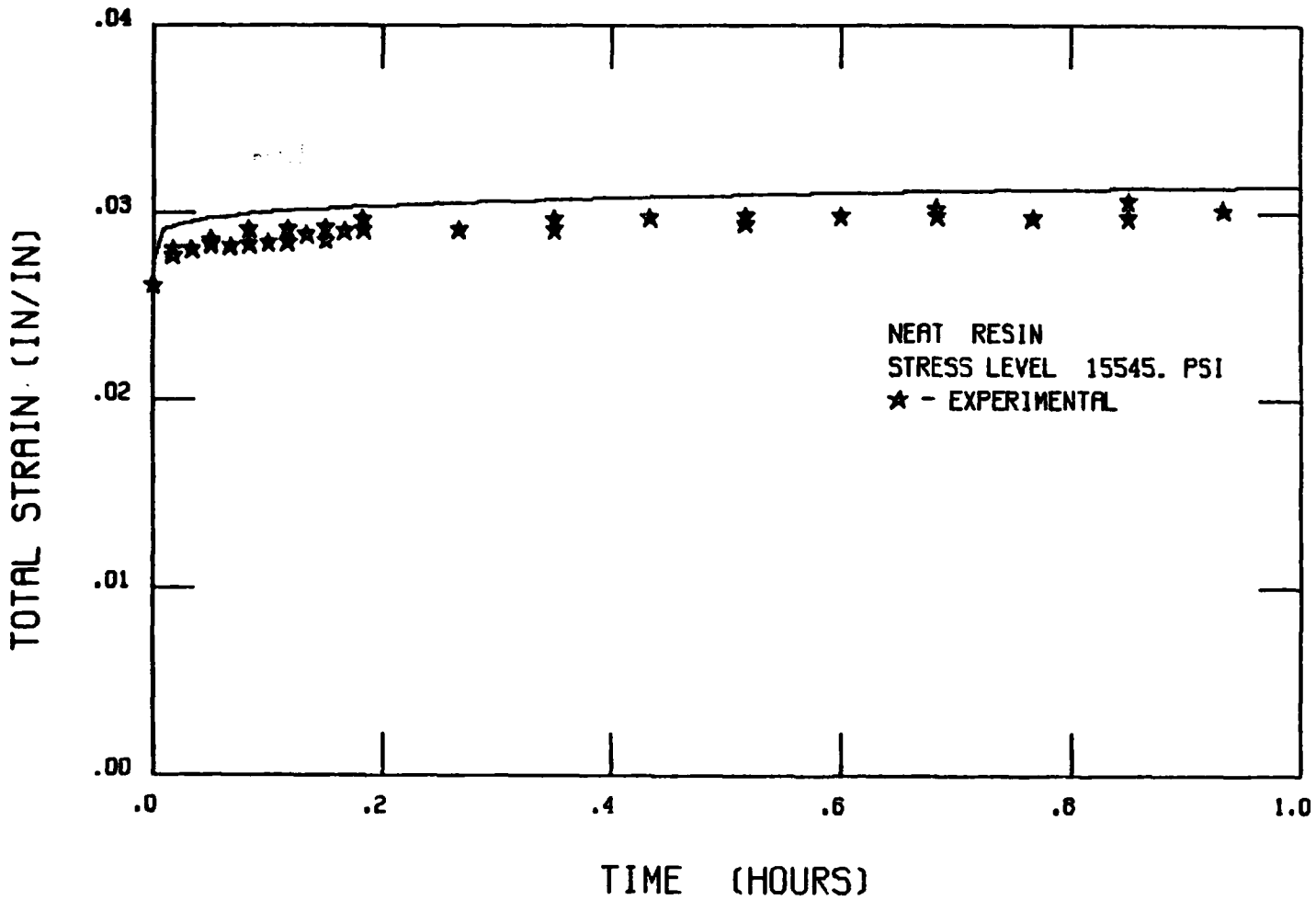

Figure C-14. Plot of strain versus time for Hercules 3501-6 epoxy resin subjected to a one hour creep test. Experimental values are shown by the stars while the solid line represents the constitutive equation.

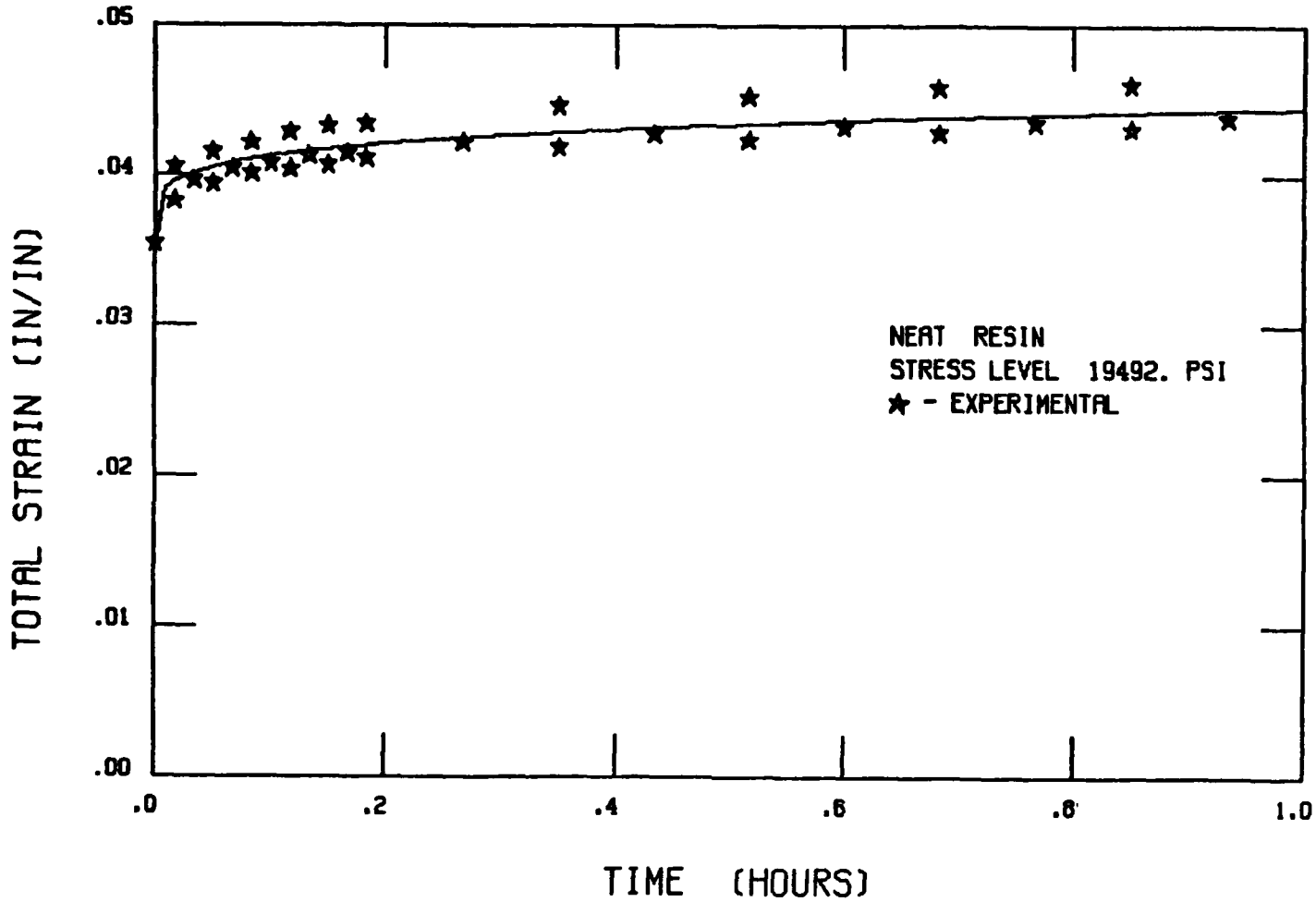

Figure C-15. Plot of strain versus time for Hercules 3501-6 epoxy resin subjected to a one hour creep test. Experimental values are shown by the stars while the solid line represents the constitutive equation.

APPENDIX D

NUMERICAL RESULTS

In Figures D-1 through D-6, predictions made for the Hercules 3501-6 epoxy resin using the computer program are plotted with the data which were input to the program. The predictions are represented by the symbols (squares) while the lines show the actual (input) response. The input response was obtained by using the constitutive equations and a hand calculator. Figures D-2, D-4, and D-6 are replotted from Figures D-1, D-3, and D-5, respectively, with the scales enlarged. This helps to magnify any errors present, which incidently are less than 6 percent in all cases.

Figures D-7 through D-18 are octahedral shear stress and strain, and normal and tangential interface stress plots for various examples presented in Chapter V. It should be mentioned that the octahedral shear stress plots have been "normalized" by dividing the contour values by the octahedral shear yield stress. This means that contour values greater than one indicate that the region has yielded. The octahedral shear yield stress is a function of temperature and moisture and was determined to be 5397 psi [27] for all plots shown except for Figures D-12a and D-12c. In these figures the temperature is 99°C, which is different from all other models where the temperature is 21°C. In this case the octahedral shear stress yield value is 2813 psi [27].

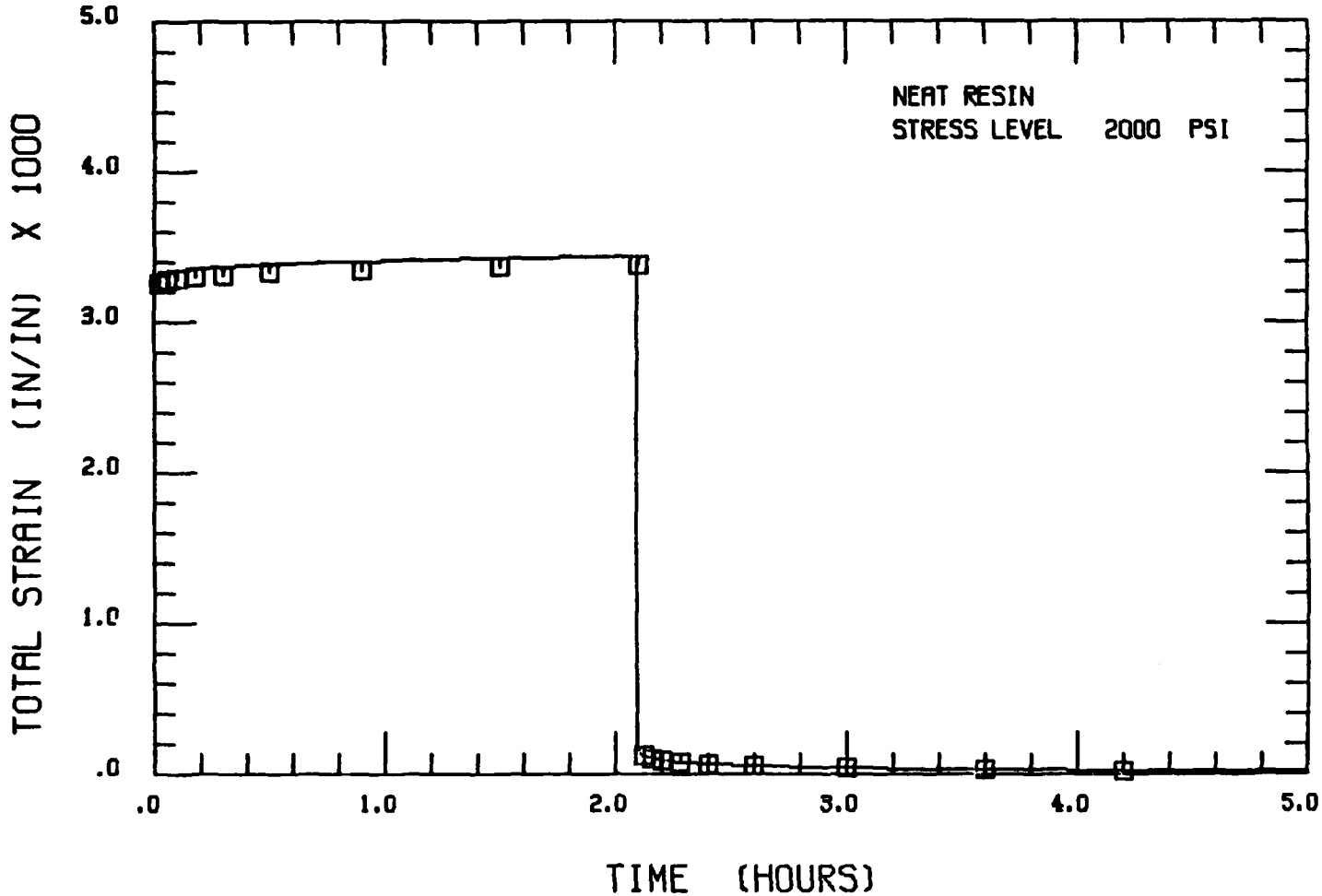

Figure D-1. Plot of strain versus time for Hercules 3501-6 epoxy resin subjected to a 2.1 hour creep and a 2.1 hour recovery test. Predicted values are shown by the symbols while the line represents the actual experimental response.

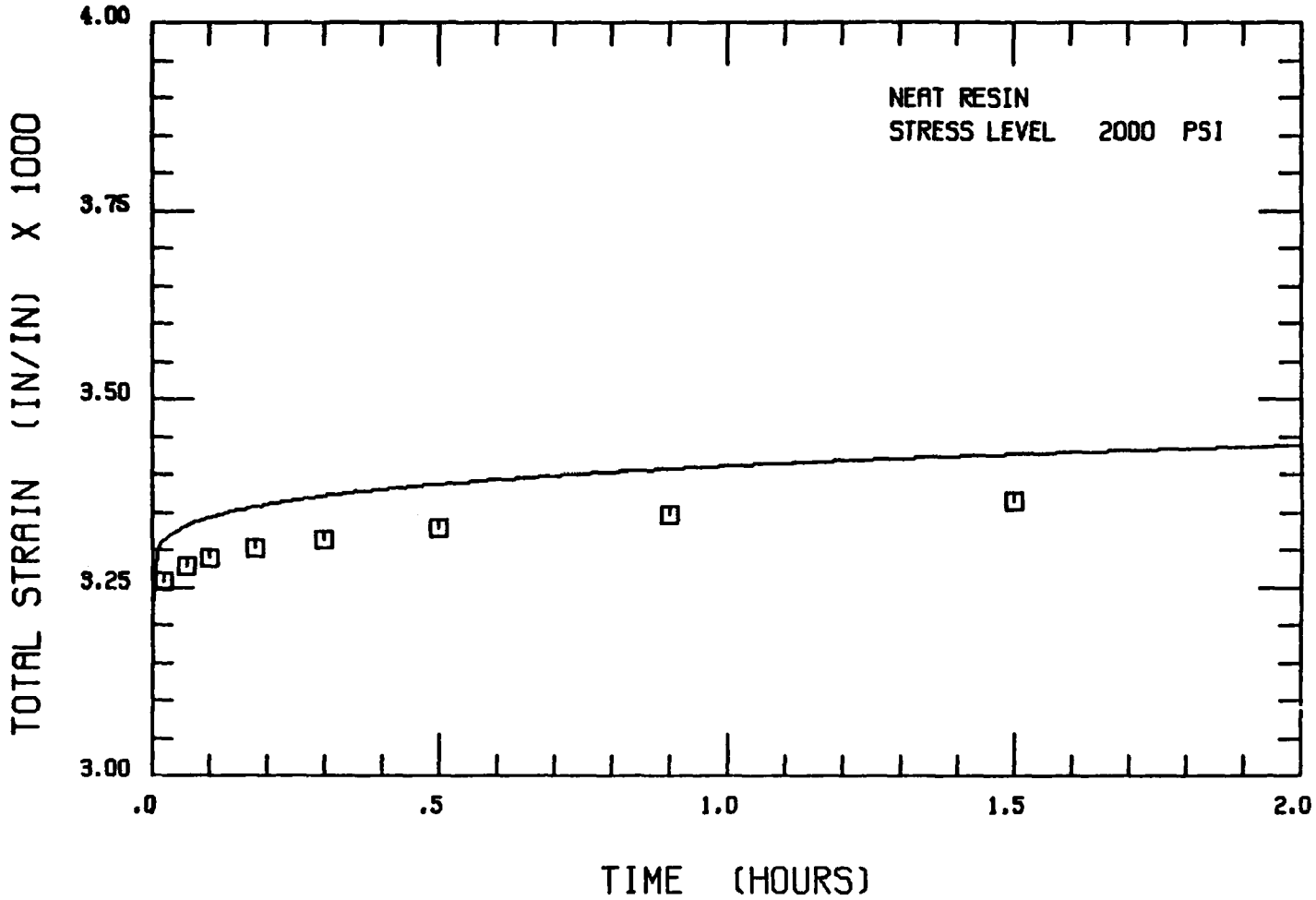

Figure D-2. Expanded scale plot of strain versus time for Hercules 3501-6 epoxy resin subjected to a 2.1 hour creep and a 2.1 hour recovery test. Predicted values are shown by the symbols while the line represents the actual experimental response.

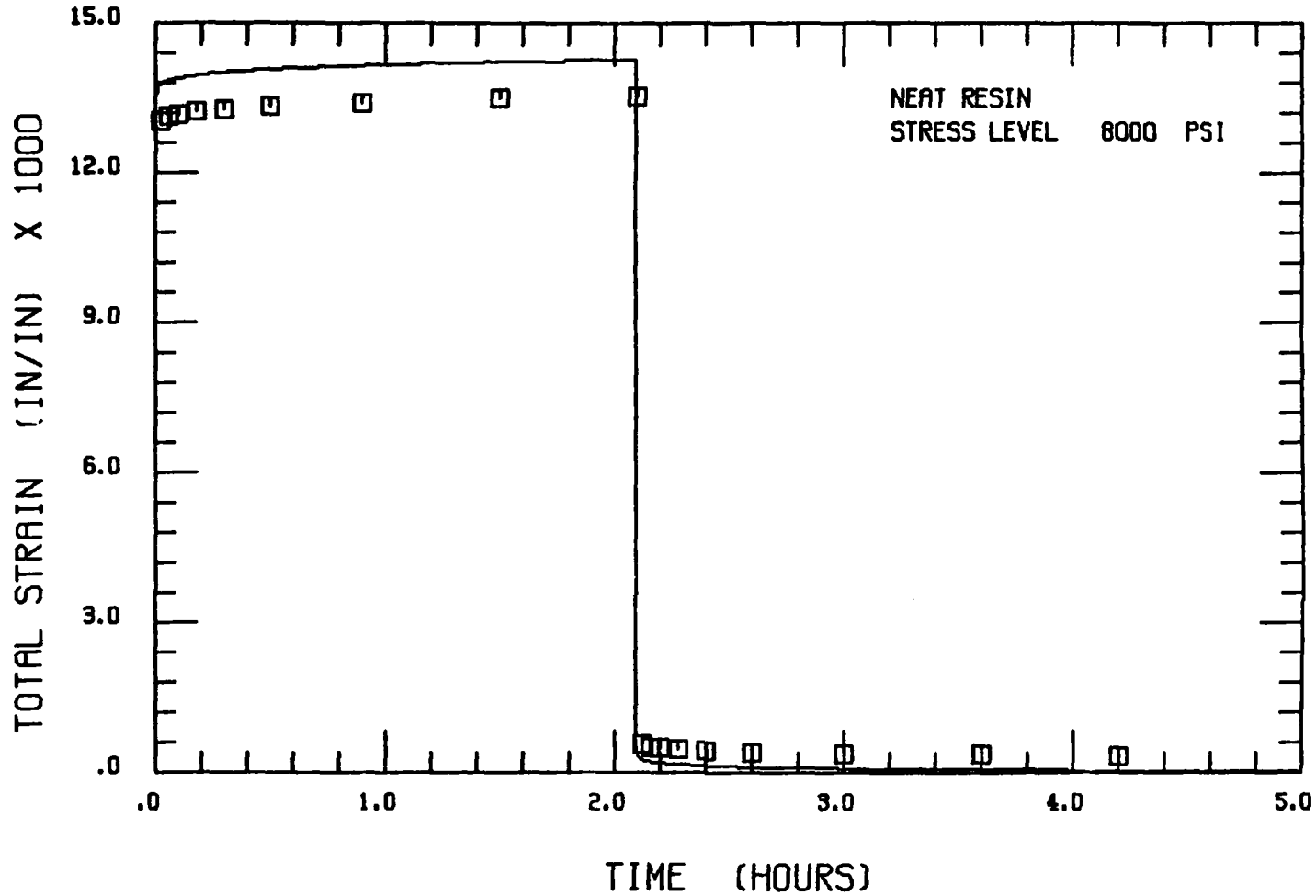

Figure D-3. Plot of strain versus time for Hercules 3501-6 epoxy resin subjected to a 2.1 hour creep and a 2.1 hour recovery test. Predicted values are shown by the symbols while the line represents the actual experimental response.

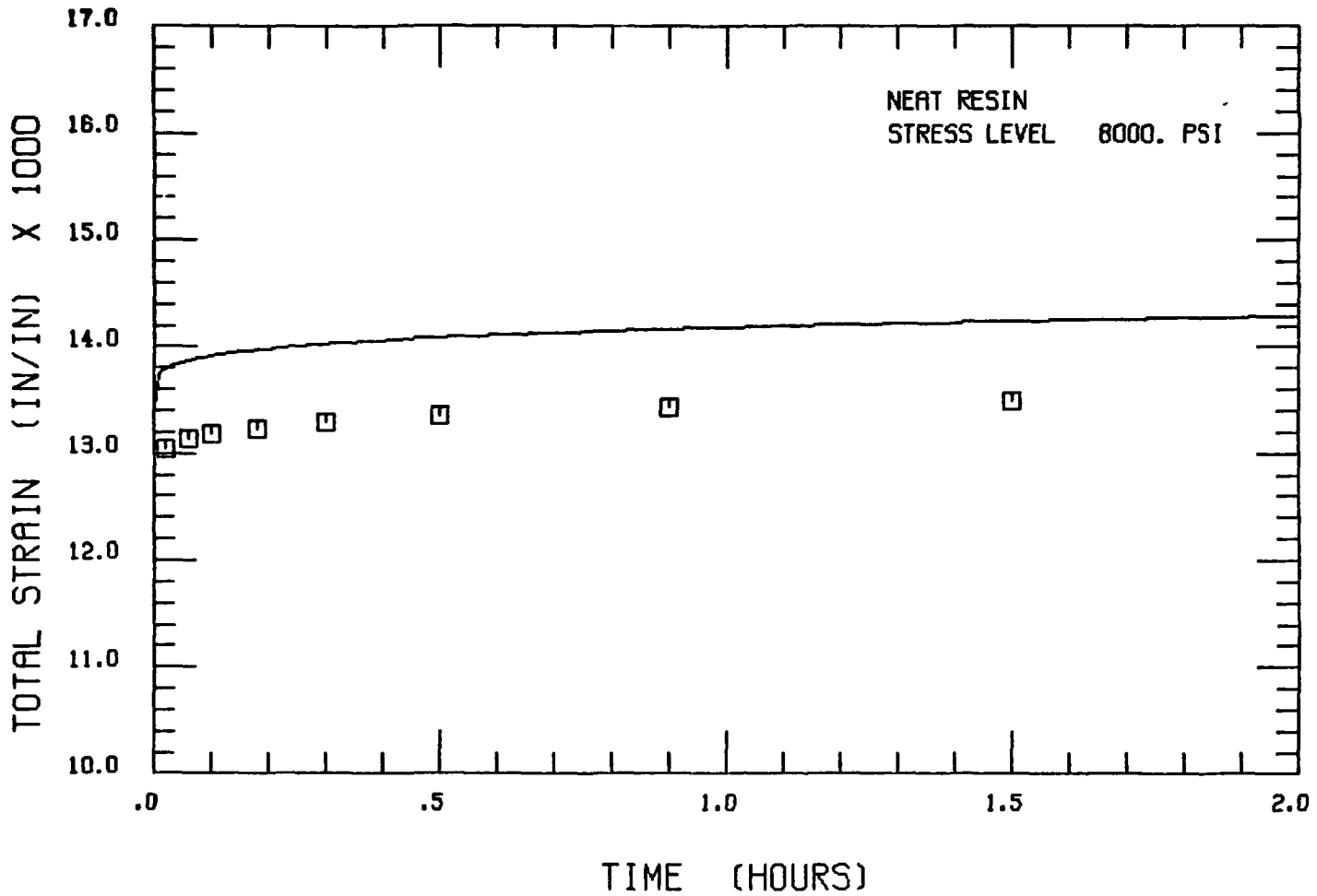

Figure D-4. Expanded scale plot of strain versus time for Hercules 3501-6 epoxy resin subjected to a 2.1 hour creep and a 2.1 hour recovery test. Predicted values are shown by the symbols while the line represents the actual experimental response.

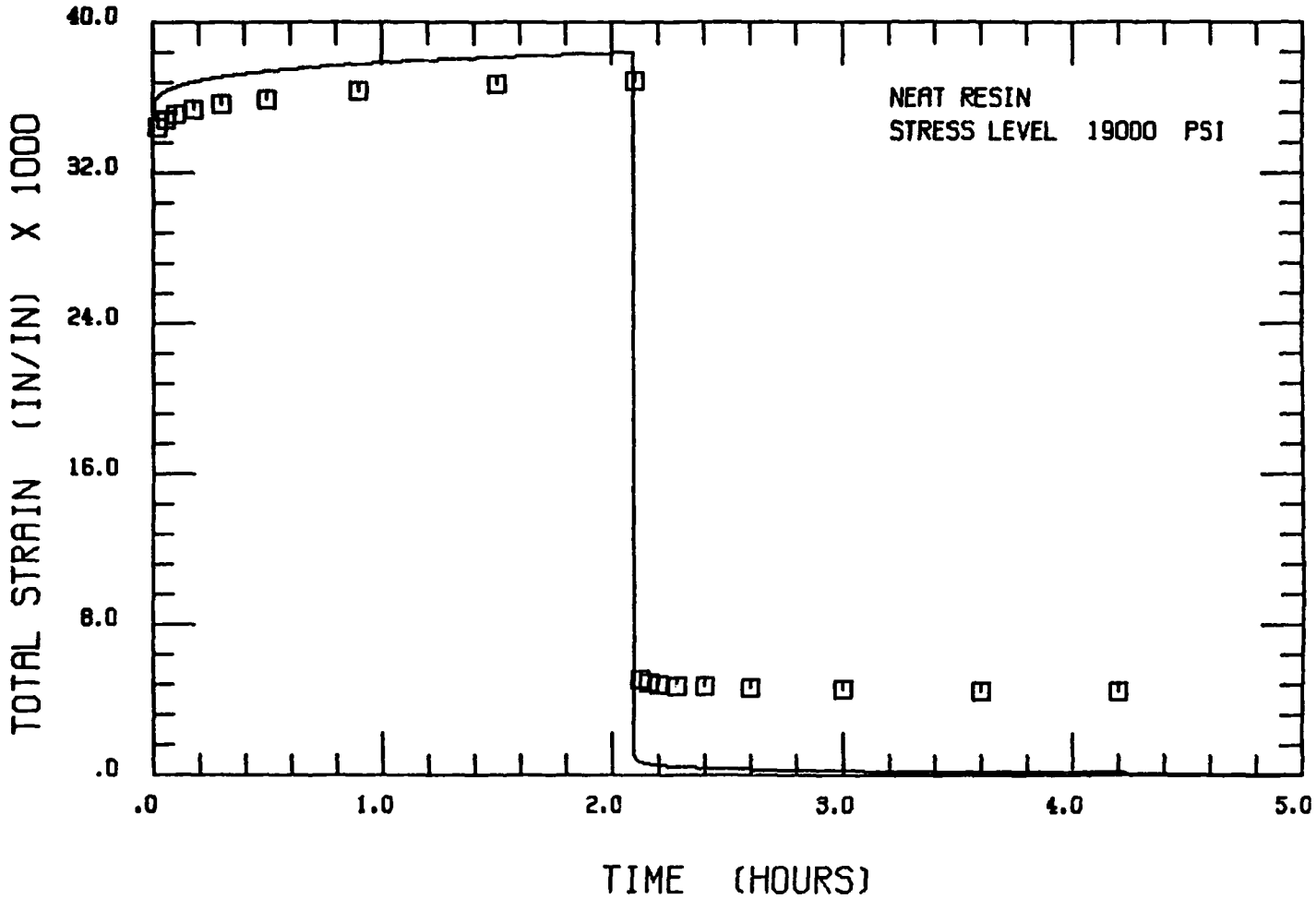

Figure D-5. Plot of strain versus time for Hercules 3501-6 epoxy resin subjected to a 2.1 hour creep and a 2.1 hour recovery test. Predicted values are shown by the symbols while the line represents the actual experimental response.

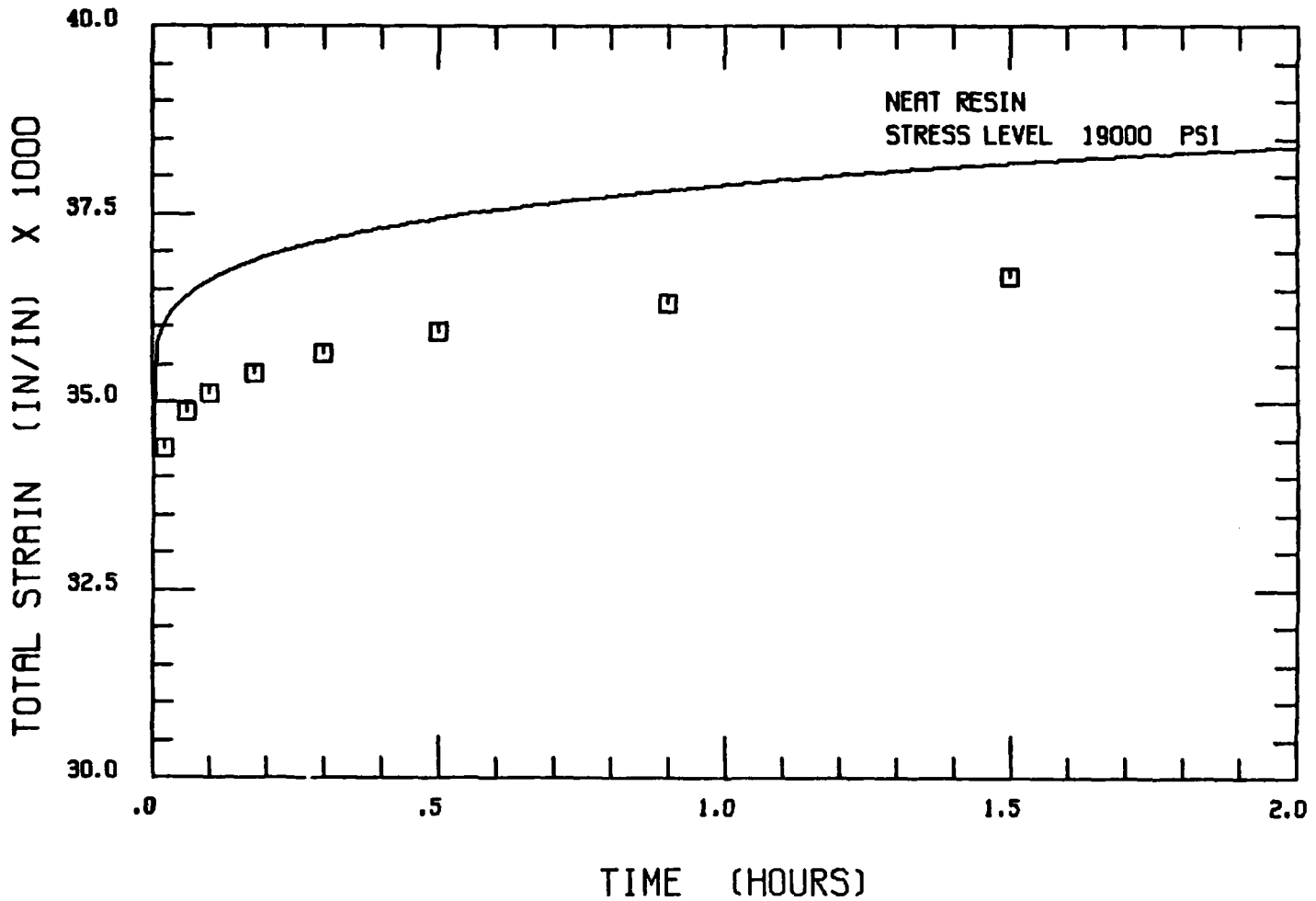

Figure D-6. Expanded scale plot of strain versus time for Hercules 3501-6 epoxy resin subjected to a 2.1 hour creep and a 2.1 hour recovery test. Predicted values are shown by the symbols while the line represents the actual experimental response.

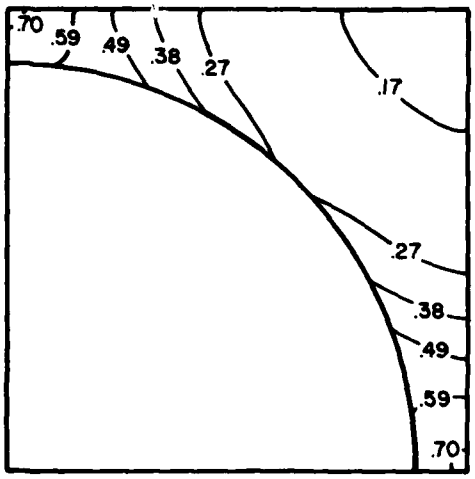

a) Octahedral shear stress
elapsed time: 0.0 hours

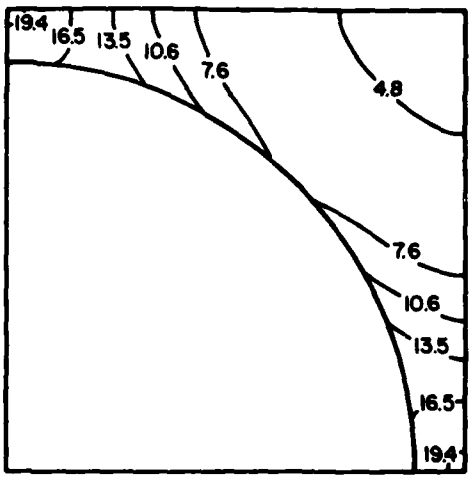

b) Octahedral shear strain
elapsed time: 0.0 hours

(immediately after cooldown to 21°C)

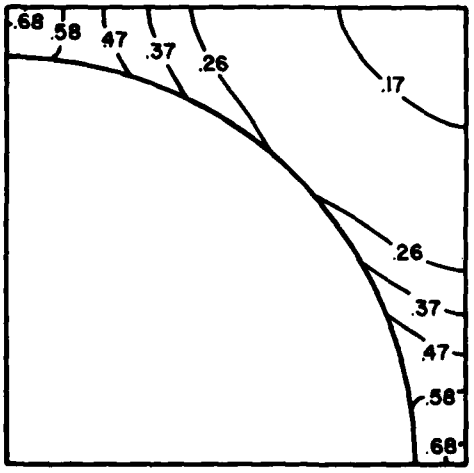

c) Octahedral shear stress
elapsed time: 0.5 hours

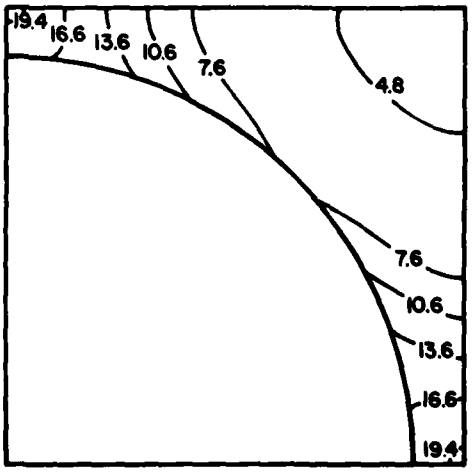

d) Octahedral shear strain
elapsed time: 0.5 hours

Figure D-7. Octahedral shear stress (normalized) and octahedral shear strain plots for glass/epoxy subjected to a cooldown from the 177°C cure temperature to 21°C, followed by a 140 hour relaxation period, and then a -20 ksi stress for another 140 hours.

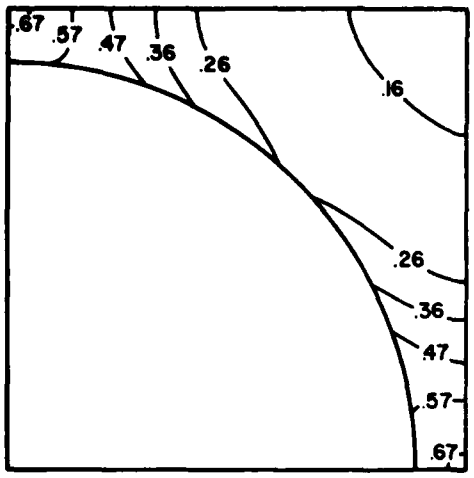

e) Octahedral shear stress
elapsed time: 2.1 hours

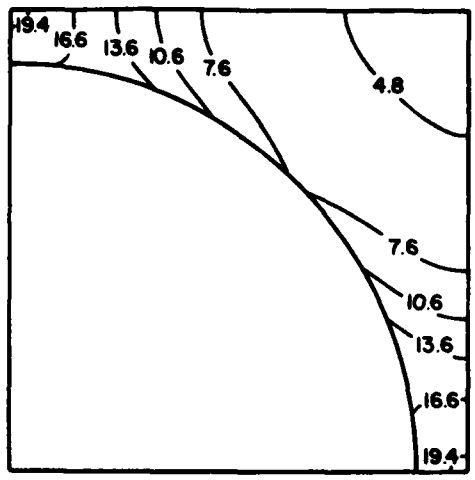

f) Octahedral shear strain
elapsed time: 2.1 hours

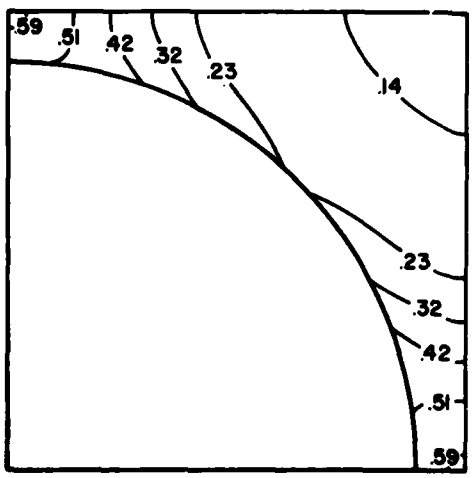

g) Octahedral shear stress
elapsed time: 140 hours

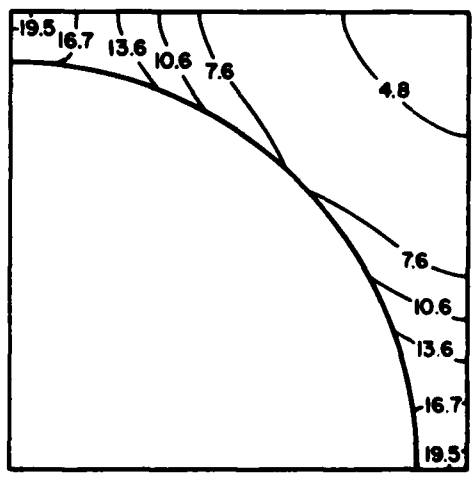

h) Octahedral shear strain
elapsed time: 140 hours

Figure D-7. (continued) Octahedral shear stress (normalized) and octahedral shear strain plots for glass/epoxy subjected to a cooldown from the 177°C cure temperature to 21°C, followed by a 140 hour relaxation period, and then a -20 ksi stress for another 140 hours.

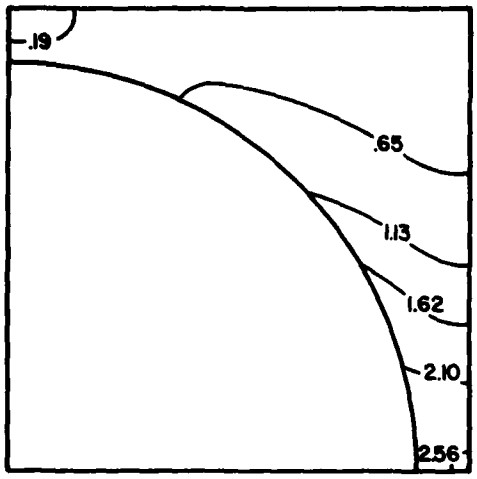

i) Octahedral shear stress
elapsed time: 140 hours

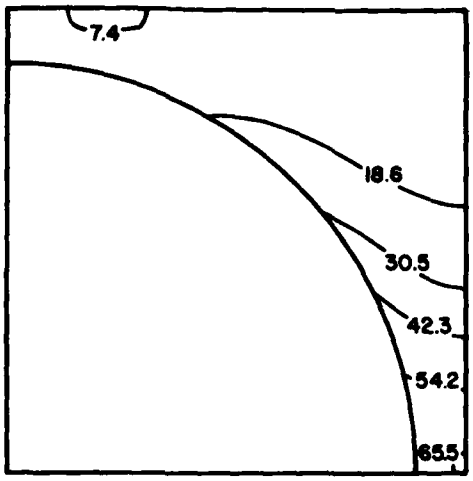

j) Octahedral shear strain
elapsed time: 140 hours

(immediately after application of $\bar{\sigma}_x$ = -20 ksi)

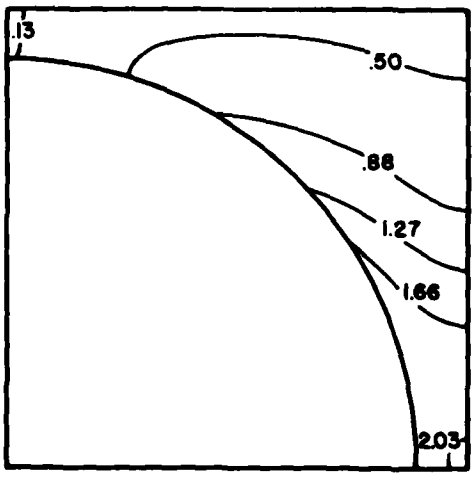

k) Octahedral shear stress
elapsed time: 280 hours

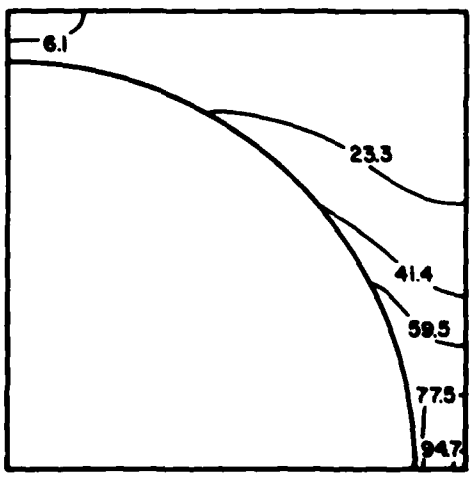

ℓ) Octahedral shear strain
elapsed time: 280 hours

Figure D-7. (continued) Octahedral shear stress (normalized) and octahedral shear strain plots for glass/epoxy subjected to a cooldown from the 177°C cure temperature to 21°C, followed by a 140 hour relaxation period, and then a -20 ksi stress for another 140 hours.

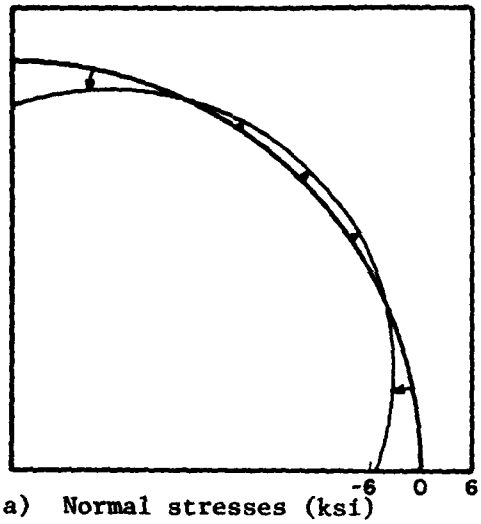

a) Normal stresses (ksi)
elapsed time: 0.0 hours

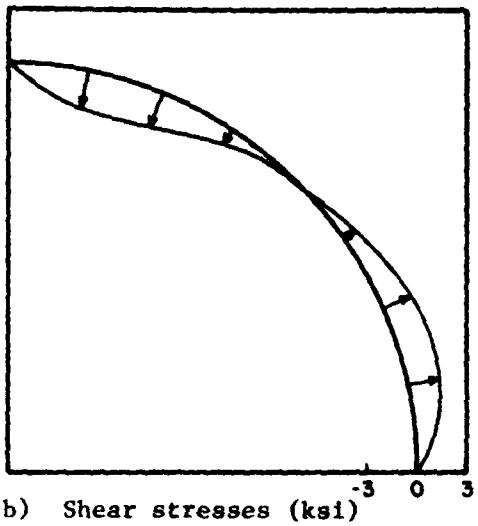

b) Shear stresses (ksi)
elapsed time: 0.0 hours

(immediately after cooldown to 21°C)

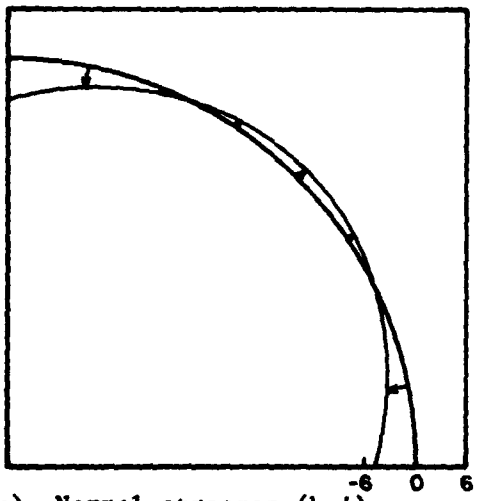

c) Normal stresses (ksi)
elapsed time: 140 hours

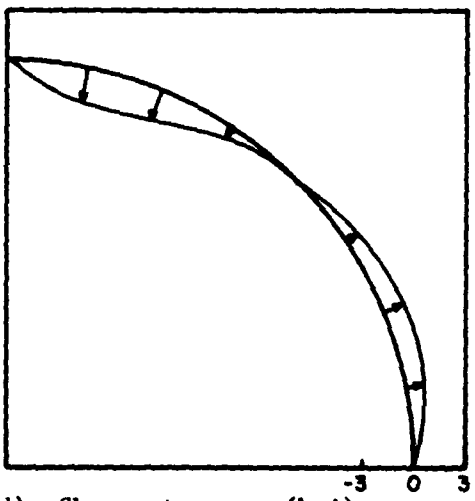

d) Shear stresses (ksi)
elapsed time: 140 hours

Figure D-8. Interface stresses for glass/epoxy subjected to a cool-down from the 177°C cure temperature to 21°C followed by a 140 hour relaxation period, and then a -20 ksi stress for another 140 hours.

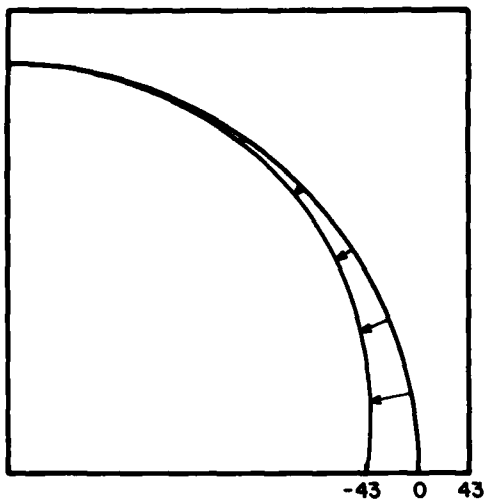

d) Normal stresses (ksi)
elapsed time: 140 hours

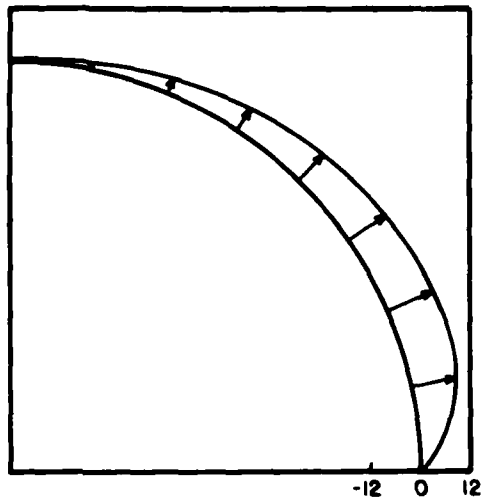

e) Shear stresses (ksi)
elapsed time: 140 hours

(immediately after application of $\bar{\sigma}_x$ = -20 ksi)

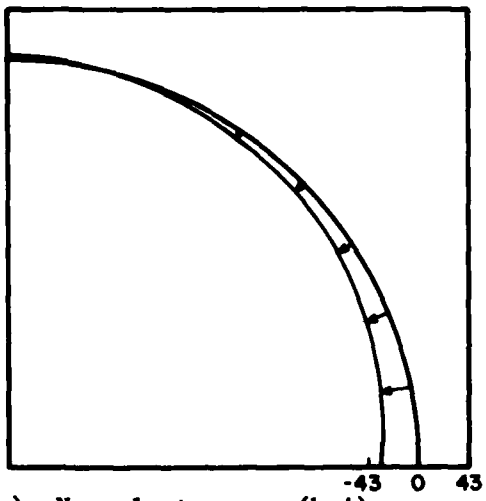

g) Normal stresses (ksi)
elapsed time: 280 hours

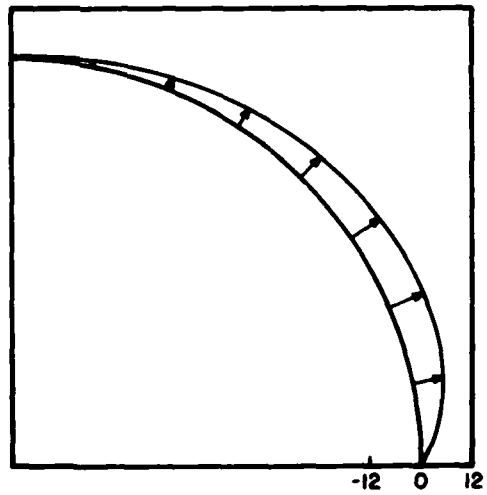

h) Shear stresses (ksi)
elapsed time: 280 hours

Figure D-8. (continued) Interface stresses for glass/epoxy subjected to a cooldown from the 177°C cure temperature to 21°C followed by a 140 hour relaxation period, and then a -20 ksi stress for another 140 hours.

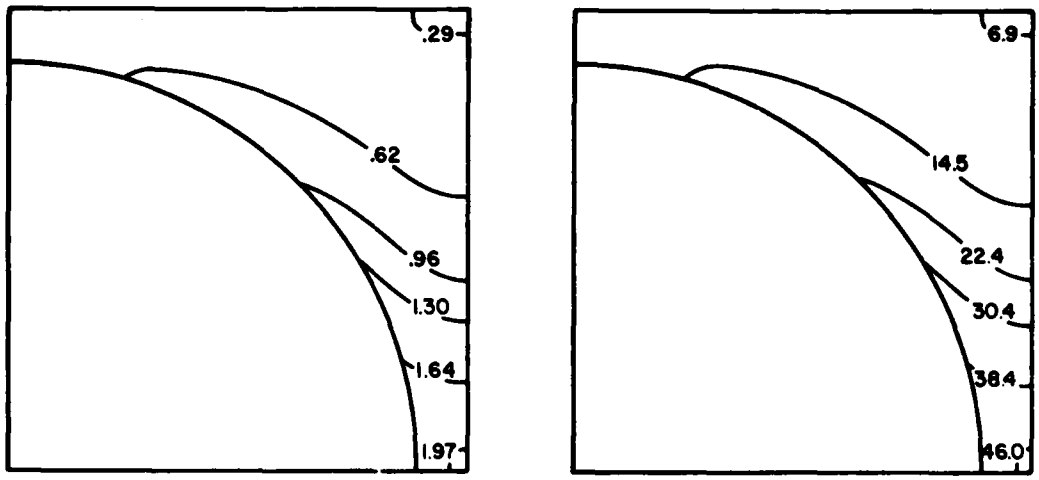

a) Octahedral shear stress
elapsed time: 0.0 hours

b) Octahedral shear strain
elapsed time: 0.0 hours

(immediately after application of $\bar{\sigma}_x$ = -20 ksi)

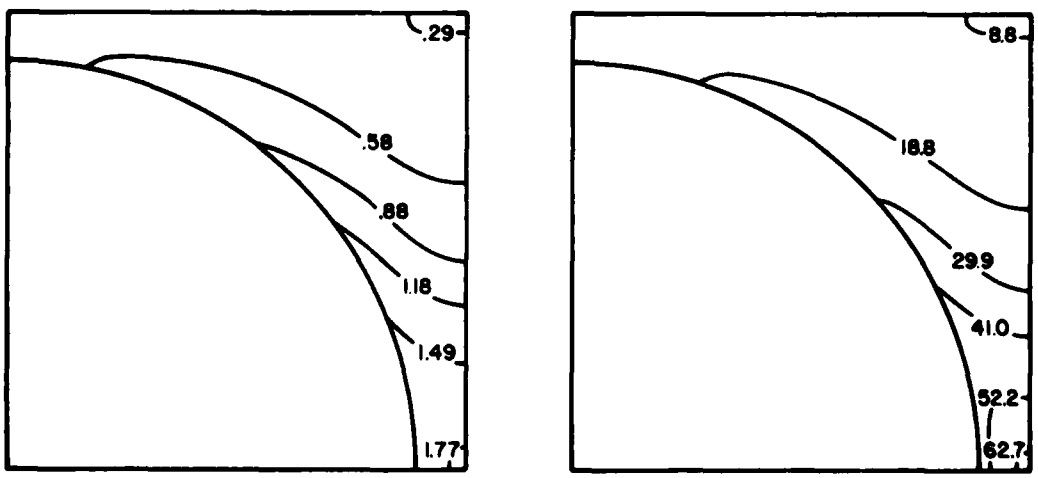

c) Octahedral shear stress
elapsed time: 140 hours

d) Octahedral shear strain
elapsed time: 140 hours

Figure D-9. Octahedral shear stress (normalized) and octahedral shear strain plots for glass/epoxy subjected to a -20 ksi stress for 140 hours (no prior temperature history).

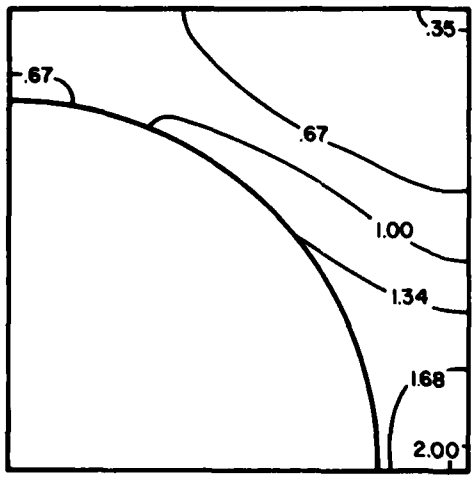

a) Octahedral shear stress
elapsed time: 0.0 hours

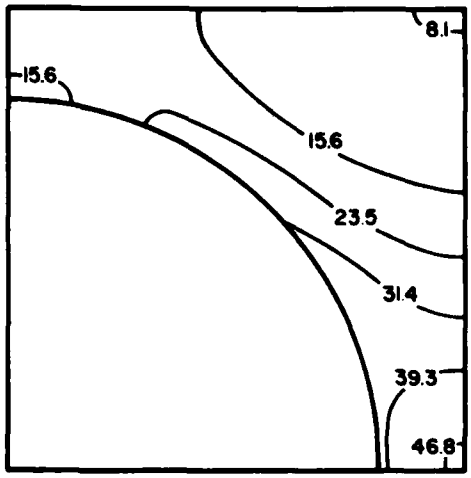

b) Octahedral shear strain
elapsed time: 0.0 hours

(immediately after application of $\bar{\sigma}_x$ = -20 ksi)

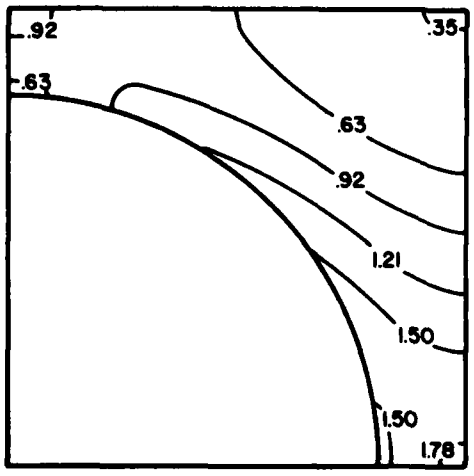

c) Octahedral shear stress
elapsed time: 140 hours

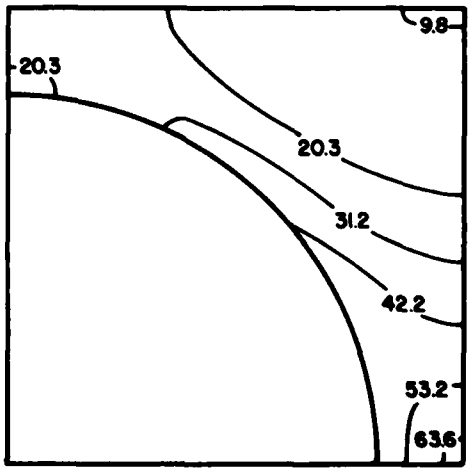

d) Octahedral shear strain
elapsed time: 140 hours

Figure D-10. Octahedral shear stress (normalized) and octahedral shear strain plots for a 50 percent fiber volume glass/epoxy composite subjected to a -20 ksi stress for 140 hours (no prior temperature history).

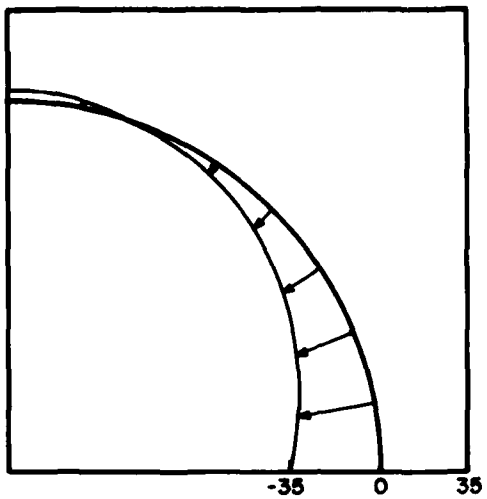

a) Normal stresses (ksi)
elapsed time: 0.0 hours

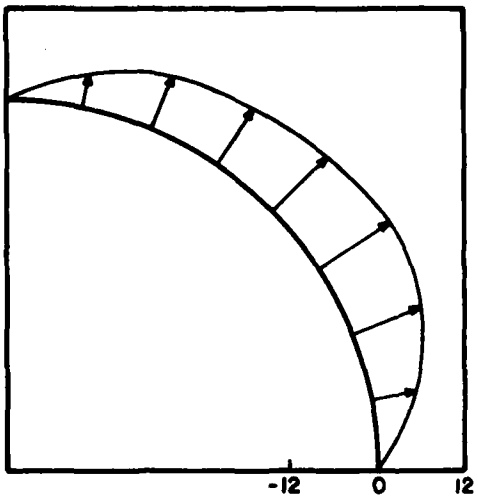

b) Shear stress (ksi)
elapsed time: 0.0 hours

(immediately after application of σ_x = -20 ksi)

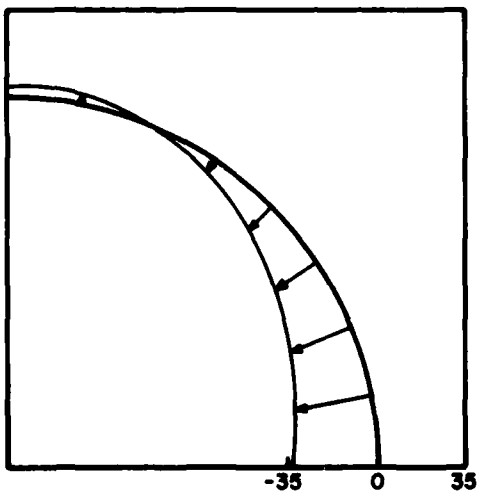

c) Normal stresses (ksi)
elapsed time: 140 hours

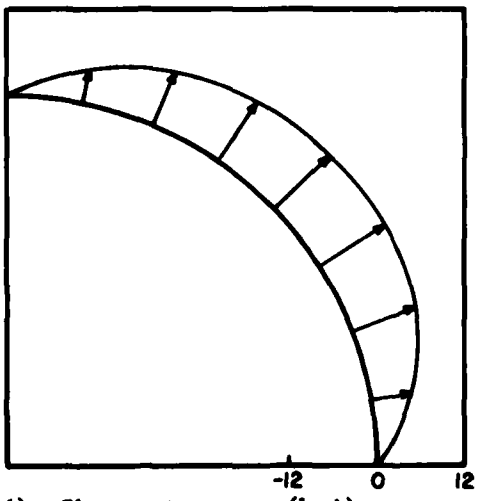

d) Shear stresses (ksi)
elapsed time: 140 hours

Figure D-11. Interface stresses for a 50 percent fiber volume glass/epoxy composite subjected to a -20 ksi stress for 140 hours (no prior temperature history).

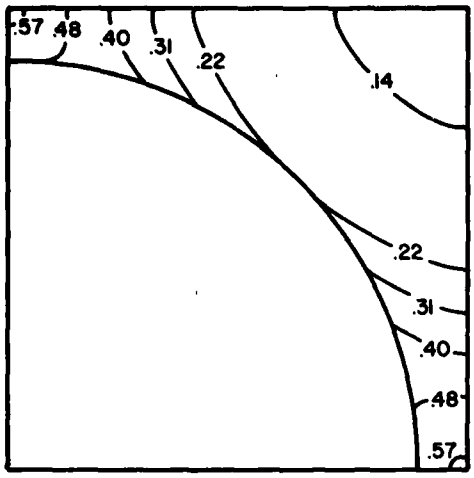

a) Octahedral shear stress
elapsed time: 0.0 hours

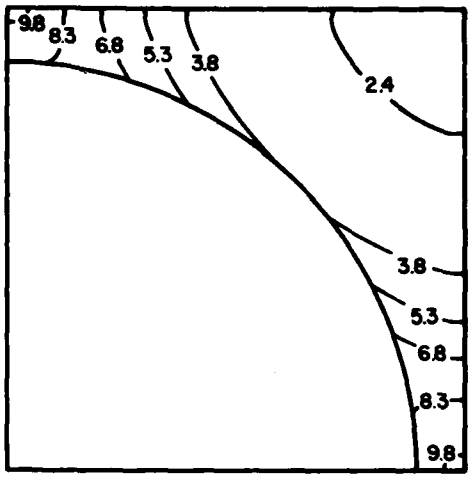

b) Octahedral shear strain
elapsed time: 0.0 hours

(immediately after cooldown to 99°C)

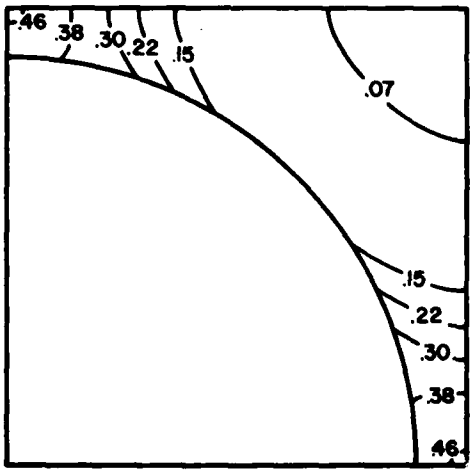

c) Octahedral shear stress
elapsed time: 2.1 hours

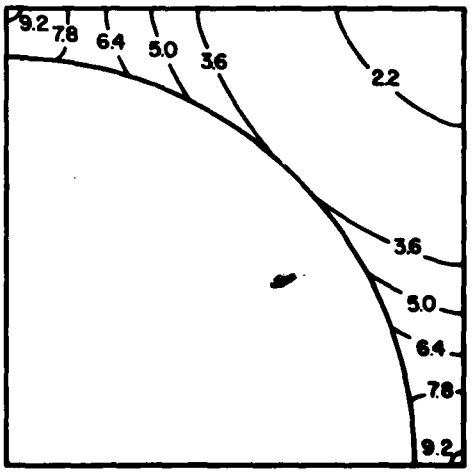

d) Octahedral shear strain
elapsed time: 2.1 hours

Figure D-12. Octahedral shear stress (normalized) and octahedral shear strain plots for glass/epoxy subjected to a cooldown from the 177°C cure temperature to 99°C, a 2.1 hours relaxation period, further cool from 99°C to 21°C, and another 2.1 hour relaxation period.

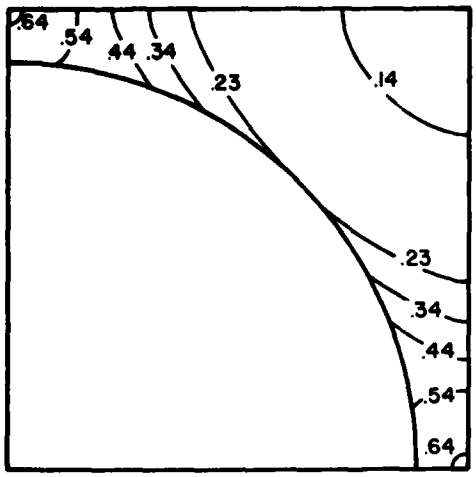

e) Octahedral shear stress
elapsed time: 2.1 hours

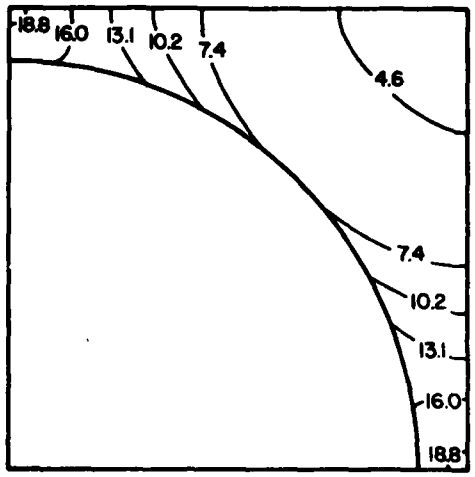

f) Octahedral shear strain
elapsed time: 2.1 hours

(immediately after cooldown to 21°C)

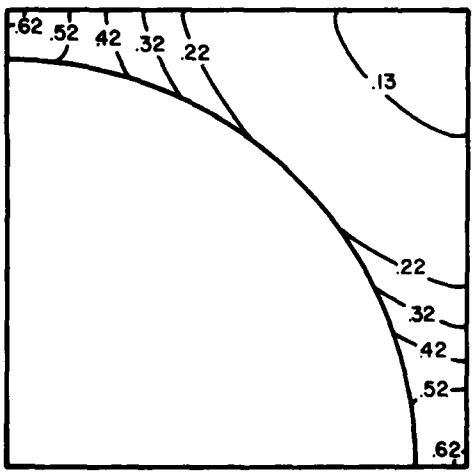

g) Octahedral shear stress
elapsed time: 4.2 hours

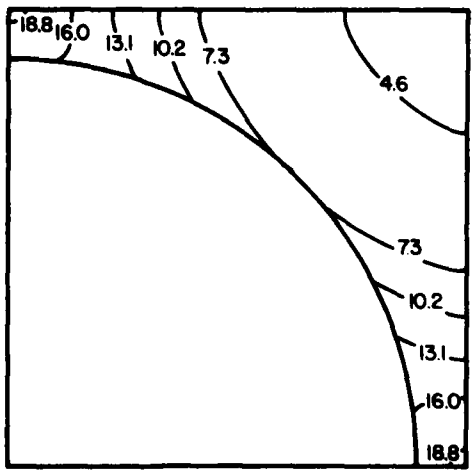

h) Octahedral shear strain
elapsed time: 4.2 hours

Figure D-12. (continued) Octahedral shear stress (normalized) and octahedral shear strain plots for glass/epoxy subjected to a cooldown from the 177°C cure temperature to 99°C, a 2.1 hour relaxation period, further cool from 99°C to 21°C, and another 2.1 hour relaxation period.

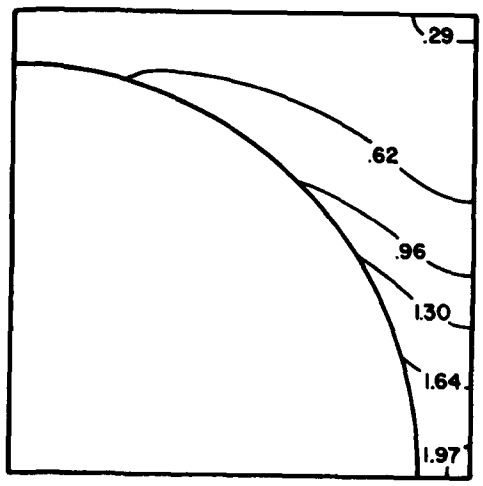

a) Octahedral shear stress
elapsed time: 0.0 hours

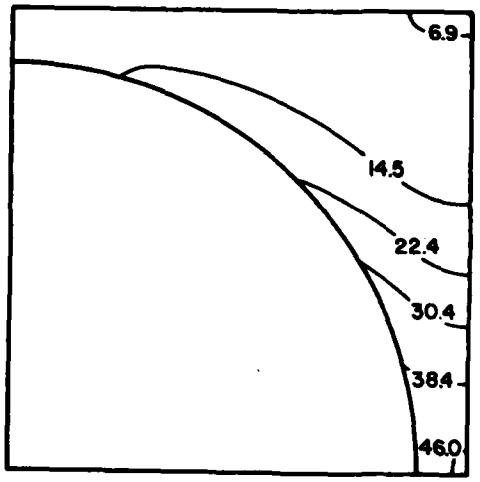

b) Octahedral shear strain
elapsed time: 0.0 hours

(immediately after application of $\bar{\sigma}_x$ = +20 ksi)

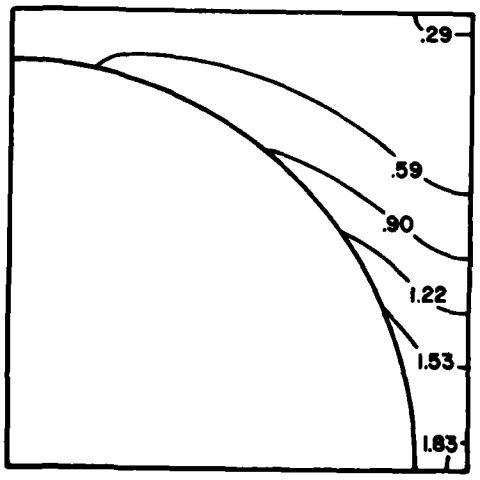

c) Octahedral shear stress
elapsed time: 2.1 hours

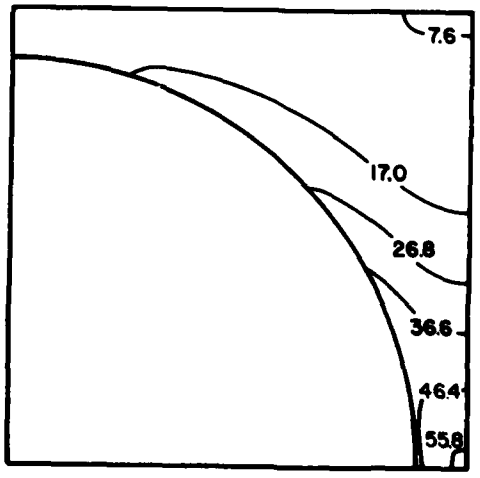

d) Octahedral shear strain
elapsed time: 2.1 hours

Figure D-13. Octahedral shear stress (normalized) and octahedral shear strain plots for glass/epoxy subjected to a +20 ksi stress for 2.1 hours, a -20 ksi stress for 2.1 hours, and a +20 ksi stress for another 2.1 hours (no prior temperature history).

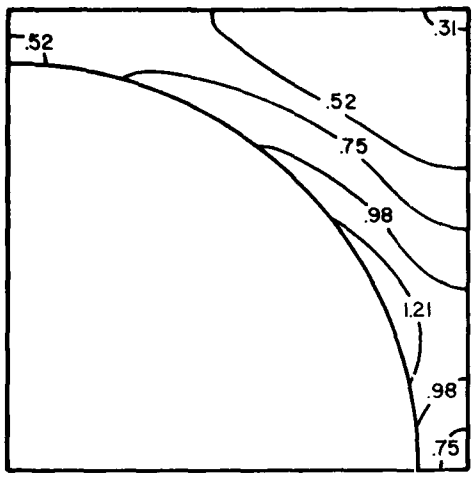

e) Octahedral shear stress
elapsed time: 2.1 hours

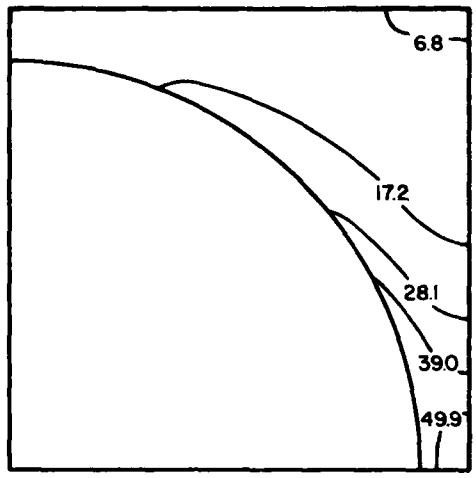

f) Octahedral shear strain
elapsed time: 2.1 hours

(immediately after stress reversal, to $\bar{\sigma}_x$ = -20 ksi)

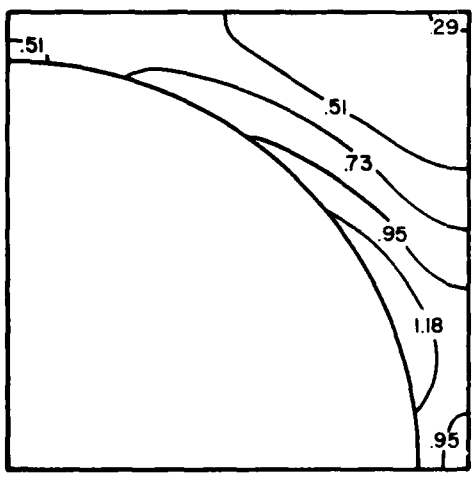

g) Octahedral shear stress
elapsed time: 4.2 hours

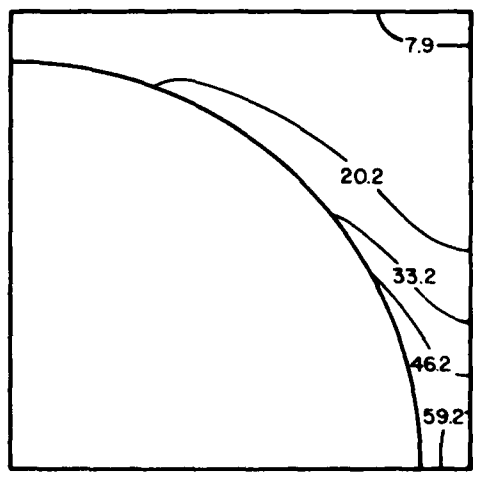

h) Octahedral shear strain
elapsed time: 4.2 hours

Figure D-13. (continued) Octahedral shear stress (normalized) and octahedral shear strain plots for glass/epoxy subjected to a +20 ksi stress for 2.1 hours, a -20 ksi stress for 2.1 hours, and a +20 ksi stress for another 2.1 hours (no prior temperature history).

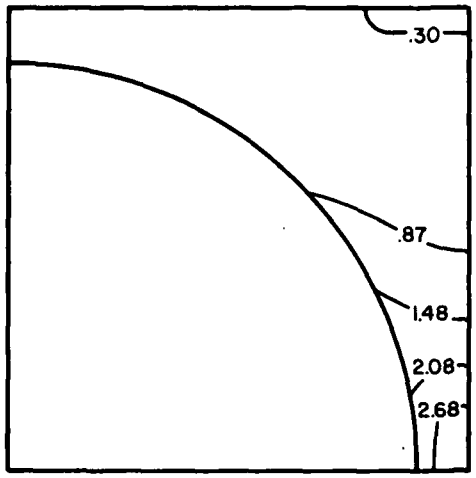

i) Octahedral shear stress
elapsed time: 4.2 hours

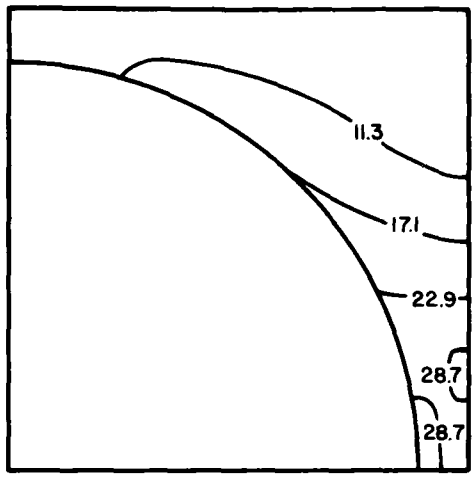

j) Octahedral shear strain
elapsed time: 4.2 hours

(immediately after stress reversal, to $\bar{\sigma}_x$ = +20 ksi)

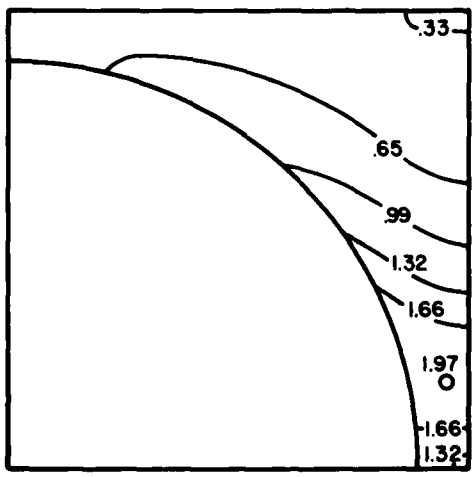

k) Octahedral shear stress
elapsed time: 6.3 hours

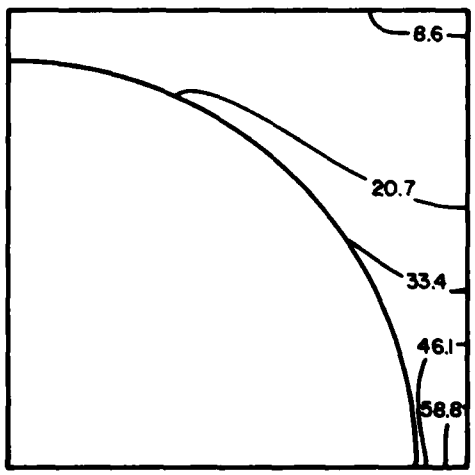

ℓ) Octahedral shear strain
elapsed time: 6.3 hours

Figure D-13. (continued) Octahedral shear stress (normalized) and octahedral shear strain plots for glass/epoxy subjected to a +20 ksi stress for 2.1 hours, and a -20 ksi stress for 2.1 hours, and a +20 ksi stress for another 2.1 hours (no prior temperature history).

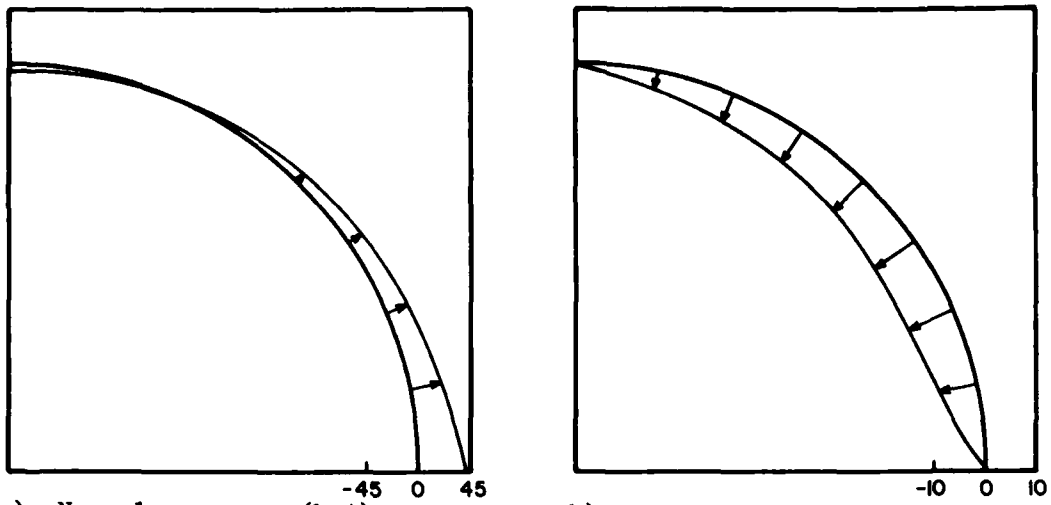

a) Normal stresses (ksi)
elapsed time: 0.0 hours

b) Shear stresses (ksi)
elapsed time: 0.0 hours

(immediately after application of $\bar{\sigma}_x$ = +20 ksi)

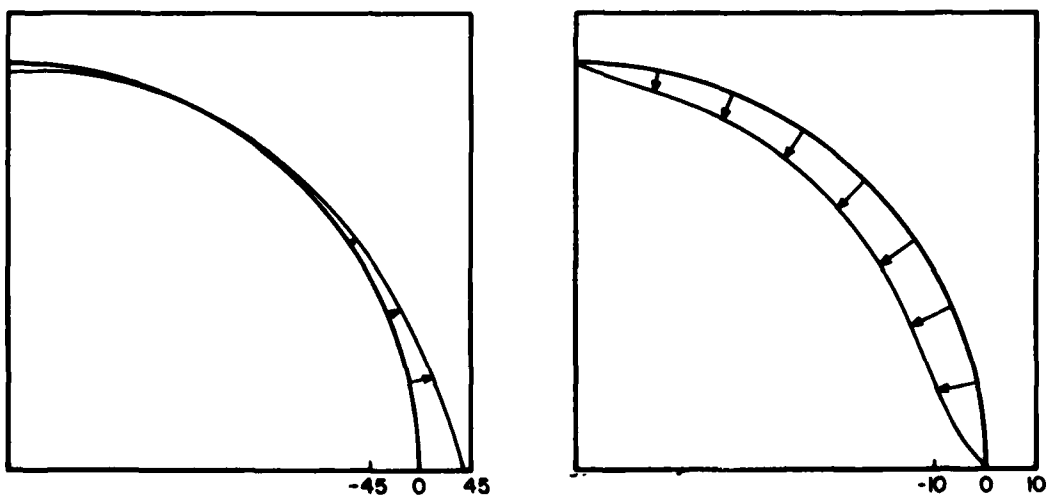

c) Normal stresses (ksi)
elapsed time: 2.1 hours

d) Shear stresses (ksi)
elapsed time: 2.1 hours

Figure D-14. Interface stresses for glass/epoxy subjected to a +20 ksi stress for 2.1 hours, a -20 ksi stress for 2.1 hours, and a +20 ksi stress for another 2.1 hours (no prior temperature history).

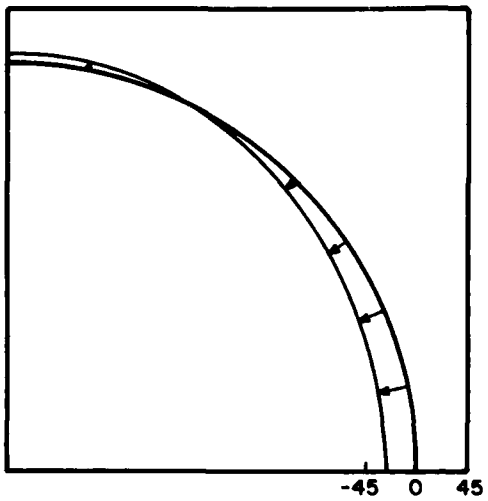

e) Normal stresses (ksi)
elapsed time: 2.1 hours

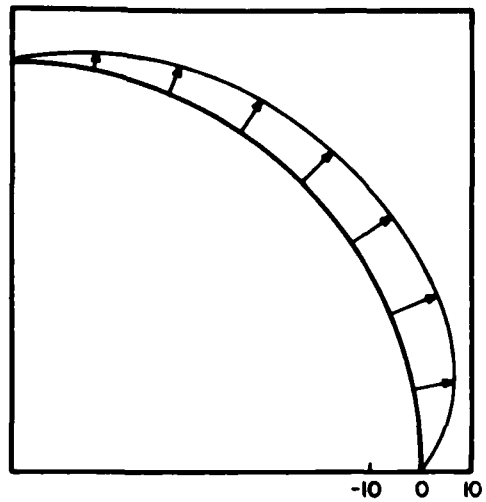

f) Shear stresses (ksi)
elapsed time: 2.1 hours

(immediately after stress reversal, to $\bar{\sigma}_x$ = -20 ksi)

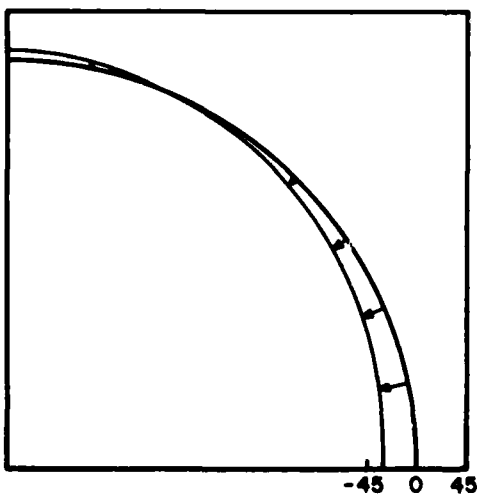

g) Normal stresses (ksi)
elapsed time: 4.2 hours

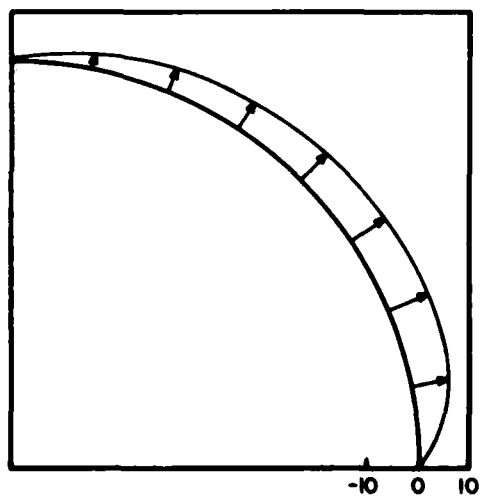

h) Shear stresses (ksi)
elapsed time: 4.2 hours

Figure D-14. (continued) Interface stresses for glass/epoxy subjected to a +20 ksi stress for 2.1 hours, a -20 ksi stress for 2.1 hours, and a +20 ksi stress for another 2.1 hours (no prior temperature history).

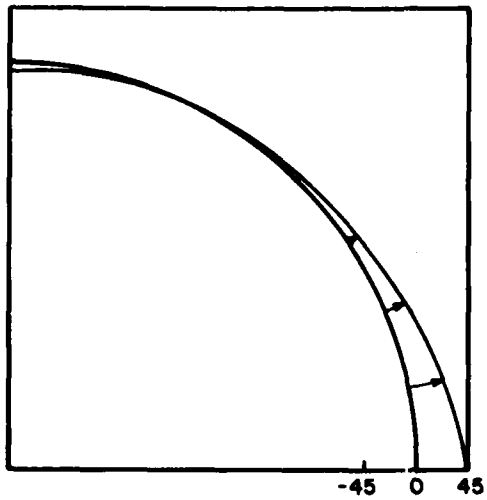

i) Normal stresses (ksi)
elapsed time: 4.2 hours

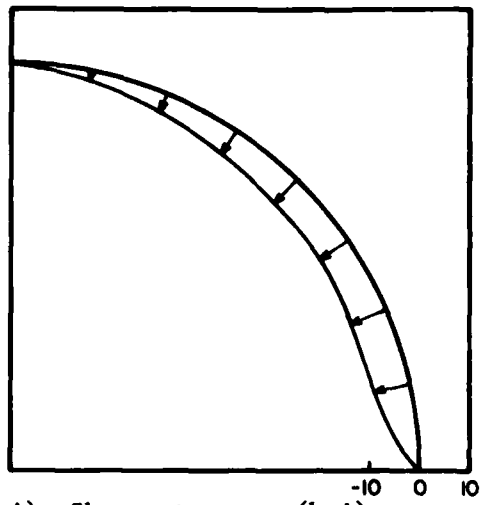

j) Shear stresses (ksi)
elapsed time: 4.2 hours

(immediately after stress reversal, to $\bar{\sigma}_x$ = +20 ksi)

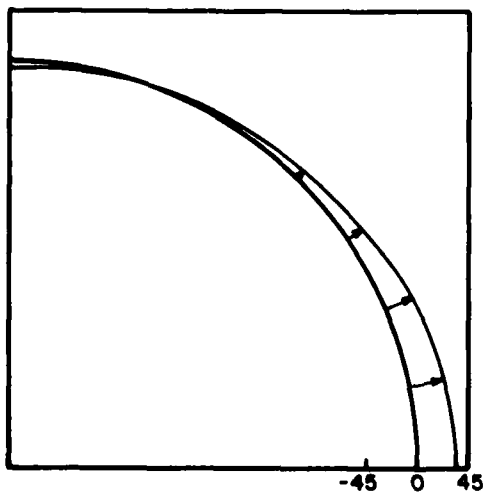

k) Normal stresses (ksi)
elapsed time: 6.3 hours

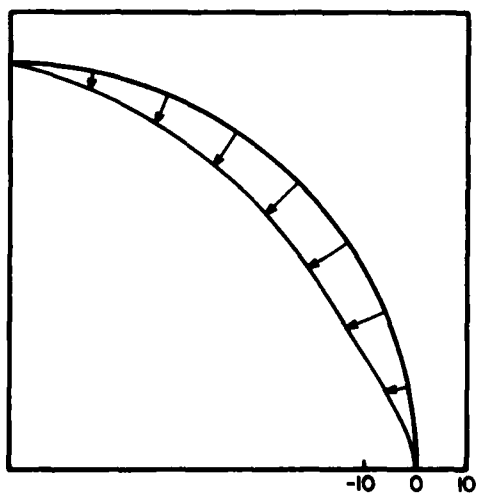

ℓ) Shear stresses (ksi)
elapsed time: 6.3 hours

Figure D-14. (continued) Interface stresses for glass/epoxy subjected to a +20 ksi stress for 2.1 hours, a -20 ksi stress for 2.1 hours, and a +20 ksi stress for another 2.1 hours (no prior temperature history).

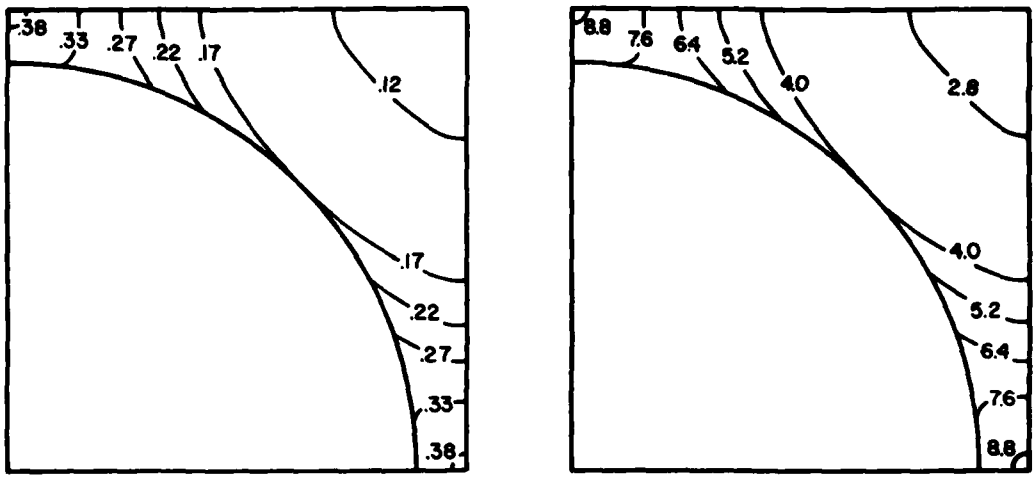

a) Octahedral shear stress
elapsed time: 0.0 hours

b) Octahedral shear strain
elapsed time: 0.0 hours

(immediately after application of $\bar{\sigma}_x = \bar{\sigma}_y = +5$ ksi)

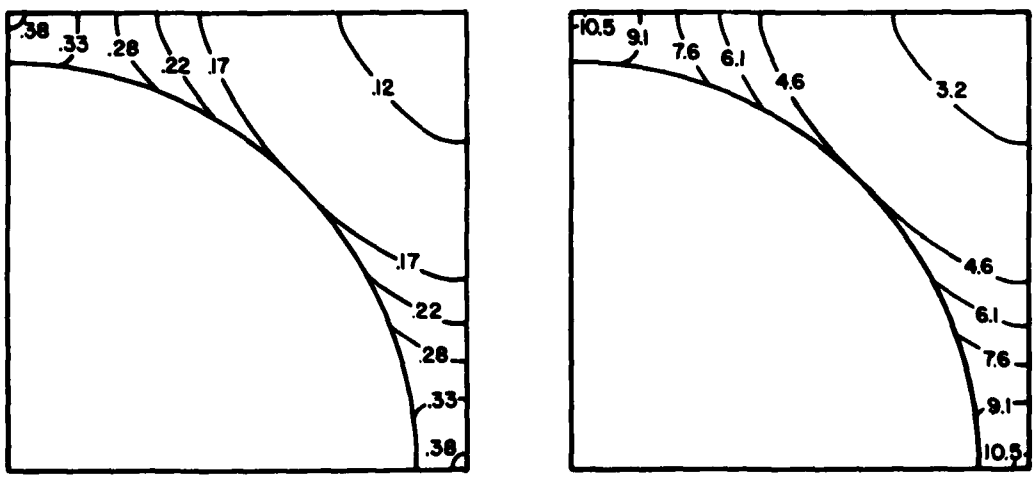

c) Octahedral shear stress
elapsed time: 140 hours

d) Octahedral shear strain
elapsed time: 140 hours

Figure D-15. Octahedral shear stress (normalized) and octahedral shear strain plots for glass/epoxy subjected to a 5 ksi stress in the x-direction and a 5 ksi stress in the y-direction (no prior temperature history).

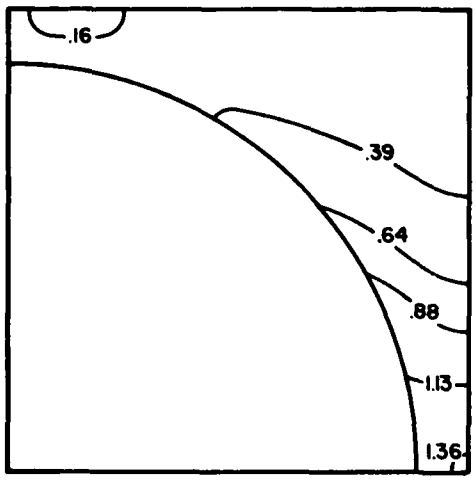

a) Octahedral shear stress
elapsed time: 0.0 hours

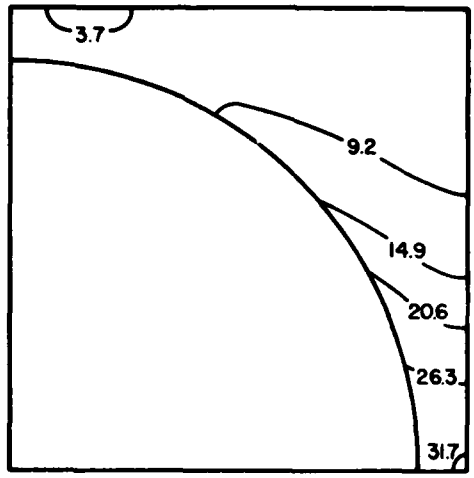

b) Octahedral shear strain
elapsed time: 0.0 hours

(immediately after application of $\bar{\sigma}_x$ = + 15 ksi, $\bar{\sigma}_y$ = + 5 ksi)

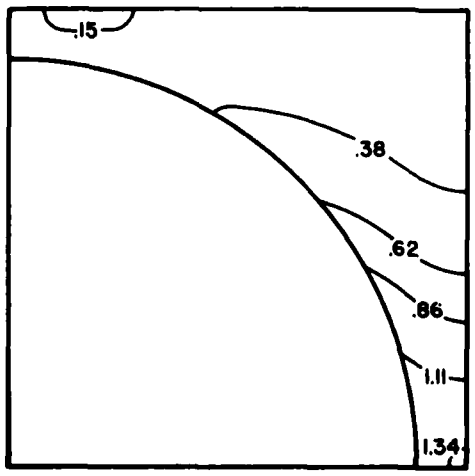

c) Octahedral shear stress
elapsed time: 140 hours

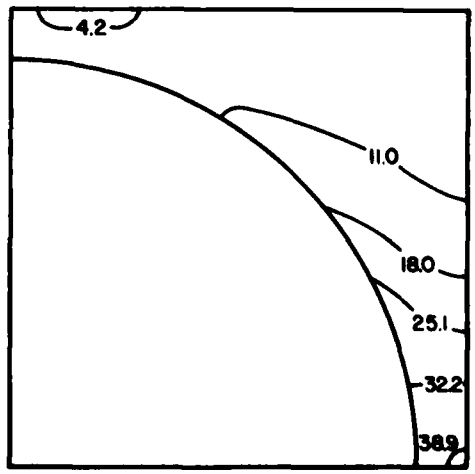

d) Octahedral shear strain
elapsed time: 140 hours

Figure D-16. Octahedral shear stress (normalized) and octahedral shear strain plots for glass/epoxy subjected to a 15 ksi stress in the x-direction and a 5 ksi stress in the y-direction (no prior temperature history).

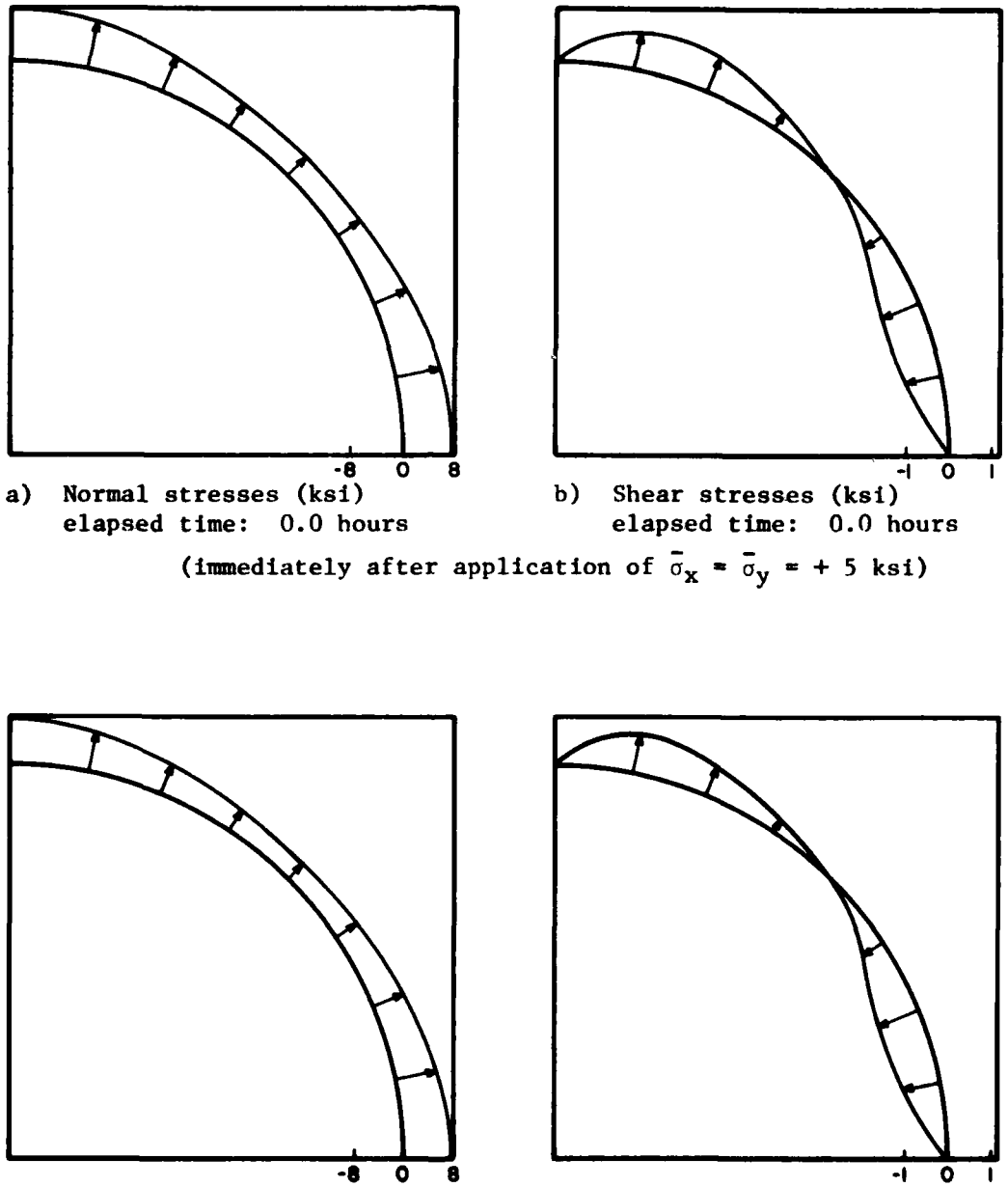

a) Normal stresses (ksi)
elapsed time: 0.0 hours

b) Shear stresses (ksi)
elapsed time: 0.0 hours

(immediately after application of $\bar{\sigma}_x = \bar{\sigma}_y = +5$ ksi)

c) Normal stresses (ksi)
elapsed time: 140 hours

d) Shear stresses (ksi)
elapsed time: 140 hours

Figure D-17. Interface stresses for glass/epoxy subjected to a 5 ksi stress in the x-direction and a 5 ksi stress in the y-direction (no prior temperature history).

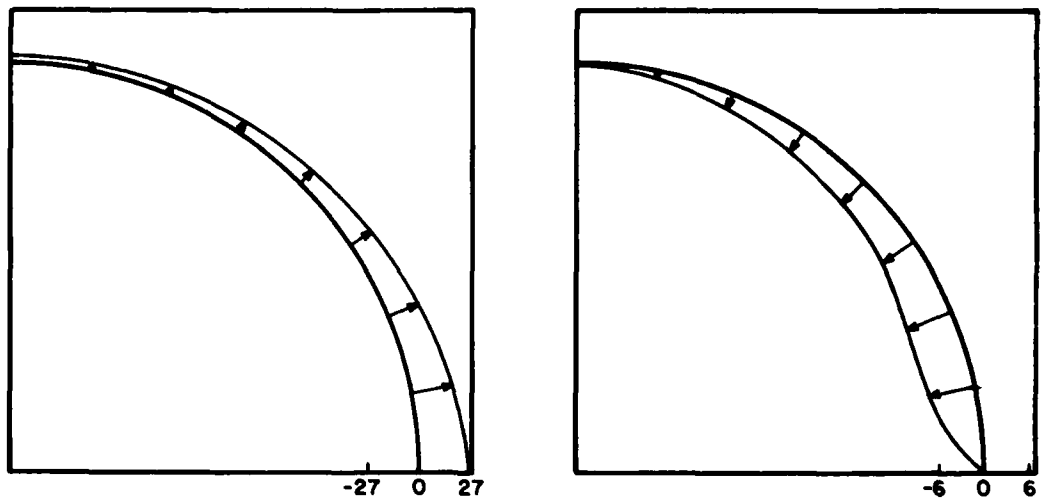

a) Normal stresses (ksi)
elapsed time: 0.0 hours

b) Shear stresses (ksi)
elapsed time: 0.0 hours

(immediately after application of $\bar{\sigma}_x$ = + 15 ksi, $\bar{\sigma}_y$ = + 5 ksi)

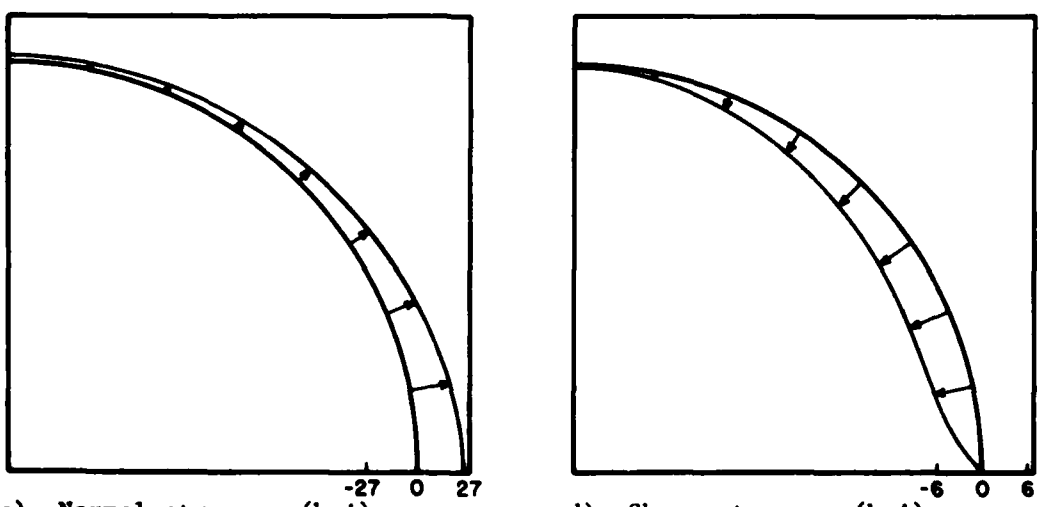

c) Normal stresses (ksi)
elapsed time: 140 hours

d) Shear stresses (ksi)
elapsed time: 140 hours

Figure D-18. Interface stresses for glass/epoxy subjected to a 15 ksi stress in the x-direction and a 5 ksi stress in the y-direction (no prior temperature history).